

EXPLORING THE MECHANISM  
AND THERAPEUTIC POTENTIAL  
OF THE EPHRIN SYSTEM IN ALS

**Lies Schoonaert**

Supervisory Committee:  
Prof. Dr. Wim Robberecht  
Prof. Dr. Philip Vandamme  
Prof. Dr. Robin Lemmens

Dissertation presented in partial  
fulfillment of the requirements for the  
degree of Doctor in Biomedical Sciences

January 2016





KU Leuven  
Biomedical Sciences Group  
Faculty of Medicine  
Department of Neurosciences  
Laboratory of Neurobiology  
Vlaams Instituut voor Biotechnologie (VIB)  
Vesalius Research Center



# Exploring the mechanism and therapeutic potential of the ephrin system in ALS

Lies SCHOONAERT

## Jury:

Promoter: Prof. Dr. Wim Robberecht  
Co-promoter: Prof. Dr. Philip Van Damme  
Prof. Dr. Robin Lemmens  
Chair: Prof. Rik Lories  
Secretary: Sophie Collart  
Jury members Prof. Dr. Albert Ludolph  
Prof. Dr. Serge Muyldermans  
Prof. Patrik Verstreken  
Prof. Mieke Dewerchin  
Prof. Matthew Holt

Dissertation presented in partial fulfilment of the requirements for the degree of Doctor in Biomedical Sciences

January 2016



# Dankwoord

Een doctoraat is als een lange bergwandeling: met veel hindernissen, veel dieptepunten, maar ook veel hoogtepunten en veel voldoening als het einde is bereikt. Het is een heel leerrijke ervaring geworden, zowel op professioneel als op persoonlijk vlak. Het is me echter enkel gelukt door de vele steun die ik heb gekregen, maar ook door het plezier dat ik vond en de energie die ik kreeg tijdens de leuke momentjes die we hebben gedeeld. Ik wil dan ook graag een aantal mensen bedanken.

Eerst en vooral wil ik mijn promotor Professor Wim Robberecht van harte danken om me de kans te geven deel te maken van zijn onderzoeksteam. Ik apprecieerde heel erg uw opmerkingen en suggesties en alle discussies die me de data terug vanuit een ander perspectief deden bekijken. U slaagde er ook steeds in om me aan te moedigen als ik het even niet meer zag zitten en om mijn enthousiasme te temperen als ik wat te veel in de wolken was met mijn data. Ik heb ook heel veel geleerd van uw manier om alles uit te leggen, zowel mondeling als geschreven. Ook wil ik u bedanken voor uw extra begrip en geduld tijdens mijn eerste doctoraatsjaar.

Mijn co-promotoren Professor Robin Lemmens en Professor Philip Van Damme wil ik graag bedanken voor de dagelijkse begeleiding. U stond altijd klaar als ik iets wilde bespreken of om mij goede raad te geven. Robin, heel erg bedankt voor alle hulp tijdens de laatste eindsprint. Ik apprecieerde het heel erg dat u steeds tijd voor me vrij maakte, zelfs tijdens heel hectische periodes. Philip, dank u voor de leuke discussies, die terug ander licht op de resultaten konden werpen. Uw rustige, kalme uitstraling tijdens presentaties op internationale conferenties en tijdens drukke momenten zijn bewonderenswaardig. Ook wil ik graag Professor Ludo Van den Bosch bedanken om me steeds verder te helpen. Uw deur stond steeds voor mij open voor zowel de wetenschappelijke als de praktische zaken.

Special thanks to the members of my jury, Professor Albert Ludolph, Professor Serge Muyldermans, Professor Patrik Verstreken, Professor Mieke Dewerchin and Professor Matthew Holt for their thorough and critical reading of my thesis manuscript. Your comments and suggestions really improved the quality of my thesis.

I am also very grateful of all the very nice collaborations. Professor Ann Van Schepdael, bedankt voor de prettige samenwerking i.v.m. de HPLC-analyse van C1. Bart, dank je wel om me op de goede weg te zetten met mijn Nanobody screen en voor de leuke samenwerking betreffende de SPR-data. Ik heb het altijd heel erg geapprecieerd dat je alles heel grondig hebt uitgelegd en dat ik altijd bij je terecht kon voor extra uitleg. Jurgen and Reza, thank you for the nice collaboration concerning the generation, production and purification of EphA4 and my Nanobodies. Annerieke, om me aan heel veel verschillende mensen voor te stellen.

Lucia, you really helped me a lot with the Alphascreen and all my biochemical questions. Sarah V. en Hermien, om me met vele kleine praktische zaken verder te helpen. Maarten, om me wegwijs te maken in de nummering van de Nanobodies en om me te helpen bij het solliciteren. Michal, Mykhailo and Chen, thank you for all the help with astrocyte isolation and astrocyte problems. Thomas, our nice talks in the animal lab have lead to a nice and successful collaboration.

Ik wil graag al mijn collega's bedanken voor de leuke tijd in het lab. Bedankt voor de steun in moeilijke momenten, de oppeppende woorden als de resultaten tegenvielen, maar ook voor al het gelach. Ook wil ik nog eens iedereen bedanken die me heeft geholpen bij de laatste eindsprint. Zonder al die hulplijnen zou het nog veel moeilijker geweest zijn.

De "oude garde" van het labo die me wegwijs heeft gemaakt in het labo, maar die ondertussen een andere weg ingeslagen hebben: Annelies V., Bea, Cindy, Hoai, Veerle C., Veerle G., Nicky, Sara, Ines, Thomas, Kim, Sarah H., Sarah D., Constantin, Louis en Elke K., Annelies V., om me wegwijs te maken in het efrineproject. Je hebt een fantastisch project opgestart en ik vond het heel leuk om dit verder te kunnen uitwerken. Thomas, jouw tips i.v.m. kleuringen en microscopie hebben me heel goed geholpen.

En natuurlijk wil ik ook de huidige mensen in het labo bedanken, beginnende bij het fantastische efrine-team. Mieke, ik vond het altijd heel leuk om samen te werken: je precieze manier van werken, je neiging alles dubbel te "sjekken", de prettige samenwerking om de Alphascreen te optimaliseren en de leuke babbels over Sieme en Lore. Je kon het presteren om steeds afwezig te zijn bij mijn presentaties of stiekem naar de keuken te vluchten. Lindsay, ik vond het heel leuk om je wegwijs te maken in het labo. Het was altijd heel prettig om samen te werken, toch totdat je in afzondering ging in de kelder. En ik denk dat ik na mijn doctoraatsverdediging die langverwachte pisco sour nu wel verdiend heb. Laura R., it is really nice that you are always prepared to help people and that you see the best in them. It was nice to work together and I'm confident you will finish my project in the best way possible. Antina, hoewel je in het begin wat problemen had om me te begrijpen, vond ik het altijd heel gemakkelijk om met je te praten. Het was leuk om samen een aantal projectjes op te starten en van onze uitstapjes samen kon ik heel erg genieten. Hoewel je met zo'n grote bos blonde krullen wel direct in het oog springt, wat ook de mensen van Sporza niet was ontgaan.

Nathalie, het was leuk om samen aan ons doctoraat te starten en samen heel wat watertjes te doorzwemmen. Je stond altijd klaar om iedereen te helpen en er kwam dikwijls heel wat schatergelach uit het vliegenlabo. Wendy, bedankt voor de fantastische celculturen en voor je luisterend oor. Ook van onze shoppinguitjes heb ik heel erg genoten. Veronick, ik vond het heel verrijkend om mijn laatste onbegrijpbare resultaten eens te bespreken met mijn achterbuur. Gelukkig waren er de wekelijkse squashpartijtjes, een ideale manier om de frustraties kwijt te geraken. Ik heb ook enorm genoten van onze tripjes samen, van Portugal tot Keulen. Caroline, bedankt voor de leuke gesprekken en pittige wetenschappelijke

discussies. Je hebt me toch dikwijls een stapje verder geholpen toen ik vast zat. En ik wist ook altijd waar ik moest zijn wanneer mijn schaar en Pritt weer eens zoek waren geraakt. Wanda, jouw vrolijkheid was altijd zo aanstekelijk, zeker als er Natalia-liedjes op de radio werden gedraaid. Spijtig dat ik je pas naar het einde toe beter leerde kennen. Begga en Séraphina, zonder jullie hulp was het kweken en onderhouden van mijn muizenkolonies nooit zo gemakkelijk geweest. Nicole, bedankt om alle problemen in het lab zo snel op te lossen en voor alle hulp bij de moleculaire biologie. Lien, bedankt voor alle praktische hulp en om toch steeds een gaatje te vinden in de agenda's, zelfs als die meestal bomvol zaten. Elke B., bedankt om me steeds verder te helpen als ik de bomen niet meer door het bos zag. Cathy, thank you for helping me with Nanobody and writing issues. Steven, buurman, jouw introductie van het to-to-to-to-tomatenplukkerslied in het labo blijft legendarisch. Lawrence, ontploffende thermoskannen, scheefgedraaide kranen, maar ook een gouden hart blijven toch jouw kenmerken. André, nobody will ever be able to perform the gangnam style like you did. Eveliina, you are the best dishwasher user ever. Raheem, Lore, Laura F. and Matthieu, it's a pity I only got to know you very late. Lore and Laura, let's meet in Ghent. Matthieu, bedankt voor alle hulp bij de eindsprint. Jolien, door al je goede raad weet ik nu hoe ik een huis moet bouwen. Sander, Tom, Rik, Bart, Benjamin and Tom, bedankt voor de praktische hulp in het lab en voor de leuke feestjes. Wenting and Annelies N., the finish is also near for both of you. Good luck! Emiel, Mathias, Annet, Kristof and Joni, veel succes met jullie thesis en verdere carrière.

Maar dit doctoraat was niet mogelijk zonder de steun van mijn familie en vrienden. Lien, samen hebben we al veel eindes en nieuwe beginnen meegemaakt. Ik ben blij dat je er ook vandaag bij bent. Greet en Lot, jullie stonden er toen ik het moeilijk had en zijn er nu bij deze nieuwe start. Eefje, Stien en Sarah, ik ben blij jullie tijdens deze periode te leren kennen. Hoewel we elkaar niet zo dikwijls zien, weet ik dat jullie er altijd zijn. Elisa and Gian Luca, it's really nice of both of you to come all the way from Italy for my defence. We had a great time together in Stockholm and I hope we'll keep in touch.

Jonas, hoewel je er niet meer bent, weet ik dat je trots op me zou zijn. Mama en papa, zonder jullie steun zou ik nu niet staan waar ik nu sta. Lieve zus, samen staan we sterk! Dank je om er altijd voor me te zijn. Jille, ik ben blij dat je deel uit maakt van onze familie. Mijn lieve, kleine vriend: mijn metekindje Sieme om met je enthousiasme en dikke knuffels steeds een grote glimlach op mijn gezicht te toveren. Mama, papa, Ine, Jille en de twee kleine wondertjes Sieme en Mathis: het doet zo veel deugd deel uit te maken van zo'n lieve, warme, hechte familie. Dank je wel!

Lies





# Table of contents

<b>Dankwoord</b>	<b>1</b>
<b>Table of contents</b>	<b>5</b>
<b>List of abbreviations</b>	<b>9</b>
<b>Introduction</b>	<b>13</b>
<b>1. Amyotrophic Lateral Sclerosis</b>	<b>13</b>
1.1 ALS genetics	13
1.1.1 Causative genes	14
1.1.2 Modifying genes	15
1.2 Pathogenesis	16
1.2.1 Disrupted RNA and protein homeostasis	16
1.2.2 Glutamate-mediated excitotoxicity	17
1.2.3 Selective vulnerability of motor neurons	17
1.2.4 ALS is a non-cell autonomous disease	20
1.2.5 Mitochondrial dysfunction	21
1.2.6 Impaired axonal transport	22
<b>2 The ephrin axonal repellent system</b>	<b>23</b>
2.1 Eph receptor structure	23
2.2 Ephrin ligand structure	26
2.3 Eph/ephrin clustering	26
2.4 Signaling	27
2.5 Regulation of Eph/ephrin signaling	28
2.6 Epha4	29
2.6.1 CNS trauma	29
2.6.2 Stroke	30
2.6.3 Multiple Sclerosis (MS)	30
2.6.4 ALS	31
2.6.5 Alzheimer's Disease (AD)	31
2.6.6 Parkinson's Disease (PD) and Huntington's Disease (HD)	32
2.6.7 Conclusion	32

<b>Aims</b>	<b>33</b>
<b>Part I: Exploring the mechanism of the beneficial effect of EphA4 inhibition in ALS</b>	<b>35</b>
<b>Introduction</b>	<b>35</b>
<b>Chapter 1. Epha4 as a vulnerability factor in motor neurons</b>	<b>37</b>
1.1 Introduction	37
1.2 Results	38
1.2.1 Vulnerable motor neurons in ALS have higher expression of Epha4	38
1.2.2 Epha4 is a determinant of the re-innervating capacity of motor neurons	40
1.3 Discussion	41
<b>Chapter 2. Exploring the Epha4 signaling direction</b>	<b>43</b>
2.1 Introduction	43
2.2 Results	45
2.2.1 Epha4 expression and phosphorylation	45
2.2.2 Abolishing Epha4 forward signaling in the SOD1 <sup>G93A</sup> mouse model	47
2.2.3 Abolishing Epha4 forward signaling negatively affects the re-innervating capacity of motor neurons	48
2.3 Discussion	50
<b>Chapter 3. The role of ephrin ligands in ALS</b>	<b>53</b>
3.1 Introduction	53
3.2 Results	54
3.2.1 Expression profile of ephrin ligands in the SOD1 <sup>G93A</sup> mouse	54
3.2.2 Expression profile of ephrinb2	56
3.2.3 Effect of ephrinb2 on ALS in the SOD1 <sup>G93A</sup> mouse model	63
3.2.4 Effect of selective deletion of ephrinb2 from astrocytes in the SOD1 <sup>G93A</sup> mouse model	64
3.3 Discussion	70
<b>Materials and methods</b>	<b>73</b>
1. Animal housing, breeding, evaluation and experiments	73
2. Histopathology	74
3. Laser capture microdissection	75
4. Molecular Biology	76
5. Stainings	78

<b>Part 2. Exploration of the therapeutic potential of EphA4 inhibitors</b>	<b>81</b>
<b>Introduction</b>	<b>81</b>
<b>Chapter 4. Exploring the use of existing EphA4 inhibitors in ALS</b>	<b>83</b>
4.1 Introduction	83
4.2 Results	84
4.3 Discussion	86
<b>Chapter 5. Identification and characterization of Nanobodies specific for the Ephrin A4 receptor</b>	<b>87</b>
5.1 Introduction	87
5.2 Results	89
5.2.1 Generation of anti-EphA4 LBD Nbs	89
5.2.2 Cloning and expression of the anti-EphA4 LBD Nbs	90
5.2.3 Analysis of EphA4 binding	91
5.2.3 Cross-reactivity with other Eph receptors	94
5.2.4 Competition with ephrin ligands for the interaction with EphA4	96
5.2.5 Inhibition of ephrin-induced EphA4 activation	97
5.3 Discussion	99
<b>Material and Methods</b>	<b>101</b>
1. Pharmacokinetics compound 1	101
2. Nanobody screening	101
<b>General discussion</b>	<b>107</b>
<b>Summary</b>	<b>113</b>
<b>Samenvatting</b>	<b>115</b>
<b>References</b>	<b>117</b>
<b>List of publications</b>	<b>133</b>
<b>Presentations at international symposia</b>	<b>135</b>



## List of abbreviations

aCSF	artificial Cerebrospinal Fluid
A $\beta$	Amyloid beta
AD	Alzheimer's Disease
ADAM	A Disintegrin and Metalloproteinase
Aldh111	10-formyltetrahydrofolate dehydrogenase
ALS	Amyotrophic Lateral Sclerosis
AMPA	$\alpha$ -amino-3-hydroxy-5-methyl-4-isoxazolepropionic acid
APP	Amyloid Precursor Protein
ATP	Adenosine Triphosphate
BBB	Blood Brain Barrier
BSCB	Blood Spinal Cord Barrier
C1	a 2-hydroxy-4(2,5-dimethylpyrrol-1-yl)benzoic acid derivative
cc1	Mouse Monoclonal APC antibody
Cd11b	Cluster of Differentiation Molecule 11B
CDR	Complementarity Determining Region
CNS	Central Nervous System
CRD	Cystein-rich Domain
CSF	Cerebrospinal Fluid
CSK	C-terminal Src kinase
CX3CR1	CX3C Chemokine Receptor 1
Cx	Cortex
Cx30	Connexin 30
Cx43	Connexin 43
DAB	3,3' diaminobenzidine tetrahydrochloride
DAPI	4',6-diamidino-2-phenylindole
DPP6	dipeptidyl-peptidase 6
DPR	dipeptide repeat proteins
EA	enzyme activator
EAE	Experimental Autoimmune Encephalomyelitis
EAAT2	Excitatory Amino-Acid Transporter 2 (=GLT1)
Efn	Ephrin
EGF	Epidermal Growth Factor
eGFP	enhanced Green Fluorescent Protein
EICD	EphA4 intracellular domain
ELP3	Elongator acetyltransferase complex subunit 3
EMG	Electromyogram
Eph	Ephrin receptor
Epha4	mouse ephrin a4 receptor

EphA4	human ephrin A4 receptor
ephrinb2	mouse ephrin b2 ligand
ephrinB2	human ephrin B2 ligand
ER	Endoplasmic Reticulum
ES	End Stage
eYFP	enhanced Yellow Fluorescent Protein
FALS	Familial ALS
Fc	Fragment crystallizable
FF	Fast-twitch fatigable
FN	Fibronectin
FR	Fast-twitch fatigue-resistant
FTD	Frontotemporal Dementia
FUS	Fused in Sarcoma/translocated in liposarcoma
GABA	gamma-aminobutyric acid
GAPDH	Glyceraldehyde 3-phosphate dehydrogenase
GFAP	Glial Fibrillary Acidic Protein
GFP	Green Fluorescent Protein
GPI	Glycosylphosphatidyl Inositol
GLAST	Glutamate Aspartate Transporter
GLT1	Glutamate Transporter 1 (=EAAT2)
GluR2	Glutamate receptor 2 subunit
GWAS	Genome-wide association studies
HD	Huntington's Disease
Hipp	Hippocampus
HPLC-UV	High Performance Liquid Chromatography (HPLC) with UV detection
HRP	Horse Radish Peroxidase
Hsp70	Heat shock protein 70
ICD	Intracellular domain
IMAC	immobilized metal-ion affinity chromatography
IP	intraperitoneal
$k_a$	association rate
$k_d$	dissociation rate
$K_D$	dissociation constant
LBD	Ligand -binding Domain
LCM	Laser Capture Microdissection
LOD	Limit of detection
LOQ	Limit of quantification
LPS	Lipopolysaccharide
LTP	Long-term Potentiation
LTD	Long-term Depression
MBP	Myelin Basic Protein

MCT1	Monocarboxylate transporter 1
MMP	Matrix Metalloproteinase
MS	Multiple Sclerosis
Nb	Nanobody
ND	Not determined
NeuN	Neuronal-specific nuclear protein
NG2	Neural/glial antigen 2
NMDA	N-methyl-D-aspartate
NSC	Neural Stem Cells
Ntg	Nontransgenic
OPC	Oligodendrocyte precursor cell
OR	Odds ratio
P60	60 days after birth
p75NTR	P75 neurotrophin receptor
PBS	Phosphate Buffered Saline
PD	Parkinson's Disease
PDZ	post synaptic density protein 95 (PSD-95) <i>Drosophila</i> discs-large imaginal disc protein (DlgA) ZO-1 tight junction
PEG	polyethyleenglycol
PFA	paraformaldehyde
PTB	Phosphotyrosine Binding
PTP	Phosphotyrosine phosphatases
qPCR	quantitative Polymerase Chain Reaction
RAN	repeat-associated non-ATG
RBD	Receptor-binding Domain
Ret	Rearranged during transfection
ROS	Reactive oxygen species
RU	Response Units
RT	Room Temperature
RT-PCR	Real-Time Polymerase Chain Reaction
rtk2	receptor tyrosine kinase 2
S	slow-twitch fatigue-resistant
SALS	Sporadic ALS
SAM	Sterile alpha Motif
SC	Spinal Cord
SCI	Spinal Cord Injury
SD	Standard Deviation
SH2	Src Homology 2
Smi32	Sternberger monoclonal-incorporated antibody 32
SOD1	Superoxide Dismutase 1
SOD1 <sup>G93A</sup>	SOD1 with substitution of a Glycine by an Alanine at position 93



SOD1 <sup>WT</sup>	Wild Type SOD1
SPE	Solid Phase Extraction
SPR	Surface Plasmon Resonance
TBI	Traumatic Brain Injury
TDP43	Tar DNA binding protein 43
TrkB	Tropomyosin receptor kinase B
Tx	Tamoxifen
UNC13A	unc-13 homolog A
UPR	Unfolded Protein Response
VEGF	Vascular Endothelial Growth Factor
VEGFR	VEGF Receptor
VH	Variable domain of heavy chain
VHH	Variable domain of heavy chain of heavy-chain antibodies
VL	Variable domain of light chain
WT	Wild Type

# Introduction

## 1. Amyotrophic Lateral Sclerosis

Neurodegenerative disorders such as Alzheimer's disease, Parkinson's disease and Amyotrophic Lateral Sclerosis (ALS) represent a major challenge for the medical world and for society. Even though ALS is a rather rare disease with an incidence of 1-2 in 100.000, the life time chance to develop this disease is 1/400 – 1/700 <sup>1</sup>.

ALS is a very dramatic disorder due to its progressive character, the short survival of the patient and the enormous impact on his/her quality of life and that of his/her caretaker. The disease typically affects adults in mid-life and is usually fatal three to five years after the first symptoms appear <sup>2-3</sup>. It is characterized by the degeneration of both the upper motor neurons in the motor cortex, and the lower motor neurons in the brain stem and the spinal cord <sup>1</sup>. Degeneration of the upper motor neurons leads to spasticity and hyperreflexia, whereas degeneration of the lower motor neurons leads to muscle atrophy and eventually paralysis. Up to now no curative treatment is available, only riluzole modestly extends lifespan with an average of 2-3 months <sup>4-5</sup>.

ALS forms a continuum with Frontotemporal Dementia (FTD), with pure ALS and pure FTD on the opposites of the spectrum <sup>2</sup>. FTD is characterized by neuronal loss in the frontal and anterior temporal lobes <sup>6</sup>. The most common symptoms are behavior changes, loss of fluent speech and loss of the knowledge of words. In the ALS-FTD spectrum many patients have features of both. A clinical overlap between both diseases has already been known for several decades. The overlap was recently confirmed at the molecular level and underscored with neuropathological and genetic studies.

### 1.1 ALS genetics

ALS is hereditary in 10% of patients (familial ALS, FALS), while 90% of patients do not report any familial occurrence (sporadic ALS, SALS). Most mutations identified so far are inherited in an autosomal dominant way, although autosomal recessive and X-linked inheritance has been observed. The most common genes in which mutations have been found are *SOD1*, *FUS*, *TARDBP* and *C9orf72* <sup>7</sup>.

### 1.1.1 Causative genes

Mutations in the *superoxide dismutase 1* (SOD1) gene were the first that have been identified in ALS<sup>8</sup>. SOD1 protects the cell against oxidative stress by converting superoxide radicals into molecular oxygen and hydrogen peroxide. The identification of mutations in SOD1 led to the development of several mutant SOD1 animal models. The mutant SOD1<sup>G93A</sup> mouse model, overexpressing the human SOD1 gene with a substitution of Glycine by Alanine at position 93, is one of the most frequently used models in ALS research<sup>9</sup>. The mice are asymptomatic until 60 days of age, a time point at which microgliosis can be observed, followed by astrogliosis around 80 days. Disease onset occurs around day 90-100 and is characterized by massive loss of motor neurons. At this symptomatic stage, initial symptoms such as hind limb weakness and tremulous movements can be observed. At late-symptomatic stage (around 140 days) major symptoms such as progressive atrophy of hind limb muscles and paralysis can be observed. Around day 150-160 the mice die preceded by disability of gait, eating and drinking<sup>9-10</sup>. Overall, mice overexpressing mutant human SOD1 show similar pathological hallmarks (motor neuron degeneration, inflammation, gliosis and paralysis) as seen in ALS patients, while control mice overexpressing wild type human SOD1 only yield a mild phenotype late in life<sup>9,11</sup>. Furthermore, SOD1 knockout mice do not show any sign of motor neuron degeneration, implying a toxic gain of function for mutant SOD1<sup>12</sup>. Overexpression of mutant human SOD1 in zebrafish embryos induces an axonal phenotype, characterized by a reduction of the axonal length and more aberrantly branched axons<sup>13</sup>.

The mutant SOD1 mouse is the best ALS model there currently is. It is the most studied animal model so far and is widely used in genetic and pharmacological studies worldwide. Alike every model, it has its drawbacks, which should be kept in mind when interpreting the results obtained with it. This animal will be used in the experiments described later.

In 2008, mutations in *TAR DNA binding protein 43* (TDP43, encoded by *TARDBP*) and *Fused in Sarcoma/translocated in liposarcoma* (FUS/TLS) were identified. TDP43 and FUS are both RNA binding proteins with functions in transcription, RNA splicing and RNA transport<sup>14-15</sup>. Interestingly, aggregates containing TDP43 and FUS are found in patients with SALS<sup>16-17</sup>. Several animal models have been generated to study the function of TDP43 and FUS. However, the use of these models to study ALS needs to be awaited. Homozygous deletion of *TARDBP* or *FUS* in mice is embryonically lethal, whereas overexpression of the wild type or the mutant protein results in a very aggressive phenotype<sup>18</sup>. This indicates that both depletion as well as overexpression of these proteins is detrimental and highlights the necessity of tight regulated TDP43 and FUS expression<sup>19</sup>.

Recently, hexanucleotide repeat expansions have been discovered in the first intron of the *C9orf72* gene<sup>20-21</sup>. The identification of this expansion mutation explains approximately 50%

of the familial ALS patients in the Belgian population <sup>22</sup>. Furthermore it also accounts for more than 5% of apparently sporadic ALS cases. The biological function of the C9Orf72 protein is still unknown, but several mechanisms of toxicity of the expansion mutation have been suggested. One is haploinsufficiency as decreased expression of different C9Orf72 transcripts has been reported in C9FTD/ALS cases <sup>23</sup>. A second is direct RNA toxicity, as the hexanucleotide repeat RNA can form highly stable RNA G-quadruplexes, which may sequester RNA-binding proteins leading to disruption of RNA metabolism <sup>24-25</sup>. A third possible mechanism is the production of dipeptide repeat (DPR) proteins from the hexanucleotide repeat through repeat-associated non-ATG (RAN) protein translation <sup>26</sup>. The relative contribution of each of these possible mechanisms in the disease pathogenesis of C9-related ALS is under investigation.

Many other genes have been identified in ALS, although most of these mutations have only been detected in a limited number of cases or within one family <sup>27</sup>.

### 1.1.2 Modifying genes

Age at disease onset, disease duration and the clinical manifestation of ALS (bulbar onset versus spinal onset, proximal versus distal weakness) can vary greatly between patients <sup>2</sup>. Even within one family carrying the same mutation, obvious variability is present <sup>28</sup>. This indicates that ALS is a multifactorial disease influenced by modifying genes and/or environmental factors. Of the latter, none has been identified convincingly <sup>29</sup>.

Generally spoken, genetic modifiers can be identified in two ways. Genome-wide association studies (GWAS) have identified several disease modifying genes, but not all of results have been replicated. The modifying genes that have been confirmed in independent GWAS studies are *ELP3* (*elongator acetyltransferase complex subunit 3*), *UNC13A* (*unc-13 homolog A*) and *DPP6* (*dipeptidyl-peptidase 6*) <sup>30-31</sup>. A second way to identify modifiers is through the screening of small animal models for ALS, such as *Drosophila*, yeast and zebrafish. We here mention only two results that have been connected to human disease.

An unbiased genetic screen in the TDP43 yeast model revealed that overexpression of ataxin2 aggravates the phenotype <sup>32</sup>. In *Drosophila*, upregulation of ataxin2 decreased survival of TDP43 flies. In humans, intermediate-length polyglutamine expansions in the ataxin2 gene are associated with an increased risk to develop ALS, suggesting the importance of this gene in the pathogenesis of ALS <sup>33-34</sup>.

In our laboratory a morpholino-based genetic screen was performed in the mutant-SOD1 zebrafish model <sup>35</sup>. Knockdown of the ephrin receptor A4 (EphA4) rescued the axonal phenotype, a finding confirmed in the ALS mouse model <sup>35</sup>. In humans, EphA4 expression is inversely correlated with disease onset and disease survival in sporadic ALS patients <sup>35</sup>.

These results show that the screening of small animal models allows to identify factors that also matter for human disease. It is important to identify such factors, as they may be targets for intervention, in particular in those forms of the disease in which we do not know the cause of disease (yet).

## **1.2 Pathogenesis**

Although many hypotheses have been generated, it is still not known what the exact mechanism of the selective motor neuron degeneration in ALS is. It is generally accepted that it is probably a combination of different ones<sup>19</sup>. We here summarize the main hypotheses.

### **1.2.1 Disrupted RNA and protein homeostasis**

In ALS, both RNA homeostasis and protein homeostasis are disrupted<sup>36</sup>. TDP43 and FUS, both RNA-binding proteins involved in multiple RNA processing steps, are major components present in pathological inclusions in ALS patients. The formation of TDP43 and FUS aggregates has been related to the biology of stress granules. In normal conditions the formation of such granules is a reversible process<sup>37</sup>. In ALS, these granules apparently do not resolve, but form the seeds of aggregation, acting as a sink for proteins, among which RNA binding proteins<sup>38</sup>. TDP43 and FUS contain low complexity domains that make them prone to aggregation and can act to recruit other proteins<sup>39-42</sup>. These proteins are thus prevented from exerting their normal function and might sequester other essential cellular components, which may contribute to cellular dysfunction. This suggests that alterations of RNA metabolism are involved in the pathogenesis of ALS<sup>36</sup>.

SOD1 on the other hand, is also present in aggregates, but is not involved in stress granule formation. To explain its toxicity, it has been suggested that the mutant SOD1 is misfolded just as is the demetallated wild type SOD1<sup>43</sup>, is aggregation-prone, and forms multimers and eventually aggregates.

It is thought that these protein multimers overload the normal protein degradation systems (the proteasome and the autophagy-lysosomal pathway), which normally protect the cell from dysfunctional and degraded proteins and thus from protein aggregation. This dysproteostasis leads to further multimerisation and finally protein aggregation. The unfolded protein response is an attempt to restore homeostasis, but when unsuccessful, it may contribute to the triggering of cell death. The presence of ubiquitin and p62 in aggregates and the upregulation of UPR (Unfolded Protein Response) genes in vulnerable motor neurons are indicative for such sequence of events<sup>44-45</sup>.

### 1.2.2 Glutamate-mediated excitotoxicity

Motor neurons in the spinal cord receive glutamatergic afferents. Glutamate receptors are subdivided in ionotropic receptors (ligand-gated cation channels) and metabotropic receptors (linked to G-protein coupled receptors). The ionotropic receptors can be further divided into three classes, based upon their pharmacological properties: AMPA ( $\alpha$ -amino-hydroxy-5-methyl-4-isoxazole propionic acid), NMDA (N-methyl-D-aspartate) and kainate receptors<sup>46-47</sup>. AMPA receptors mediate fast excitatory transmission and NMDA receptors mediate the late component of excitatory transmission. The excitatory transmission is terminated by glutamate removal from the synaptic cleft by glutamate transporter proteins in neurons and astrocytes. The most important astrocytic glutamate transporter is Excitatory Amino-Acid Transporter 2 (EAAT2/GLT1)<sup>48-49</sup>.

Stimulation of ionotropic glutamate receptors induces calcium entry. The intracellular calcium levels are tightly controlled by calcium-binding proteins, mitochondria and the endoplasmic reticulum (ER)<sup>50-51</sup>. When the calcium storage capacity is saturated, intracellular calcium levels rise, which can induce neuronal death<sup>52</sup>. Motor neurons are very sensitive to this phenomenon, called glutamate-mediated excitotoxicity because of their low calcium buffering capacity and because of the high calcium permeability of their AMPA receptors. The latter is explained by the fact that motor neurons express little glutamate receptor 2 subunit (GluR2), which renders the AMPA receptors less permeable to calcium<sup>53</sup>. In addition to this, EAAT2 expression is decreased in ALS, which results in increased synaptic glutamate concentrations<sup>54-58</sup>. The only drug that has been shown to affect disease course in ALS patients, is riluzole. It is thought, but unproven, that this drug works through its glutamate receptor blocking activity<sup>5</sup>.

### 1.2.3 Selective vulnerability of motor neurons

It is unclear why motor neurons are selectively affected in ALS, but some mechanisms that may at least partially explain their vulnerability have been suggested. Motor neurons are very sensitive to excitotoxicity due to their low expression of calcium buffering proteins and of the GluR2 subunit of AMPA receptors, as explained above<sup>59-60</sup>. Furthermore, motor neurons are very large cells with a somatic diameter of up to 100  $\mu\text{m}$  and axons up to one meter long. The high energy demand and metabolic rate of such large cells, and the high level of mitochondrial activity with the possible generation of oxidative stress that is associated with it, has been suggested to be a vulnerability factor<sup>61</sup>. A third vulnerability factor is the high threshold for the induction of the stress response, including the activation of heat shock protein 70 (Hsp70), compared to other types of neurons<sup>62</sup>. Heat shock proteins protect neuronal cells against stress such as oxidative stress and excitotoxicity<sup>62-65</sup>. Overexpression of Hsp70 in motor neurons delayed mutant SOD1 mediated formation of aggregates and cell toxicity<sup>66</sup>.

Interestingly, not all motor neurons are equally vulnerable. There appear to be subpopulations of neurons that are less vulnerable. Oculomotor neurons (generating the oculomotor, trochlear and abducens nerve controlling eye movement) and neurons in Onuf's nucleus (controlling sphincter muscles) are more resistant to neurodegeneration as they are preserved until the very late stages of disease both in ALS patients as in the SOD1 mouse model<sup>67-70</sup>.

Transcription profile analysis of resistant and vulnerable motor neurons revealed differential expression of genes involved in synaptic transmission, ubiquitin-mediated protein degradation, mitochondrial function, transcriptional regulation, immune system functions and the extracellular matrix, both in rodents as in humans<sup>71</sup>. The resistant motor neurons show higher expression of the protective AMPA receptor subunit GluR2 and gamma-aminobutyric acid (GABA) receptor subunit GABA<sub>A</sub>R $\alpha$ 1, both involved in synaptic transmission<sup>72</sup>. Those motor neurons also have increased expression of genes involved in mitochondrial oxidative phosphorylation, leading to higher calcium buffering capacity<sup>73</sup>. The vulnerable motor neurons show higher expression of Matrix metalloproteinase 9 (MMP9)<sup>71</sup>. In wild type mice MMP9 is only expressed by the vulnerable motor neurons and inhibition of its activity in the mutant SOD1 mice delayed muscle denervation<sup>74</sup>. Expression of MMP9 in the presence of mutant SOD1 enhanced the activation of the UPR thereby triggering axonal dieback.

Motor neurons with different physiological characteristics are also differentially vulnerable in ALS. The alpha motor neurons can be subdivided into three different groups based on the contractile properties of their target muscle fibers: fast-twitch fatigable (FF), fast-twitch fatigue-resistant (FR), and slow-twitch fatigue-resistant (S).

The S motor neurons are small, highly active, and have a low activation threshold. They innervate slow contracting muscle fibers which are dependent on oxidative metabolism. These fibers are very resistant to fatigue because of their rich content of mitochondria and their rich capillary blood supply. FF motor neurons are large, and have a higher activation threshold. They innervate fast contracting muscle fibers, which generate more force. These fibers rely on glycolysis for energy generation. The FR motor neurons are intermediate in size and innervate FR fibers, which are intermediate between the S and FF fibers.

In mutant SOD1 mice, the FF motor neurons are the first to degenerate and are almost all lost by P50<sup>75</sup>. Also in ALS patients the FF motor neurons are the ones affected earliest<sup>76</sup>. The motor end plates, from which the degenerating FF axons have retracted, will subsequently be innervated by FR motor neuron axons. This leads to a switch in muscle fiber phenotype from FF to FR<sup>77</sup>. Later in the disease process, the FR-motor neurons become involved, cannot maintain their neuromuscular junctions anymore and will retract their axons and degenerate. The S motor neurons will compensate for the degeneration of these axons by re-innervating motor end plates left by degenerating FF and FR motor neurons<sup>75</sup>.

The axons of S motor neurons are involved in the terminal stages of the disease only. Moreover, electromyogram (EMG) patterns show similar cycles of denervation and re-innervation in ALS patients as shown in the mutant SOD1 mouse <sup>78</sup>.

Interestingly, these physiologically different motor neurons also have different regeneration capacity. Mice treated with Botulinum toxin A, which blocks transmitter release, showed ultraterminal nerve sprouting <sup>79</sup>. More sprouting synapses were detected in slow muscle fibers, while the FF motor neurons failed to sprout in fast muscle fibers <sup>75</sup>.

In summary, the large FF motor neurons are more vulnerable and degenerate first in ALS, followed by degeneration of the FR, intermediate in size, and only later by the small S motor neurons (Figure 1). The exact mechanism underlying this sequence is unknown. This vulnerability correlates with the intrinsic regeneration/sprouting capacity of these types of neurons.

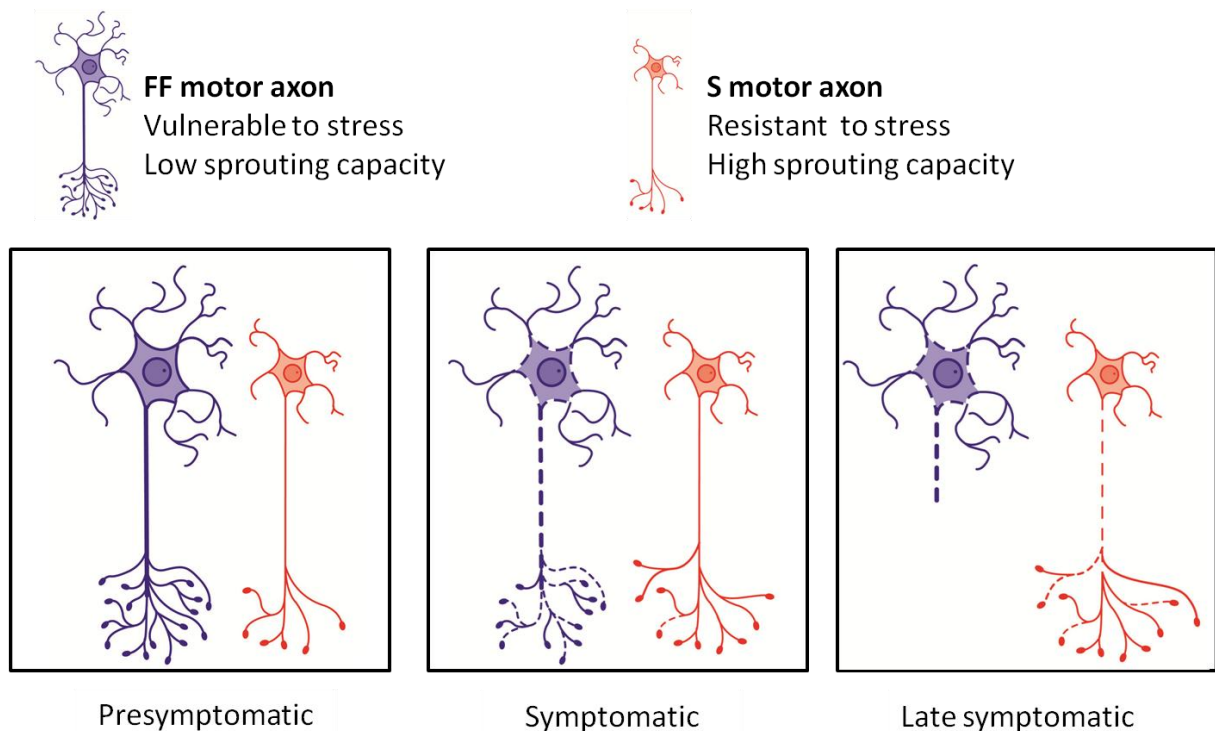


**Figure 1 Vulnerability of motor neurons in ALS.** The large FF motor neurons are more vulnerable to stress and have low sprouting capacity. These motor neurons degenerate first in ALS, followed by degeneration of the FR and S motor neurons.

However, we have to keep in mind that this look at vulnerability of motor neurons is from the perspective of ALS. As previously mentioned, ALS forms a disease spectrum with FTD with mutations in certain genes giving rise to phenotypes throughout the spectrum <sup>80</sup>. Furthermore, hexanucleotide expansions in C9Orf72 can give rise to several neurodegenerative diseases such as ALS, FTD and Huntington's Disease (HD) <sup>81</sup>. It is still unknown how mutations in one gene can give rise to different phenotypes as in FTD the



frontal and temporal lobe are affected and in ALS it are the motor neurons that degenerate. The concept of vulnerability awaits to be expanded in view of these considerations.

#### 1.2.4 ALS is a non-cell autonomous disease

Expression of mutant SOD1 in the motor neurons solely is not sufficient to cause motor neuron degeneration<sup>82-85</sup>. Indeed, a number of transgenic and transplantation experiments have demonstrated that other cells such as microglia, astrocytes and oligodendrocytes may be involved in the biology of ALS, at least in the mutant SOD1 mouse. Transgenic deletion or siRNA based downregulation of mutant SOD1 in motor neurons delayed disease onset, but did not alter disease progression<sup>86-88</sup>. Deletion of mutant SOD1 from microglia slowed disease progression as did replacement of microglia expressing mutant SOD1 by nontransgenic microglia<sup>86, 89-90</sup>. Deletion of mutant SOD1 from astrocytes slowed disease progression as well as transplantation of nontransgenic astrocyte precursor cells<sup>91-92</sup>. Deletion of mutant SOD1 from oligodendrocytes dramatically delayed disease onset and prolonged survival<sup>93</sup>. These experiments show that the presence of mutant SOD1 in motor neurons and oligodendrocytes may determine disease onset, while its presence microglia, astrocytes and oligodendrocytes accelerates disease progression.

**Astrocytes** have pivotal functions in the healthy central nervous system, but also in pathological conditions<sup>94</sup>. They can regulate synaptic transmission, maintain synaptic homeostasis and secrete components into the synapse such as lactate, glutamate and growth factors<sup>94</sup>. Astrocytes are tightly linked through gap junctions and form a network enabling them to rapidly shuttle small molecules. Astrocytes also establish the blood brain barrier (BBB) by encircling endothelial cells with so called astrocytic end-feet<sup>95</sup>. In response to Central Nervous System (CNS) injury and neurodegeneration, astrocytes become highly reactive in a process called astrogliosis<sup>96</sup>. In this process, they upregulate glial fibrillary acidic protein (GFAP), nestin and connexin 43 (Cx43), which are used as markers for activation<sup>97-98</sup>. Reactive astrocytes become hypertrophic which refers to the increased thickness of their processes<sup>94, 99</sup>. Reactive astrocytes produce pro- and anti-inflammatory molecules, indicating that they have a dual effect, similar to what is seen for microglia (see below)<sup>94</sup>. In ALS, familial and sporadic, reactive astrogliosis starts before disease onset and increases as the disease progresses. It is most pronounced in the ventral horn around the descending fibers of the corticospinal tract<sup>100-101</sup>. Astrogliosis is also present in the motor cortex<sup>101-102</sup>. Upon disease progression, there is a decrease in expression of glutamate transporter EAAT2, resulting in reduced glutamate clearance from the synaptic cleft rendering the motor neuron more vulnerable for glutamate-mediated excitotoxicity (see above)<sup>54-58</sup>. ALS reactive astrocytes produce more nitric oxide compared to controls, which can contribute to the oxidative damage in ALS<sup>103</sup>. Furthermore astrocytes containing mutant SOD1 secrete a toxic factor that selectively kills motor neurons but leaves dorsal root

ganglion neurons and interneurons unaffected, while they fail to secrete trophic factors that are secreted by control astrocytes<sup>104-108</sup>.

**Microglia** are the resident macrophages of the CNS and consequently act as the first and main form of immune defense in the CNS<sup>109-110</sup>. They are constantly scanning their environment for damaging factors and change from a surveying state into an activated state when detecting one. Microglia can exert a deleterious function (M1 microglia) or a benign function (M2 microglia) depending on the microenvironment and the pathological insult<sup>111-112</sup>. M1 microglia secrete proinflammatory molecules and upregulate oxidant molecules to clear hazards and repair damage. M2 microglia release anti-inflammatory molecules and trophic factors contributing to repair and limiting inflammation. A shift from M1 to M2 predominance is necessary for the shift from inflammation to repair<sup>110, 112-113</sup>. In the spinal cord and brain of ALS patients strong microglial activation and proliferation is present<sup>114-117</sup>. In the mutant SOD1 mouse, this microgliosis is already present before disease onset and escalates with disease progression<sup>45, 118</sup>. Microglia isolated from mutant SOD1 mice at disease onset have an M2 phenotype whereas microglia isolated at end-stage have an M1 phenotype<sup>113</sup>.

**Oligodendrocytes** are glial cells responsible for myelination in the CNS allowing rapid and efficient propagation of action potentials<sup>119</sup>. Myelination is a key process in the developing brain and continues after birth up to 30 years of age<sup>120</sup>. Remyelination also occurs during neuronal injury or degeneration<sup>119</sup>. This process is not performed by existing mature oligodendrocytes, but involves generation of new oligodendrocytes from oligodendrocyte precursor cells (OPCs). OPCs can be found throughout grey and white matter and start proliferating in response to neuronal insult<sup>121</sup>. In spinal cords of ALS mice and patients oligodendrocytes show morphological and functional changes starting before disease onset<sup>15, 122-124</sup>. Similarly to neurons, oligodendrocytes show mislocalisation of TDP43 which is a pathological hallmark of ALS<sup>125</sup>. In spinal cords of ALS patients and mutant SOD1 mice, oligodendrocyte degeneration is observed<sup>124</sup>. This degeneration of oligodendrocytes is compensated by enhanced proliferation and differentiation of OPCs. However these newly formed oligodendrocytes are dysfunctional as suggested by reduced expression of monocarboxylate transporter 1 (MCT1), a lactate transporter essential for the metabolic support of motor axons. This reduced MCT1 expression was also detected in ALS patients is also decreased in ALS mice and patients<sup>15, 124</sup>. As a result the motor neurons lose an important source of trophic support<sup>15, 93, 124</sup>.

### 1.2.5 Mitochondrial dysfunction

The large dimensions of the motor neurons implicit a high demand of energy and a high metabolic rate, which is supplied through a high level of mitochondrial activity<sup>126</sup>. During mitochondrial oxidative phosphorylation reactive oxygen species (ROS) are formed, which

have important effects on cell signaling and homeostasis <sup>127-128</sup>. ROS levels can increase dramatically upon stress which may result in an imbalance between production and decomposition of ROS. This oxidative stress can damage several cellular components such as proteins, lipids and DNA <sup>128</sup>. In sporadic ALS patients, increased oxidative stress was detected compared to control samples <sup>61</sup>. Furthermore, mitochondrial abnormalities such as vacuolization and swelling have been detected in mutant SOD1 mice, even in presymptomatic stages, as well as in ALS patients <sup>129</sup>. It is uncertain whether these changes are primary or secondary in nature, but they may contribute to cell death in ALS as mitochondria contribute to calcium buffering (see below for excitotoxicity) and the regulation of apoptosis <sup>59, 130</sup>. Mutant SOD1 mice show decreased levels of anti-apoptotic proteins and increased levels of pro-apoptotic proteins <sup>131</sup>. These mice also showed an increased mitochondrial release of cytochrome c into the cytosol initiating the caspase pathway <sup>132</sup>.

### **1.2.6 Impaired axonal transport**

Motor neurons have very long axons that connect the cell body with the synapses. Impairment of axonal transport, both forward and reverse, has been shown to be affected even before disease onset <sup>133-136</sup>. Both in ALS patients and mutant SOD1 mice abnormal accumulation of microfilaments in the cell body and in the axons has been observed <sup>137-141</sup>. Abnormalities of the location of mitochondria throughout the motor neuron have been observed as well in ALS <sup>126</sup>. Again, it is uncertain whether these changes are primary or secondary phenomena.

## 2 The ephrin axonal repellent system

The family of Eph receptors is the largest of receptor tyrosine kinases and is named after the high EphA1 expression in an Erythropoietin-Producing human Hepatocellular carcinoma cell line <sup>142</sup>. This family is subdivided in two classes (EphA and EphB) based on sequence similarity and ligand affinity <sup>143</sup>. They interact with ephrin ligands that are also subdivided into two classes: ephrinA and ephrinB ligands. In the mammalian system there are nine EphA receptors (EphA1-EphA8, EphA10) that interact with five ephrinA ligands (efnA1-efnA5) and five EphB receptors (EphB1-EphB4, EphB6) that interact with three ephrinB ligands (efnB1-efnB3). There is some interclass promiscuity as EphA4 also interacts with efnB ligands and EphB2 also interacts with efnA5 <sup>144-147</sup>. As both Eph receptors and ephrin ligands are membrane bound, cell-cell interaction is required for activation. Eph-ephrin interaction can induce both repulsion and attraction between cells as observed during cell migration and axon guidance <sup>148-149</sup>.

The ephrin system has major functions both in development and in adulthood. During embryonic development, the ephrin system plays a role in axon guidance, formation of tissue boundaries, cell migration, segmentation and angiogenesis <sup>150-153</sup>. In adulthood it plays an important role in long-term potentiation, bone mineral metabolism, T-cell and stem cell differentiation <sup>154-157</sup>. Eph-ephrin signaling has also been implicated in the pathogenesis of several diseases <sup>158-160</sup>. Both Eph receptors and ephrin ligands are expressed in cancer cells and tumor vasculature. They have been shown to affect growth, migration, invasiveness, angiogenesis and metastasis of different types of tumors. Furthermore, the ephrin system is also involved in repair after nervous system injury, neurodegenerative disorders, diabetes, viral infections and bone remodeling diseases <sup>159</sup>.

### 2.1 Eph receptor structure

The Eph receptor extracellular domain consists of an N-terminal ligand-binding domain (LBD), a cysteine-rich domain (CRD) with a Sushi domain and an Epidermal Growth Factor (EGF)-like domain and two fibronectin (FN) type III repeats (Figure 2) <sup>161</sup>. The intracellular domain consists of a juxtamembrane domain with two conserved tyrosine residues, a kinase domain, a sterile  $\alpha$ -motif (SAM) and a PDZ-binding motif (post synaptic density protein 95 (PSD-95) *Drosophila* discs-large imaginal disc protein (DlgA) ZO-1 tight junction).

The LBD determines the affinity for the ephrin ligands. It contains a hydrophobic channel and a polar docking site on the lower site of the LBD, of which the latter is only of importance for interaction with ephrinB ligands <sup>144, 146</sup>.

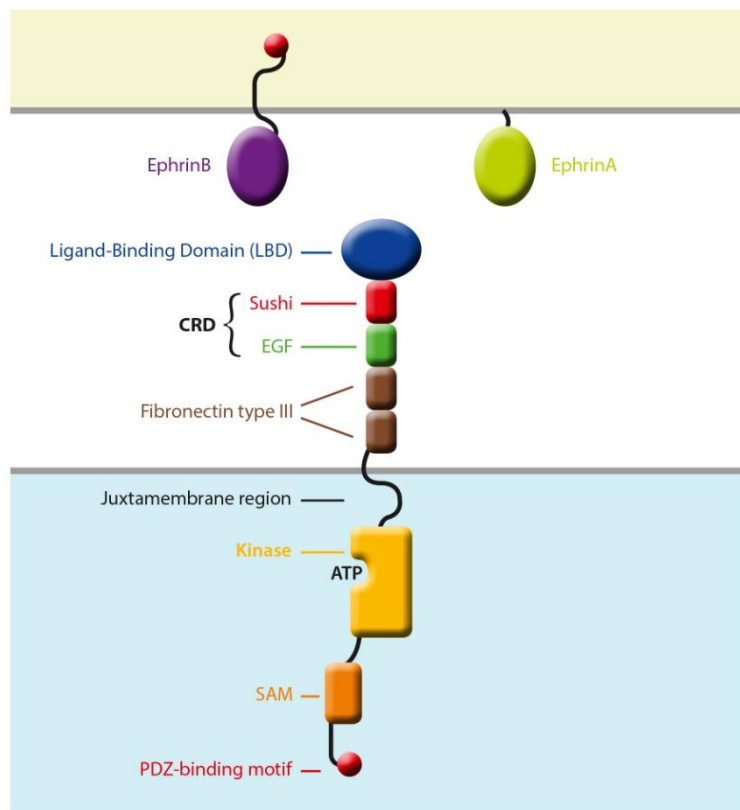


**Figure 2 Schematic representation of the Eph receptor and the ephrin ligands.** The Eph extracellular domain contains a ligand-binding domain (LBD), a cysteine-rich domain (CRD) with a Sushi domain and an Epidermal Growth Factor (EGF)-like domain and two fibronectin type III repeats. The Eph intracellular domain consists of a juxtamembrane region, a kinase domain, a Sterile alpha (SAM) domain and a PDZ-binding motif. EphrinB ligands contain cytoplasmic domain with a PDZ-binding domain at the C-terminus. EphrinA ligands are attached to the cell-membrane with a Glycosylphosphatidyl Inositol (GPI)-anchor. Figure based on several articles <sup>161-163</sup>.

In the inactive state, the juxtamembrane region tightly associates with the kinase domain (Figure 3) <sup>164</sup>. Upon ephrin binding, Eph receptors are activated, which is characterized by the phosphorylation of two tyrosine residues in the juxtamembrane region and one tyrosine residue in the kinase domain (Figure 3) <sup>165-166</sup>. Phosphorylation of the tyrosine residue in the kinase domain induces repositioning of this segment, unblocking the kinase active site. It is still unclear how ephrin binding induces Eph receptor autophosphorylation. One possibility is that ephrin binding increases the local concentration of receptors thereby promoting transphosphorylation. Another possibility is that Eph receptor clustering physically destabilizes the juxtamembrane region initiating receptor activation (Figure 3, further discussed in 2.3 Eph/ephrin clustering) <sup>167</sup>.

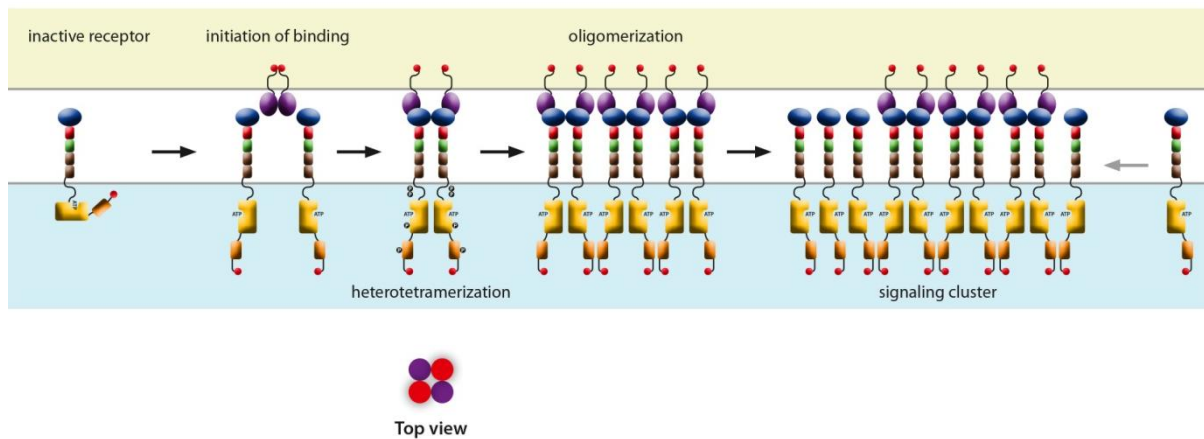


**Figure 3 Schematic representation of Eph/ephrin clustering.** In the inactive state the juxtamembrane region associates tightly with the kinase domain. Eph/ephrin clustering starts with the recognition and binding of Eph receptors and ligands on opposing cell surfaces. Heterodimers are formed, which can tetramerize into heterotetramers, thereby forming a ring structure in which each receptor interacts with two ligands and each ligand interacts with two receptors. Receptor activation includes the phosphorylation of tyrosine residues in the juxtamembrane region and in the kinase domain. These clustering interfaces allow binding of other heterotetramers resulting in an array of well-ordered Eph receptors. This clustering also results in lateral recruitment of non-ligand-bound Eph receptors. Figure based on several articles <sup>149, 161-162, 168-169</sup>.

Several of the extracellular and intracellular domains are involved in the formation of Eph/ephrin clusters, including the CRD, FNIII repeats, SAM <sup>170</sup>. The FNIII repeats are also involved in *cis*-interaction with ephrin ligands <sup>163, 171-172</sup>. The SAM domain is not essential for Eph clustering, but may stabilize the array of clustered Eph receptors <sup>161, 173-174</sup>.

After clustering, several tyrosine residues are phosphorylated forming binding sites for intracellular adaptors <sup>175</sup>. Phosphorylation of the tyrosine residues in the juxtamembrane region form binding sites for cytoplasmic targets with Src Homology 2 (SH2) or Phosphotyrosine binding (PTB) domains. Oligomerization and phosphorylation of the SAM domain creates interaction sites for downstream signaling molecules such as protein tyrosine phosphatases (PTP) <sup>176-177</sup>.

## 2.2 Ephrin ligand structure

All ephrin ligands contain a conserved receptor-binding domain (RBD). The RBD contains a hydrophobic loop that is inserted into the hydrophobic core of the LBD upon receptor binding. Ephrin ligands are subdivided in two classes based on the way they are attached to the cell membrane (Figure 2). EphrinA ligands are attached to the cell membrane via a Glycosylphosphatidyl Inositol (GPI) anchor. However, as they lack a cytoplasmic domain, they depend on the association with co-receptors (p75NTR (p75 neurotrophin receptor), Ret (rearranged during transfection) and TrkB (Tropomyosin receptor kinase B)) for further signaling<sup>178-180</sup>. EphrinB ligands contain a transmembrane domain followed by a conserved cytoplasmic region and a C-terminal PDZ-binding motif<sup>181</sup>. This cytoplasmic region contains tyrosine residues that become phosphorylated upon receptor binding<sup>182-183</sup>.

## 2.3 Eph/ephrin clustering

To obtain full biological activity Eph receptors need to be clustered, through a seeding mechanism<sup>168</sup>. This mechanism involves two interaction interfaces: the heterodimerization interface between receptor and ligand, and the clustering interface between two adjacent Eph receptors. Eph/ephrin clustering starts with the recognition and binding of Eph receptors and ligands on opposing cell surfaces (Figure 3)<sup>161</sup>. Heterodimers are formed, which can tetramerize into heterotetramers, thereby forming a ring structure in which each receptor interacts with two ligands and each ligand interacts with two receptors (Figure 3)<sup>184</sup>. This heterotetramerization has been observed both for EphA/efnA and EphB/efnB clustering<sup>184-185</sup>. The Eph/ephrin heterotetramers assemble into hetero-oligomeric clusters via direct Eph/Eph interactions. Most likely these clustering interfaces allow them to bind to other heterotetramers resulting in an array of well-ordered Eph receptors. This clustering also results in lateral recruitment of non-ligand-bound Eph receptors<sup>186</sup>. The clustering interfaces involve LBD-LBD interactions through salt bridges and hydrogen bonds, and CRD-CRD interactions through van der Waals interactions<sup>170, 185, 187</sup>. Interaction between fibronectin repeats has also been suggested, but this has not been confirmed<sup>163, 185</sup>.

Only ligands that are clustered (both membrane-bound ligands and artificially clustered ligands) can trigger signaling, while non-clustered or soluble ligands act as antagonists<sup>175, 188-191</sup>. Moreover, clustering of ephrin ligands increases the local Eph receptor concentration, thereby stimulating downstream signaling<sup>168</sup>.

In normal conditions, Eph receptors and ephrin ligands are present at the cell surface in distinct membrane regions, the cholesterol-rich lipid rafts<sup>192</sup>. These rafts enable trans-signaling between Eph receptors and ephrin ligands on opposing cells, and block *cis*-interactions between Eph receptors and ephrin ligands on the same cell<sup>192-193</sup>. *Cis*-interaction makes Eph receptors less responsive to ephrin ligands *in trans* abolishing the induction of tyrosine phosphorylation (Figure 4)<sup>149</sup>.

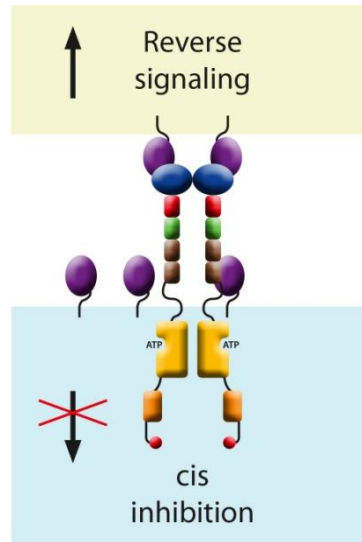


**Figure 4** *Cis*-interaction between ephrin ligands and Eph receptors. This *cis*-interaction abolishes the induction of tyrosine phosphorylation and makes Eph receptors less responsive to ephrin ligands *in trans*. Adapted from Pitulescu *et al.*, 2010<sup>149</sup>.

## 2.4 Signaling

Interaction between Eph receptors and ephrin ligands can result in bidirectional signaling: forward signaling in the Eph-bearing cell and reverse signaling in the ephrin-bearing cell (Figure 5)<sup>159</sup>. The Eph-ephrin signal is complex due to a large number of possible Eph-ephrin interactions, co-expression of different Eph receptors, *cis*-interaction influencing the signal and cross-talk with other signaling pathways<sup>175</sup>. This complexity makes it difficult to clearly define the signaling pathways underlying many Eph functions<sup>175</sup>. Signaling from the same Eph-ephrin pair can result in opposing responses, such as adhesion and retraction, depending on cell type, tissue and organ context. In general, Eph receptor phosphorylation results in cell-cell segregation while the same Eph receptor can stimulate cell-cell adhesion via kinase-independent signaling pathways<sup>149, 194</sup>. Many of the functions of Eph receptors involve signaling in both ways regulating cytoskeleton dynamics and morphology. One of the most common cellular responses to Eph receptor activation is actin stress fiber depolymerisation leading to cytoskeletal collapse, inducing cell-cell segregation<sup>194</sup>.



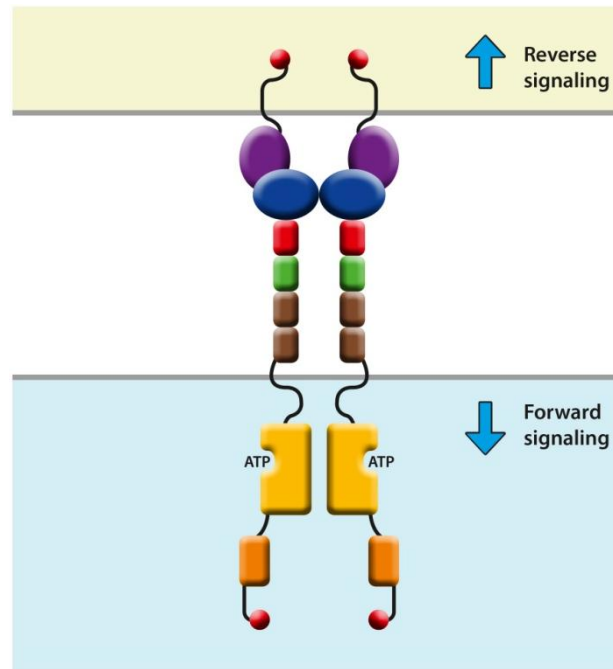


**Figure 5 Bidirectional signaling.** Interaction between Eph receptors and ephrin ligands can result in signaling in two directions: signaling in the Eph-bearing cell (forward signaling) and signaling in the ephrin-bearing cell (reverse signaling). Adapted from Pitulescu *et al.*, 2010<sup>149</sup>.

## 2.5 Regulation of Eph/ephrin signaling

The Eph/ephrin interaction and subsequent signaling is regulated in different ways and at different levels. At the RNA level there is transcriptional and post-transcriptional regulation<sup>195</sup>. Eph/ephrin signaling is also influenced by different interaction partners such as ligand-interaction *in cis*, protein tyrosine phosphatases (PTPs),  $\gamma$ -secretases and matrix metalloproteinases (MMP) such as A Disintegrin and Metalloproteinase (ADAM). Ligand interactions *in cis* make Eph receptors less responsive to ephrin ligands *in trans*<sup>149, 172</sup>. PTPs block Eph receptor phosphorylation and counteract Eph receptor endocytosis<sup>196-197</sup>. ADAM interaction with Eph receptors is promoted by ephrin-induced clustering (Figure 6A). ADAM cleaves ephrinA ligands, thereby disrupting the Eph/ephrin interaction, resulting in cell de-adhesion. EphrinB ligands are cleaved both by MMPs and  $\gamma$ -secretases, producing an intracellular domain (ICD) which activates downstream signaling<sup>198</sup>. This process of cleavage has been reported for the EphA4 and EphB2 receptor<sup>199-201</sup>. Another mechanism to terminate Eph/ephrin interaction is trans-endocytosis involving the uptake of full-length transmembrane EphB-ephrinB signaling complexes in the cell, enabling cell de-adhesion (Figure 6B)<sup>149</sup>. Whether the Eph/ephrin complex is taken up by the cell with the Eph receptor or the cell with the ephrin ligand, is determined by the Eph/ephrin signaling as this

process requires a functional Eph kinase. However, the exact mechanism is not completely understood<sup>202</sup>.

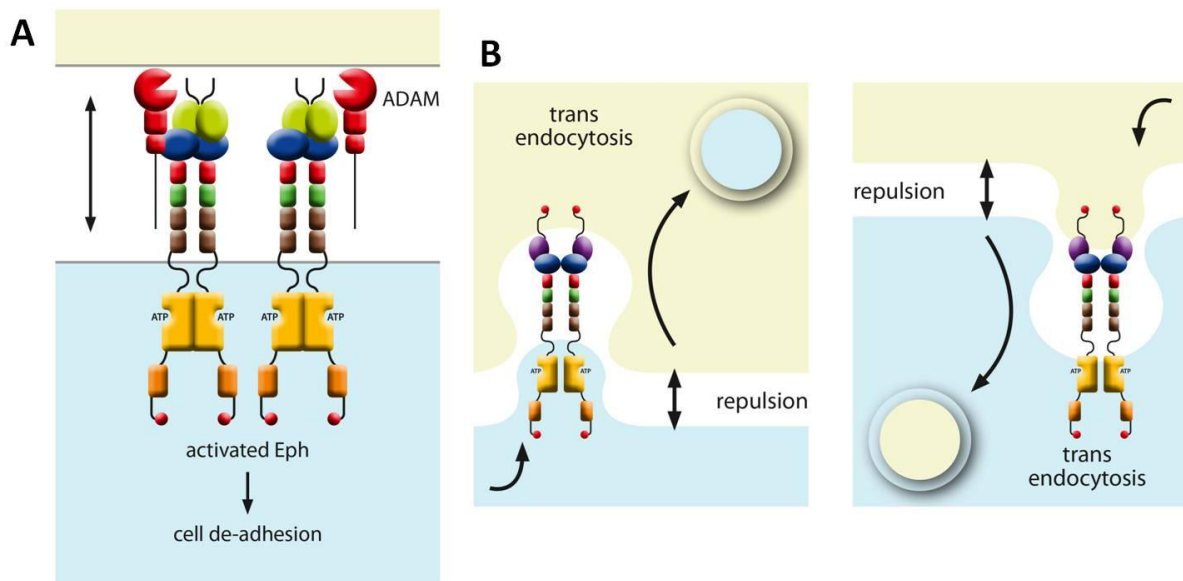


**Figure 6 Regulation of Eph/ephrin signaling.** (A) Upon clustering ADAM cleaves ephrinA ligands, thereby disrupting the Eph/ephrin interaction and inducing cell de-adhesion. (B) Trans-endocytosis involving the uptake of full-length transmembrane EphB-ephrinB signaling complexes in the cell, enabling cell de-adhesion. Adapted from Pitulescu et al., 2010<sup>149</sup>.

## 2.6 Epha4

In the CNS, Epha4 is highly expressed in cell bodies, dendritic spines and axons of neurons in various brain regions<sup>203-204</sup>. Neuronal Epha4 expression regulates dendritic spine morphology, which plays an important role in synaptic plasticity including long-term potentiation (LTP) and long-term depression (LTD)<sup>201, 205-206</sup>, while synaptic activity itself is able to increase Epha4 phosphorylation<sup>207</sup>. Furthermore, Epha4 has been shown to be involved in several neurological disorders including acute injuries, neuroinflammation and neurodegenerative diseases<sup>175</sup>.

### 2.6.1 CNS trauma

Total Epha4 expression has been found to be upregulated in reactive astrocytes in brains of traumatic brain injury (TBI) patients who deceased more than one day after the injury<sup>208</sup>, while phosphorylated Epha4 levels were significantly increased both in the ipsi- and contralateral hemisphere of individuals who died more than 8 hours after TBI<sup>208</sup>. In mouse models, this upregulation was only found in the cortex ipsilateral to the injury, but not in the hippocampus. Disappointingly, transgenic reduction of Epha4 levels in the hippocampus and

cortex did not result in improved outcome<sup>209</sup>.

The results obtained in studies on spinal cord injury (SCI) have been somewhat inconsistent. Some<sup>210-212</sup> but not all<sup>213-214</sup> studies have found Epha4 to be upregulated in reactive astrocytes at the lesion site<sup>210-211</sup> and in the proximal axonal stumps<sup>212</sup>. Epha4<sup>-/-</sup> mice showed increased axonal regeneration, which was shown by forward labeling of axons crossing the lesion site in Epha4<sup>-/-</sup> mice<sup>210</sup>. Furthermore, in rats treated with an EphA4 inhibitor, corticospinal tract axons sprouting was enhanced<sup>213</sup>. Both genetic knockdown as well as pharmacological blocking of Epha4 improved functional recovery including walking, climbing and grasping in mice after SCI<sup>210, 213</sup>. Disappointingly, this enhanced functional recovery was not seen in a rat model for SCI in which Epha4 expression was reduced using Epha4 antisense-oligodeoxynucleotides<sup>215</sup>.

### 2.6.2 Stroke

Epha4 was found to be highly upregulated in several experimental stroke models. In a focal cerebral ischemia rat model, Epha4 was highly upregulated in the glial scar 7 and 14 days after ischemia<sup>214</sup>. In a forebrain ischemia-reperfusion rat model, Epha4 was also found to be upregulated in the CA1 region<sup>216</sup>. Furthermore, higher expression of Epha4 was also shown in sprouting neurons after stroke in aged mice compared to sprouting neurons in younger mice, which may contribute to the reduced functional recovery in aged mice<sup>217</sup>. Inhibiting Epha4 by Epha4-Fc delivery in mice seven days post-stroke enhanced sprouting within the motor cortex<sup>218</sup>.

Downregulation as well as inhibition of Epha4 enhanced recovery after stroke in two different experimental stroke models<sup>216, 219</sup>. In a mouse model of photothrombotic stroke, enhanced motor recovery was observed in mice with reduced expression of Epha4<sup>219</sup>. Blocking Epha4 by Epha4-Fc delivery 30 minutes after ischemia-reperfusion in rats, lead to attenuated apoptotic neuronal death, suggesting a neuroprotective effect of Epha4 inhibition<sup>216</sup>.

### 2.6.3 Multiple Sclerosis (MS)

In active MS lesions in the human brain, EphA4 was found to be upregulated in inflammatory cells, macrophages, reactive astrocytes and axons<sup>220</sup>. In mice with experimental autoimmune encephalomyelitis (EAE), a model for MS, Epha4 was expressed on reactive astrocytes surrounding lesions<sup>221</sup>. In Epha4<sup>-/-</sup> mice with EAE, disease onset was delayed and its course less severe. Pharmacological blocking of Epha4 using soluble Epha4-Fc also delayed disease onset and slowed disease evolution. Genetic and pharmacological inhibition of Epha4 did not affect histopathological characteristics of the lesions including the numbers of infiltrating T-cells and macrophages, the number and size of the lesions and the extent of

astrocytosis, although axonal abnormalities were attenuated in *Epha4*<sup>-/-</sup> mice with EAE <sup>221</sup>.

#### 2.6.4 ALS

The clinical presentation of ALS varies greatly between ALS patients. Even within one family carrying the same mutation, disease onset and disease progression can be very heterogeneous <sup>2, 28</sup>. This suggests that ALS is a multifactorial disease influenced by modifying genes and environmental factors. In previous experiments in our laboratory, a zebrafish model of ALS was used to screen for modifying genes that could rescue the axonal phenotype. This axonal phenotype, shorter and more aberrantly branched motor axons, is caused by overexpression of mutant SOD1 in zebrafish embryos <sup>13</sup>. A morpholino-based knockdown of receptor tyrosine kinase 2 (*rtk2*), the zebrafish orthologue of human EphA4, completely rescued the axonal phenotype <sup>35</sup>. This result was confirmed in the SOD1<sup>G93A</sup> ALS mouse model where deletion of only one *Epha4* allele resulted in a longer survival compared to controls. In blood samples of ALS patients an inverse correlation was identified between EphA4 expression and disease onset suggesting lower levels of EphA4 to be associated with a less severe phenotypic expression of the disease. Sequencing of EphA4 in humans with ALS identified two previously unknown mutations which are associated with unusual long survival.

As genetic interference had a beneficial effect in the ALS fish and mouse model, it was also tested whether pharmacological inhibition could result in a beneficial effect. The small compound, a 2-hydroxy-4(2, 5-dimethylpyrrol-1-yl) benzoic acid derivative (C1), completely rescued the axonal phenotype in the zebrafish model of ALS. Intracerebroventricular delivery of the KYL-peptide delayed onset and increased survival in the SOD1<sup>G93A</sup> rat model. This dodecapeptide is a specific EphA4 antagonist which has been extensively studied *in vitro* and *in vivo* with beneficial effects in spinal cord injury <sup>213, 222</sup>. The properties of C1 will be further discussed in Chapter 4.

#### 2.6.5 Alzheimer's Disease (AD)

In the hippocampus of AD patients in the initial stage of the disease, EphA4 expression was found to be decreased and in their frontal lobe, the expression of the EphA4 intracellular domain (EICD) was reduced <sup>223-224</sup>. This fragment is obtained after cleavage of EphA4 by  $\gamma$ -secretase and enhances the formation of dendritic spines <sup>201</sup>. Furthermore, increased abundance of EphA4 has been found in neuritic plaques, although this study did not find a difference in EphA4 expression <sup>225</sup>.

In the hippocampus of two AD mouse models <sup>223</sup>, but not in two other ones <sup>226-227</sup>, *Epha4* expression was reduced, even before the occurrence of behavioral changes. However, in the

AD mouse models where no difference in Epha4 expression was found, an increase in Epha4 activity could be detected <sup>226-227</sup>. This enhanced Epha4 activation was also seen in hippocampal slices, cultured neurons and synaptoneurosomes exposed to amyloid beta (A $\beta$ ) oligomers <sup>227-228</sup>.

Experimental AD mice showed decreased long-term potentiation (LTP) that was rescued when Epha4 was genetically or pharmacologically downregulated <sup>227</sup>. Pharmacological blocking of the Epha4 receptor also rescued LTP in an *in vitro* model for A $\beta$  toxicity <sup>228</sup>.

### **2.6.6 Parkinson's Disease (PD) and Huntington's Disease (HD)**

In a study searching for biomarkers in cerebrospinal fluid (CSF) of PD patients, a peptide derived from EphA4 was found to be abundantly present <sup>229</sup>. In HD brains, decreased EphA4 mRNA levels have been found, and decreased EphA4 protein levels in the CSF of HD patients have been reported <sup>230</sup>. No functional studies in models for these disorders have been performed.

### **2.6.7 Conclusion**

In spite of some inconsistencies in terms of Epha4 expression, an increase in Epha4 activity as measured by Epha4 phosphorylation was observed in all disorders. In agreement with this, and again in spite of inconsistencies of results obtained using different strategies, blocking Epha4 positively affected the functional outcome in all neurological disorders tested, suggesting that Epha4 activation negatively affects the pathogenesis of these disorders.

# Aims

The variability of the phenotypic expression of ALS is unexplained, but it is thought to be genetic and/or environmental in nature. We previously identified the Epha4 receptor to be contributing to this variability. Knockdown of Epha4 in the zebrafish model of ALS resulted in a rescue of the axonal phenotype. Epha4 deletion and inhibition of the receptor resulted in increased survival in the ALS mouse and rat model respectively. Furthermore Epha4 expression in blood of sporadic ALS patients inversely correlated with survival indicating that patients with higher Epha4 expression have shorter survival. With the present work, we aim to gain more insight in the pathogenesis of ALS by studying the mechanism of action of Epha4 (I) and to test the therapeutic potential of modifying Epha4 in ALS (II).

The aim of **part one** is to investigate the **mechanism of action** of the hazardous effect of Epha4 on ALS. The ephrin system is a very complex system due to a large number of possible Eph-ephrin interactions, bidirectional signaling, co-expression of different Eph receptors, *cis*-interaction influencing the signal and cross-talk with other signaling pathways. To unravel the mechanism of action of the hazardous effect of Epha4 on ALS, we will focus on the effect of the Epha4 receptor on motor neuron degeneration and on the role of its interaction partners.

The aim of **part two** is to explore the **therapeutic potential** of EphA4 antagonists in the pathogenesis of ALS. We will test the potential of existing EphA4 antagonists. In addition, as most existing EphA4 inhibitors lack specificity and only block EphA4 activation at higher concentration, we will use Nanobody technology to generate a new, selective EphA4 inhibitor.



# Part I: Exploring the mechanism of the beneficial effect of EphA4 inhibition in ALS

## Introduction

We previously showed that EphA4 is a modifier of ALS both in animal models and in patients<sup>35</sup>. In a mouse model of ALS, the SOD1<sup>G93A</sup> mouse, genetically reducing the levels of EphA4 to half of the normal levels resulted in increased motor performance and survival. Histopathological analysis showed that more ventral horn motor neurons were preserved in mice with reduced EphA4 levels, *Epha4*<sup>+/-</sup>; SOD1<sup>G93A</sup> mice, compared to their littermate controls. Furthermore, *Epha4*<sup>+/-</sup>; SOD1<sup>G93A</sup> mice had a higher percentage of fully innervated neuromuscular junctions. These data indicate that 50% reduction of EphA4 expression slows motor neuron degeneration in the SOD1<sup>G93A</sup> ALS mouse model. Interestingly, these findings could be translated to human ALS, as an inverse correlation between EphA4 expression in blood samples and disease onset was identified in sporadic ALS patients.

We next studied the mechanism through which EphA4 exerted its role as a modifier of motor neuron degeneration. We previously studied the possible effect of decreased EphA4 expression on gliosis and excitotoxicity. Indeed, in an animal model for spinal cord injury a reduction of EphA4 was shown to be associated with a decrease in gliosis, which is of interest since astrocytes are important contributors to motor neuron degeneration in ALS<sup>210</sup>. However, in ALS mice with reduced EphA4 no reduction in gliosis was observed<sup>35</sup>. Furthermore, the expression of the glial glutamate transporter (GLT1) was demonstrated to be upregulated in the hippocampus of mice with lower levels of EphA4<sup>205</sup>. Excitotoxicity is a generally accepted mechanism in ALS, and therefore, we hypothesized that the beneficial effect of reduced EphA4 expression may be explained by an upregulation of GLT1 in the spinal cord of ALS mice. However, although an upregulation of GLT1 was confirmed in the hippocampus, no change of GLT1 expression was found in the spinal cord of *Epha4*<sup>+/-</sup>; SOD1<sup>G93A</sup> mice<sup>35</sup>.

In part I of this thesis, we further studied the mechanism through which EphA4 modifies ALS. We explored the contribution of EphA4 to the vulnerability of motor neurons and their sprouting potential following injury (Chapter 1). Furthermore, we studied whether the effect of EphA4 on motor neuron degeneration is mediated through forward or reverse signaling (Chapter 2). Finally, we investigated the possible involvement of one particular EphA4 ligand, ephrinb2, in the pathogenesis of ALS (Chapter 3).





# Chapter 1. Epha4 as a vulnerability factor in motor neurons

Published in: Van Hoecke A et al., Nature Medicine, 2012

Experiments in collaboration with Annelies Van Hoecke

## 1.1 Introduction

In previous work studying the spinal cord of mice overexpressing human wild type SOD1 (SOD1<sup>WT</sup>) or mutant SOD1 (SOD1<sup>G93A</sup>), we found Epha4 to be mainly or even exclusively present in spinal cord motor neurons, as it was below detection threshold in other cell types, such as astrocytes or microglia<sup>35</sup>.

In ALS, motor neurons are selectively affected. Some mechanisms that may at least partially explain the vulnerability of motor neurons have been discussed above. Interestingly, not all motor neurons are equally vulnerable. There are subpopulations of motor neurons such as the oculomotor neurons and neurons in Onuf's nucleus that are more resistant to neurodegeneration. Furthermore, there are motor neurons with different physiological characteristics that are also differentially vulnerable in ALS.

The aim of the present study was to further study the role of Epha4 in motor neurons during disease development and progression in ALS and to elucidate whether Epha4 contributes to the vulnerability of motor neurons.

## 1.2 Results

### 1.2.1 Vulnerable motor neurons in ALS have higher expression of Epha4

Epha4 protein expression in lysates of lumbar spinal cord decreases during disease progression in mutant SOD1 mice<sup>35</sup>. We first studied whether this decrease merely reflects the decrease of the number of motor neurons known to occur during ALS. To this end, we quantified Epha4 expression in motor neurons of the anterior horn of the spinal cord. Motor neurons from the spinal cord of SOD1<sup>G93A</sup> mice were isolated at different time points during the disease using Laser Capture Microdissection (LCM) followed by quantification of Epha4 mRNA expression using quantitative Polymerase Chain Reaction (qPCR) (Figure 1.1A). Surprisingly, Epha4 levels in motor neurons were reduced in late-symptomatic mice, compared to pre-symptomatic mice. This suggests that expression within the motor neuron is decreasing when the disease progresses or that motor neurons with higher levels of Epha4 are the most vulnerable as they die off first, while motor neurons with low Epha4 levels are less vulnerable, as they appear to survive until the late stages of the disease (Figure 1.1B).

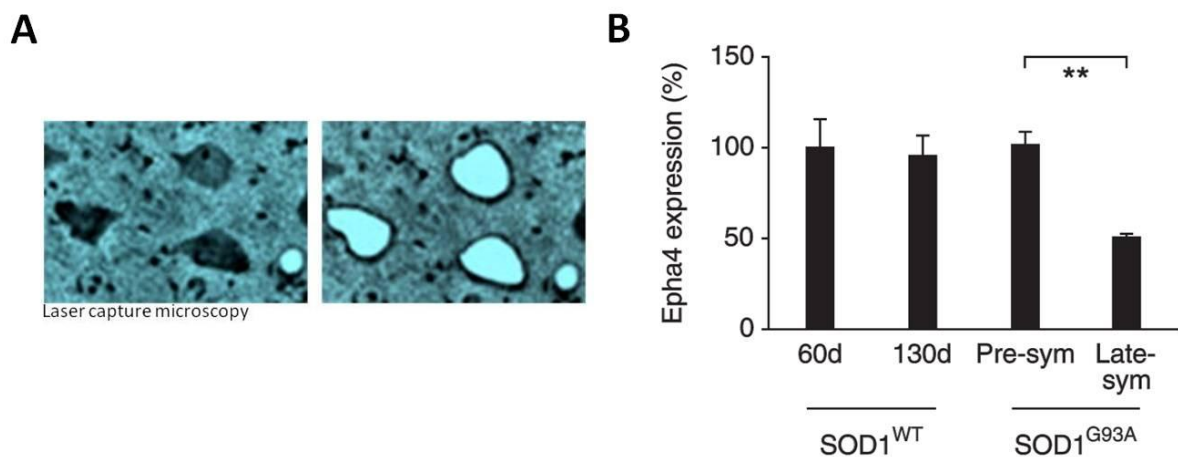


**Figure 1.1 Motor neurons in late-symptomatic mice have lower levels of Epha4.** (A) Image of ventral horn of lumbar spinal cord before (left) and after (right) LCM. (B) Epha4 mRNA expression in microdissected motor neurons of presymptomatic (Pre-sym) and late-symptomatic (Late-symp) SOD1<sup>G93A</sup> mice and age-matched SOD1<sup>WT</sup> mice (ANOVA  $p = 0.0033$ ,  $n = 3$ ). Polr2a was used as internal control, and levels were subsequently normalized to the 60-d value obtained in SOD1<sup>WT</sup> mice. Adapted from Van Hoecke *et al.*, 2012.

Differential vulnerability of motor neurons in ALS has been related to size and physiological subtype. Large, FF motor neurons are more vulnerable<sup>231</sup>. We therefore studied the expression of Epha4 in relation to size of the motor neuron. As shown in figure 1.2A., large motor neurons appear to be more susceptible to ALS, as has been described previously<sup>231</sup>.

Interestingly, Epha4 expression was significantly higher in microdissected large motor neurons ( $> 600 \mu\text{m}^2$ ) compared to that in smaller motor neurons ( $250 - 400 \mu\text{m}^2$ ) (Figure

1.2B). In agreement with this, we found that the protective effect of a reduction of Epha4 in  $SOD1^{G93A}$  mice was most pronounced in the large motor neurons (Figure 1.2C). Thus, expression levels of Epha4 correlate with vulnerability of neurons to ALS.

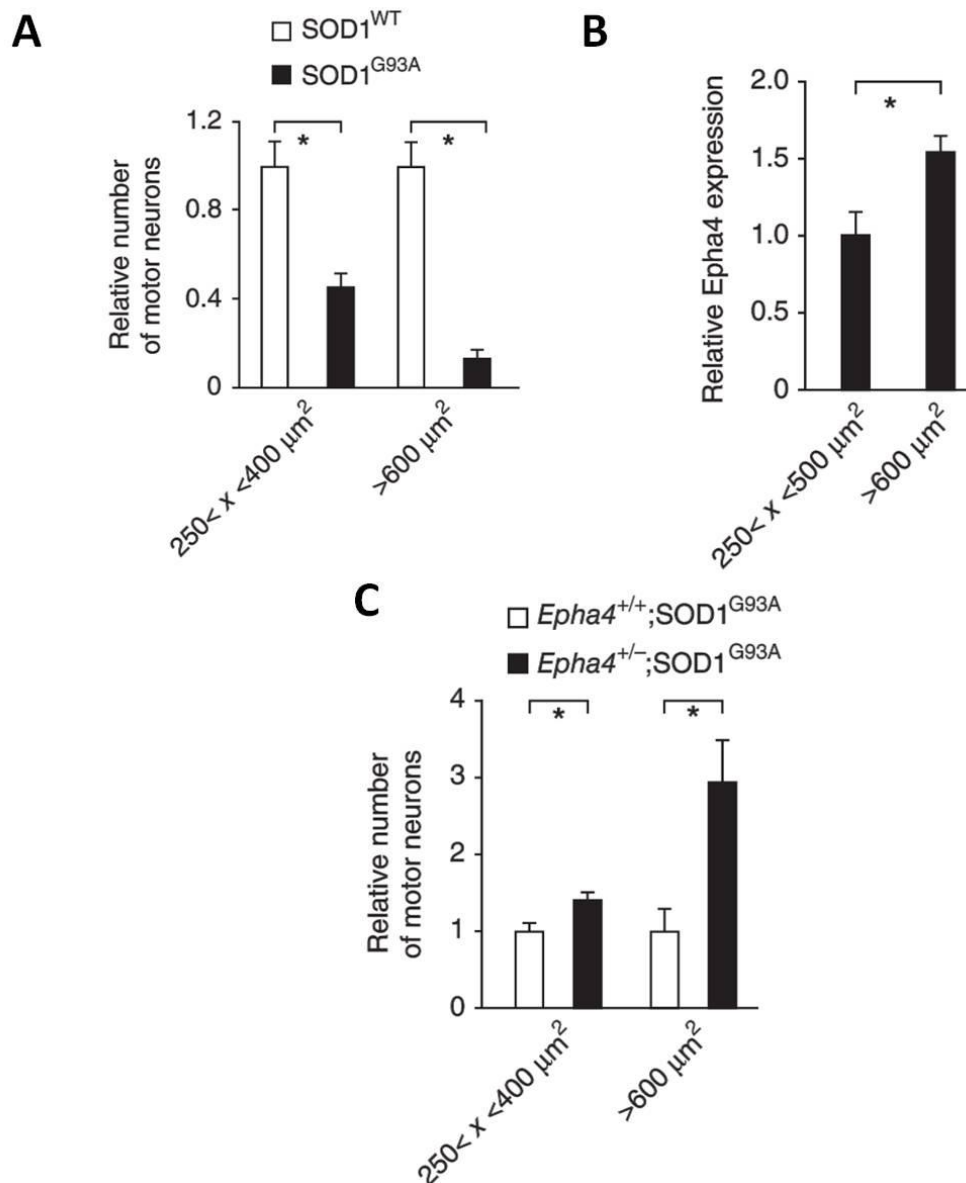


**Figure 1.2 Vulnerable motor neurons in ALS have higher expression of Epha4.** (A) Relative number of small ( $250\text{--}400 \mu m^2$ ) and large ( $>600 \mu m^2$ ) motor neurons in the ventral horn of spinal cord of late-symptomatic  $SOD1^{G93A}$  mice ( $n = 9$ ) and age-matched  $SOD1^{WT}$  controls ( $n = 6$ ; two-way ANOVA,  $p_{\text{genotype} \times \text{motor neuron size}} = 0.018$ , t-test small motor neurons  $p = 8.1 \times 10^{-4}$ , t-test large motor neurons  $p = 2.80 \times 10^{-5}$ ). (B) Epha4 expression in small and large laser-captured microdissected motor neurons of nontransgenic mice ( $n = 3$ , t-test  $p = 0.044$ ). Polr2a was used as internal control. (C) Relative number of small and large motor neurons in the spinal cord of late-symptomatic  $Epha4^{+/-}; SOD1^{G93A}$  mice ( $n = 9$ ) compared to age-matched  $Epha4^{+/+}; SOD1^{G93A}$  littermates ( $n = 9$ ; two-way ANOVA  $p_{\text{genotype} \times \text{motor neuron size}} = 0.031$ , t-test small motor neurons  $p = 0.018$ , t-test large motor neurons  $P = 0.011$ ). Adapted from Van Hoecke *et al.*, 2012.

## 1.2.2 Epha4 is a determinant of the re-innervating capacity of motor neurons

We then wondered whether Epha4 is just a marker of vulnerable neurons, or whether it plays a mechanistic role. Large motor neurons have limited regenerating capacity as evaluated by sprouting and reduced re-innervation capacity. Therefore, vulnerability and regeneration capacity are thought to be interrelated<sup>75</sup>. We therefore studied the role of Epha4 in re-innervation capacity of the motor neuron by investigating its effect on neuromuscular re-innervation following axotomy of the sciatic nerve (Figure 1.3A). As shown in figure 1.3B, the re-innervation capacity in Epha4 knockout mice was significantly and dose-dependently improved compared to wild type mice, suggesting that Epha4 reduces the re-innervating capacity of spinal motor neurons (Figure 1.3B).

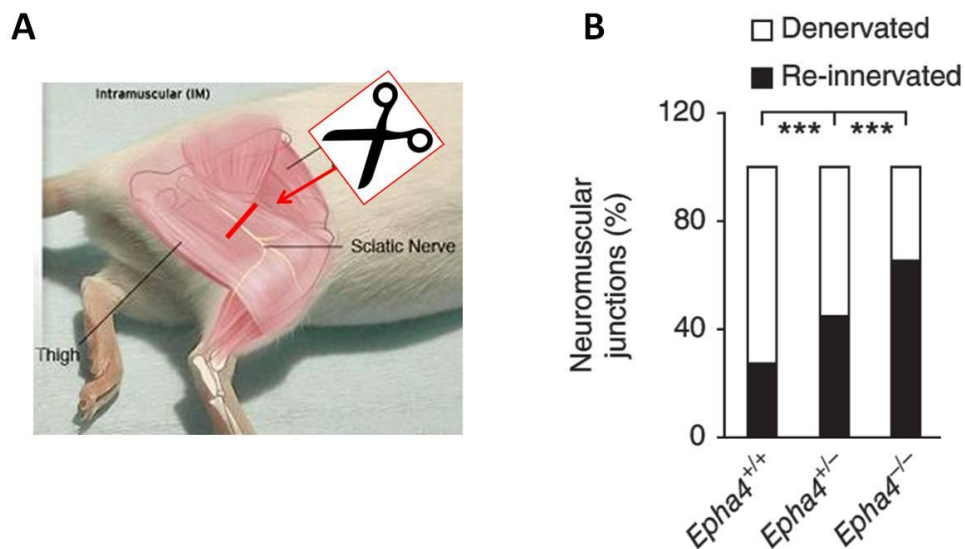


**Figure 1.3 Epha4 is a determinant of the re-innervating capacity of motor neurons .** (A) Schematic representation of sciatic nerve axotomy. (B) Re-innervation of gastrocnemius neuromuscular junctions after sciatic nerve axotomy in Epha4<sup>+/+</sup> (n = 10), Epha4<sup>+/-</sup> (n = 8, OR 2.15 ± [1.76–2.63]) and Epha4<sup>-/-</sup> mice (n = 5, OR 4.98 ± [3.93–6.31]). \*\*\*p < 0.001. Adapted from Van Hoecke *et al.*, 2012. OR, Odds ratio

### 1.3 Discussion

Previous work in our laboratory has shown that Epha4 is a modifier of ALS. However, the mechanisms by which Epha4 reduction/inhibition attenuate motor neuron degeneration remain unknown. In  $SOD1^{G93A}$  mouse with 50% reduction of Epha4 expression, astrogliosis and GLT1 expression were not altered. In this chapter we showed that motor neurons with lower levels of Epha4 are less vulnerable as they survived until the late stages of the disease. Large motor neurons that are more vulnerable have higher Epha4 expression compared to smaller motor neurons. In agreement with this, the protective effect of reduced Epha4 expression in the  $SOD1^{G93A}$  mouse was most pronounced in the large motor neurons. Furthermore, reduced Epha4 expression improved the re-innervating capacity of spinal motor neuron axons in a model of sciatic nerve axotomy. Together these results suggest that Epha4 contributes to the differential vulnerability of motor neurons in ALS and that high Epha4 expression reduces the re-innervating capacity of large motor neurons, possibly making them vulnerable for degeneration and thereby attenuating ALS disease progression (Figure 1).

Mutant  $SOD1$  mice resemble to a remarkable degree the precise pattern in selective motor neuron degeneration both in terms of regional vulnerability and motor neuron subtype seen in patients with sporadic ALS. Similar to what is seen in mutant  $SOD1$  mice, the large motor neurons are the ones affected earliest in ALS patients<sup>78</sup>. Moreover, EMG patterns of single motor units in a distal muscle in ALS patients show similar patterns of denervation and re-innervation<sup>76</sup>. This de- and re-innervation results in fiber type grouping, characteristic for what is seen in ALS patients<sup>232</sup>. It is thought that sprouting from surviving motor neurons can compensate for the motor neuron degeneration in early stages of the disease. Even though a similar pattern in selective motor neuron degeneration is observed in ALS patients, we don't know whether EphA4 also contributes to the vulnerability in motor neurons in ALS patients. Further experiments, including determining EphA4 expression within human motor neurons, might help to elucidate whether EphA4 contributes to the vulnerability of motor neurons in ALS patients.

Several other factors have been identified that contribute to the differential vulnerability of motor neurons in ALS. MMP9 has been identified to be selectively expressed in the vulnerable motor neurons, more specifically in the fast motor neurons<sup>74</sup>. These fast motor neurons (FF) are the ones affected earliest both in mutant  $SOD1$  mice as in ALS patients<sup>75-77</sup>. The degeneration of these FF motor neurons is followed by degeneration of the FR motor neurons and only later by the S motor neurons. There is compensatory re-innervation which differs between the different motor neuron subtypes. The motor end plates, from which the degenerating FF axons have retracted, will subsequently be innervated by FR motor neuron axons. Later in the disease process, the FR-motor neurons become involved, cannot maintain their neuromuscular junctions anymore and will retract their axons and degenerate. The S

motor neurons will compensate for the degeneration of these axons by re-innervating motor end plates left by degenerating FF and FR motor neurons<sup>75</sup>. The axons of S motor neurons are involved in the terminal stages of the disease only. This regeneration/sprouting capacity of different motor neuron subtypes correlates with its vulnerability and is important in the pathogenesis of ALS. Experimental increase of motor unit activity in the hind limbs of mutant SOD1 mice saved the motor units that are normally lost during early stages of the disease suggesting that the vulnerable motor units are saved by increasing their neuromuscular activity thereby converting them to more resistant motor units<sup>233</sup>. Furthermore, FF and FR motor neurons in mutant SOD1 mice lacking MMP9 both adopt an axonal dieback phenotype comparable to that of S motor neurons as their rate of muscle denervation was similar to that of S motor neurons with normal MMP9 levels<sup>74</sup>. The exact mechanism underlying this sequential degeneration of the different motor neuron subtypes is unknown. However, it has been shown that UPR activation is initiated selectively in the vulnerable motor neurons and activated in resistant motor neurons late in disease, shortly before they start to degenerate<sup>45</sup>. In mutant SOD1 mice with a deletion of MMP9 the UPR was initiated at later stages, suggesting MMP9 enhances the activation of the UPR thereby inducing axonal degeneration<sup>74</sup>.

## Chapter 2. Exploring the Epha4 signaling direction

Experiments in collaboration with Laura Rué

### 2.1 Introduction

Interaction between Eph receptors and ephrin ligands can result in signaling in two directions: signaling in the Eph-bearing cell (forward signaling) and signaling in the ephrin-bearing cell (reverse signaling) (Figure 5). Reduction of Epha4 expression results in decreased Epha4 signaling in both directions. It is unknown which signaling direction is involved in the modifying effect of Epha4 (Figure 2.1). To study the contribution of forward and reverse signaling on the beneficial effect observed upon Epha4 reduction, we obtained a transgenic mouse in which the Epha4 receptor is modified to lack forward signaling, but in which reversed signaling is unaffected<sup>206</sup>. In this Epha4<sup>eGFP/eGFP</sup> mouse the cytoplasmic domain has been replaced by an enhanced Green Fluorescent Protein (eGFP), removing all intracellular binding sites. Previous studies already used this mouse model to distinguish between forward and reverse signaling. Both homozygous Epha4<sup>eGFP/eGFP</sup> and Epha4<sup>-/-</sup> mice show aberrant organization of thalamocortical projections<sup>234-235</sup>. However, in contrast to Epha4<sup>-/-</sup> mice, long-term potentiation (LTP) is not affected in Epha4<sup>eGFP/eGFP</sup> mouse<sup>206</sup>. These data indicate that Epha4 forward signaling is required for corticospinal tract formation, while Epha4 reverse signaling is involved in LTP. These aberrations in the formations of the corticospinal tract result in a rabbit-like hopping gate in both the Epha4<sup>-/-</sup> and Epha4<sup>eGFP/eGFP</sup> mice<sup>234, 236</sup>. Since the motor performance is difficult to assess in these homozygous Epha4<sup>-/-</sup> and Epha4<sup>eGFP/eGFP</sup> mice due to the hopping gate, survival and motor performance were assessed using Epha4<sup>+/-</sup>; SOD1<sup>G93A</sup> and Epha4<sup>eGFP/+</sup> mice<sup>234</sup>.

We first molecularly characterized the Epha4<sup>eGFP/+</sup> mice and then investigated the effect of replacing Epha4 by Epha4eGFP on the course of ALS. We hypothesized that if a similar protective effect on ALS is observed in the Epha4<sup>eGFP/+</sup>; SOD1<sup>G93A</sup> mice as in the Epha4<sup>+/-</sup>; SOD1<sup>G93A</sup>, the beneficial effect is mediated by a decrease of forward signaling. However, if no effect is observed in the Epha4<sup>eGFP/+</sup>; SOD1<sup>G93A</sup> mice, the beneficial effect observed in the Epha4<sup>+/-</sup>; SOD1<sup>G93A</sup> mice is caused by a decrease in reverse signaling.



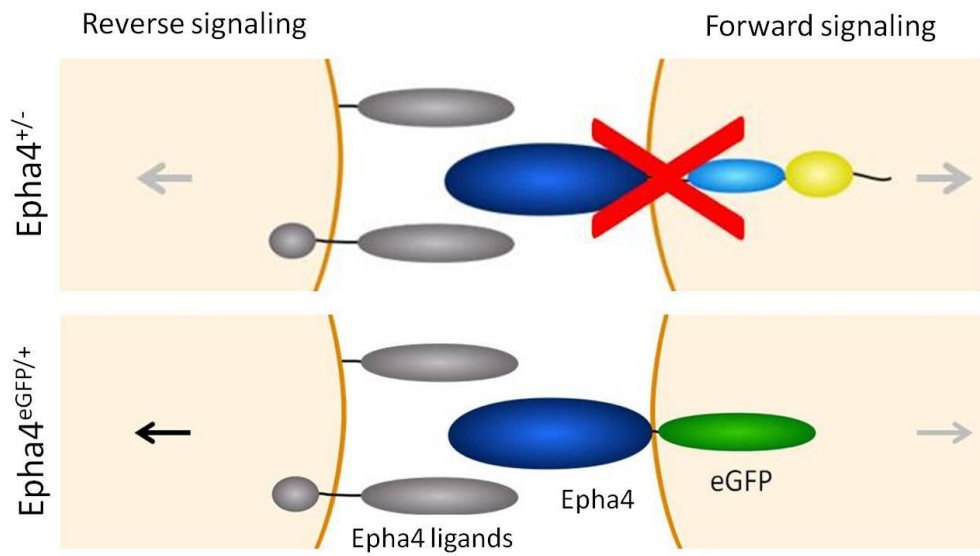


**Figure 2.1 Schematic representation of the *Epha4<sup>+/-</sup>* mouse and the *Epha4<sup>eGFP/+</sup>* mouse.** In the *Epha4<sup>+/-</sup>* mouse, Epha4 is deleted abolishing both the forward and the reverse signaling. In the *Epha4<sup>eGFP/+</sup>* mouse, one Epha4 allele is replaced with an Epha4eGFP isoform abolishing only the forward signaling.

## 2.2 Results

### 2.2.1 Epha4 expression and phosphorylation

We determined the expression of the Epha4eGFP isoform and wild type Epha4 protein in lysates of spinal cord, hippocampus and cortex using an N-terminal Epha4 antibody since this detects both wild type Epha4 as well as the Epha4eGFP isoform (Figure 2.2A,B). Quantification of their expression levels in the heterozygous Epha4<sup>eGFP/+</sup> mice showed higher expression of the Epha4eGFP isoform compared to wild type Epha4 (Figure 2.2C,D).

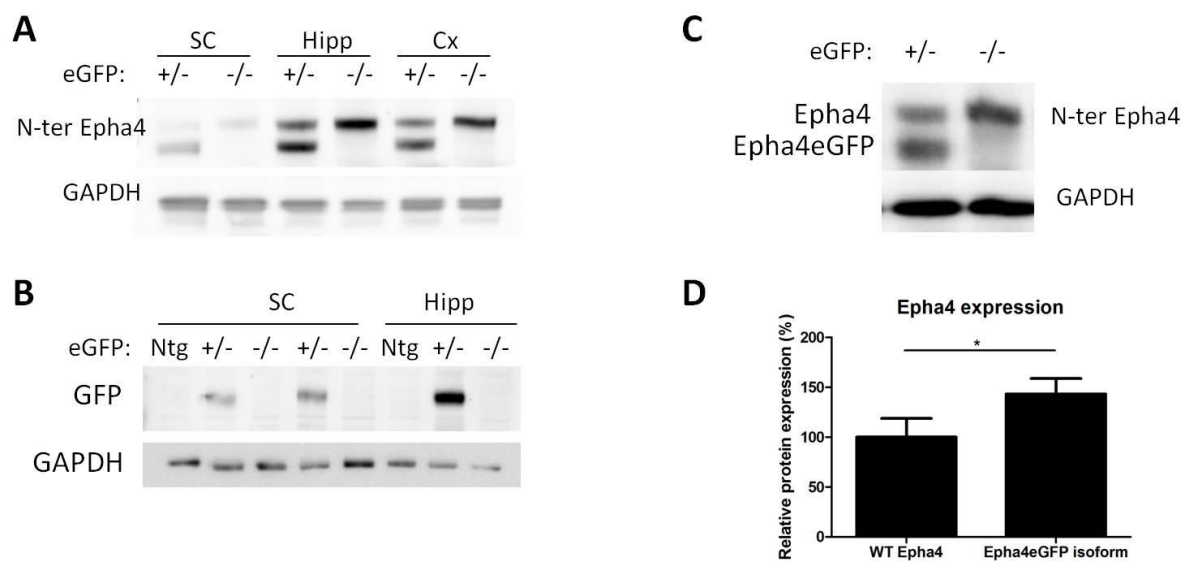


**Figure 2.2 Expression levels of wild type Epha4 and Epha4eGFP in CNS of adult mice.** (A) A monoclonal antibody against the extracellular part of Epha4 recognised wild type Epha4 and Epha4eGFP in adult spinal cord (SC), hippocampus (Hipp) and cortex (Cx). (B) An antibody against GFP identified the lower band as Epha4eGFP. (C,D) Expression levels of wild type Epha4 (n = 4, 100%) and Epha4eGFP (n = 4, 143%) in the spinal cord of Epha4<sup>eGFP/+</sup> mice (p = 0.0122). GAPDH (37 kDa) was used as a loading control. \*p<0.05. Error bars denote standard deviation.

Epha4 expression levels in the spinal cord of nontransgenic, Epha4<sup>+/-</sup> and Epha4<sup>eGFP/+</sup> were compared. Using a C-terminal Epha4 antibody, Epha4<sup>+/-</sup> mice and Epha4<sup>eGFP/+</sup> mice had similar levels of the Epha4 cytoplasmic domain, which are 50% compared to the Epha4 levels in nontransgenic animals (Figure 2.3A,C). Next, we determined to what extent Epha4 phosphorylation was affected in the heterozygous Epha4<sup>eGFP/+</sup> mouse. Replacement of the Epha4 wild type protein by the Epha4eGFP isoform removes the kinase domain and the phosphorylation sites present in the kinase domain and the juxtamembrane region. We focused on the phosphorylation levels of Y779, located in the kinase domain of the Epha4 receptor. Phosphorylation of Y779 was comparable in the Epha4<sup>eGFP/+</sup> mice and the Epha4<sup>+/-</sup>

mice, but reduced compared to nontransgenic animals (Figure 2.3B,D). These results indicate that Epha4 expression and phosphorylation status is similar in Epha4<sup>eGFP/+</sup> and in Epha4<sup>+/-</sup> mice.

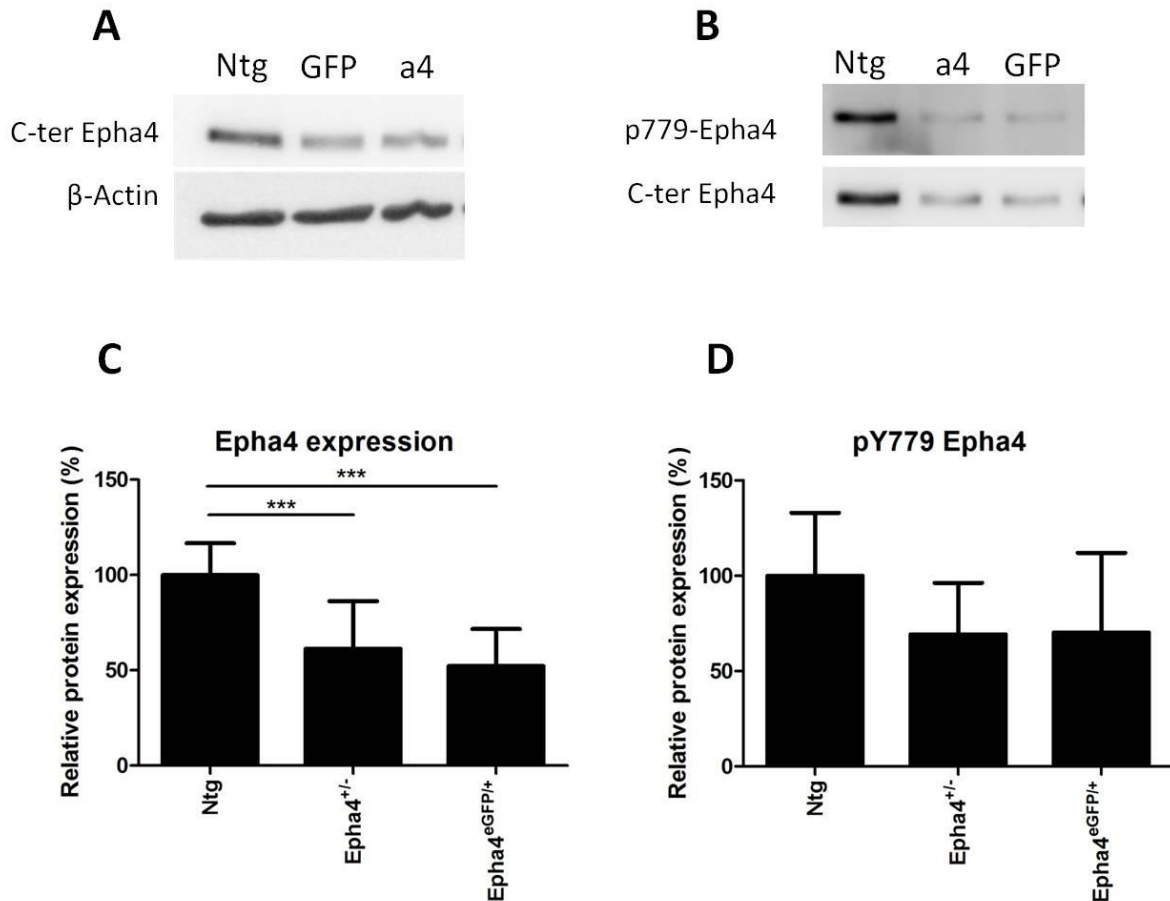


**Figure 2.3 Phosphorylation levels of Epha4 in the spinal cord of Epha4<sup>+/-</sup>, Epha4<sup>eGFP/+</sup> and nontransgenic mice.** (A, C) Epha4 expression in lumbar spinal cords of Ntg mice (n = 14, 100% expression), Epha4<sup>+/-</sup> mice (n = 8, 61% expression) and Epha4<sup>eGFP/+</sup> mice (n = 8, 52% expression). (B, D) Phosphorylation of Y779, a Epha4 kinase domain residue, in lumbar spinal cords of Ntg mice (n = 9, 100% expression), Epha4<sup>+/-</sup> mice (n = 4, 69% expression) and Epha4<sup>eGFP/+</sup> mice (n = 4, 70% expression). GAPDH (37 kDa) was used as a loading control. ANOVA tests were used for statistical analysis, \*\*\*p<0.001. Error bars denote standard deviation.

## 2.2.2 Abolishing Epha4 forward signaling in the SOD1<sup>G93A</sup> mouse model

Epha4<sup>eGFP/+</sup> mice were crossbred with the SOD1<sup>G93A</sup> mouse model. Replacement of one *Epha4* allele in the SOD1<sup>G93A</sup> mouse with an Epha4eGFP isoform, did not affect disease onset, assessed by hanging wire and rotarod performance (Figure 2.4A,B). Survival and disease duration was unaltered in the Epha4<sup>eGFP/+</sup>; SOD1<sup>G93A</sup> mouse, in contrast to the Epha4<sup>+/-</sup>; SOD1<sup>G93A</sup> which showed a beneficial effect on survival and disease duration (Figure 2.4C,D)<sup>35</sup>.

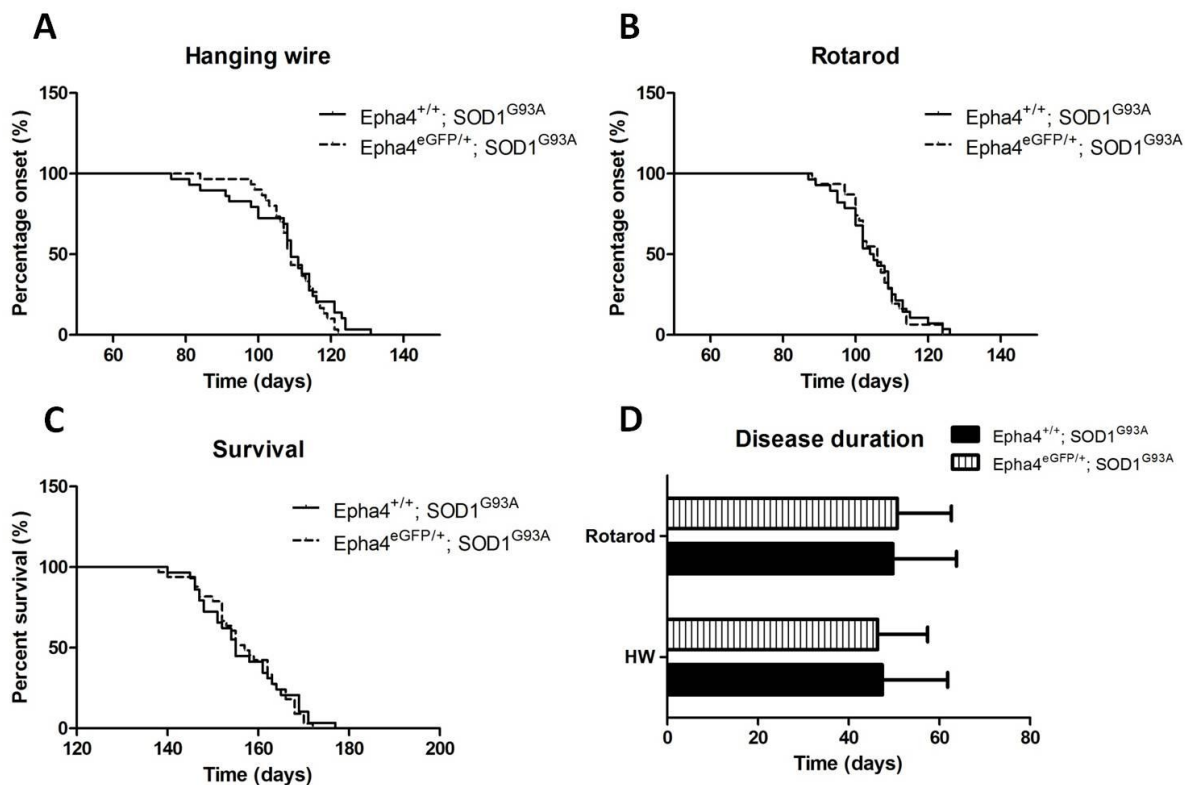


**Figure 2.4 Deletion of the Epha4 cytoplasmic domain did not affect disease onset and survival in SOD1<sup>G93A</sup> mice. (A) Disease onset as determined by hanging wire.** Median disease onset: 109 d (Epha4<sup>+/+</sup>; SOD1<sup>G93A</sup>, n = 29) and 109 d (Epha4<sup>eGFP/+</sup>; SOD1<sup>G93A</sup>, n = 30). (B) Disease onset as determined by rotarod. Median disease onset: 104.5 d (Epha4<sup>+/+</sup>; SOD1<sup>G93A</sup>, n = 28) and 106 d (Epha4<sup>eGFP/+</sup>; SOD1<sup>G93A</sup>, n = 31). (C) Median survival: 155 d (Epha4<sup>+/+</sup>; SOD1<sup>G93A</sup>, n = 29) and 157 d (Epha4<sup>eGFP/+</sup>; SOD1<sup>G93A</sup>, n = 33). (D) Average disease duration as determined by hanging wire or rotarod respectively: 47 and 50 d (Epha4<sup>+/+</sup>; SOD1<sup>G93A</sup>, n = 29), 46 and 51 d (Epha4<sup>eGFP/+</sup>; SOD1<sup>G93A</sup>, n = 30).

In order to assess subtle effects on motor neuron degeneration too small to affect the clinical status of the animals, we quantified the number of motor neurons in the spinal ventral horn, and studied the degree of neuromuscular innervation. Histopathological analysis of age-matched mice showed no difference in preserved ventral horn motor neurons nor neuromuscular junctions in  $Epha4^{eGFP/+}; SOD1^{G93A}$  mice as compared to littermate controls ( $Epha4^{+/+}; SOD1^{G93A}$ ) (Figure 2.5).

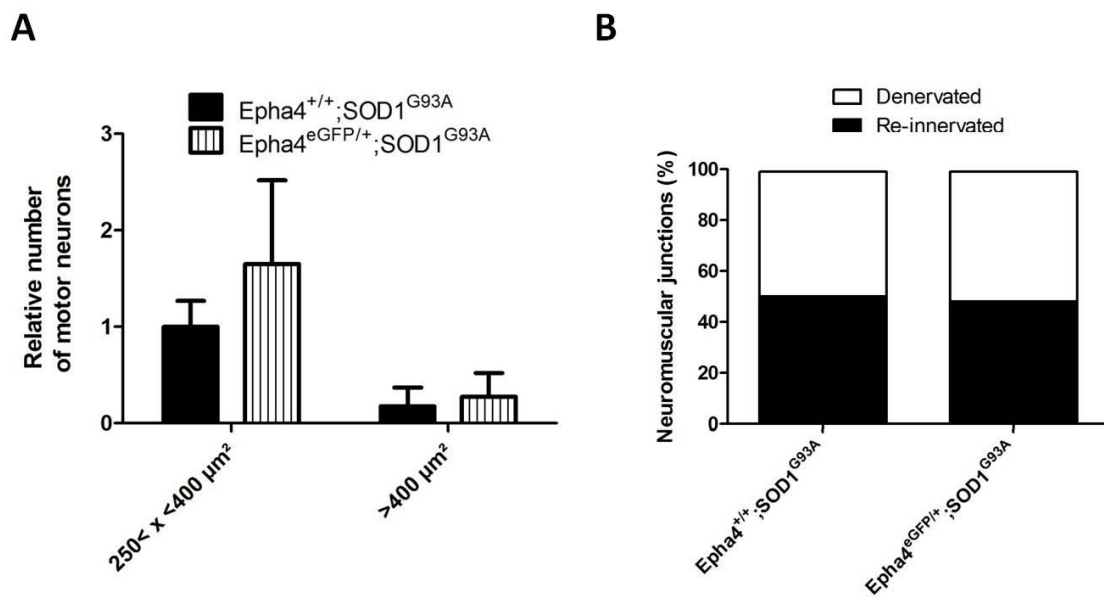


**Figure 2.5 Ventral horn motor neurons and neuromuscular junctions were not preserved in the  $Epha4^{eGFP/+}; SOD1^{G93A}$  mice compared to their age-matched littermate controls ( $Epha4^{+/+}; SOD1^{G93A}$ ).** (A) Relative number of small and large motor neurons in the spinal cord of late-symptomatic  $Epha4^{eGFP/+}; SOD1^{G93A}$  mice (n = 3) compared to age-matched  $Epha4^{+/+}; SOD1^{G93A}$  littermates (n = 5) (B) Percentage completely innervated neuromuscular junctions: 48% ( $Epha4^{eGFP/+}; SOD1^{G93A}$ , n = 8) versus 50% ( $Epha4^{+/+}; SOD1^{G93A}$ , n = 9, age-matched controlled).

These data show that replacement of one *Epha4* allele by an *Epha4*eGFP isoform did not affect disease onset and survival in a mouse model of ALS. Thus, abolishment of *Epha4* forward signaling by deleting the *Epha4* cytoplasmic domain did not influence ALS, suggesting that it is a reduction of *Epha4* reverse signaling that is beneficial for motor neuron degeneration in ALS.

### 2.2.3 Abolishing *Epha4* forward signaling negatively affects the re-innervating capacity of motor neurons

Previously, we showed that *Epha4* determines the re-innervating capacity of motor neurons (Figure 1.3). In general, sprouting of motor neurons is increased when *Epha4* is deleted and/or blocked<sup>212-213, 217</sup>. More specifically, it is thought to be mediated by abolishing *Epha4*

forward signaling<sup>234</sup>. We therefore studied the role of Epha4 forward signaling in re-innervation capacity of the motor neuron by investigating the effect of replacing the Epha4 cytoplasmic domain with a eGFP protein on neuromuscular re-innervation following axotomy of the sciatic nerve. As shown in figure 2.6A, the re-innervation capacity in Epha4 knockout mice was significantly improved compared to wild type mice. Surprisingly, Epha4<sup>eGFP/eGFP</sup> mice showed reduced re-innervation capacity compared to wild type mice (Figure 2.6B). These data show that we have to be cautious to interpret the data of this transgenic mouse model as replacement of the Epha4 cytoplasmic domain not only abolishes forward signaling, but most likely interferes with different aspects of Epha4 signaling such as cleavage and clustering.

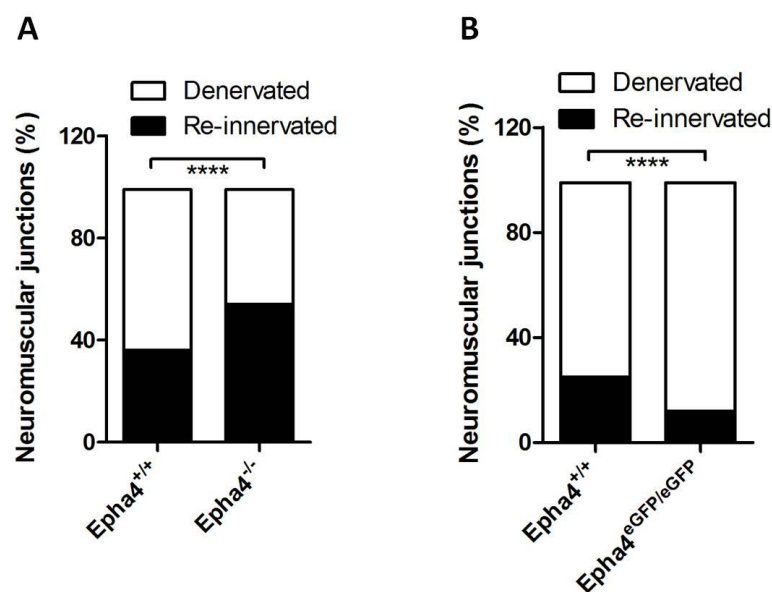


**Figure 2.6 Re-innervation of gastrocnemius neuromuscular junctions after sciatic nerve axotomy.** (A) Re-innervation of gastrocnemius neuromuscular junctions after sciatic nerve axotomy in Epha4<sup>+/+</sup> (n = 11) and Epha4<sup>-/-</sup> mice (n = 8, OR 2.014 ± [1.675–2.422]). (B) Re-innervation of gastrocnemius neuromuscular junctions after sciatic nerve axotomy in Epha4<sup>+/+</sup> (n = 13) and Epha4<sup>eGFP/eGFP</sup> mice (n = 8, OR 0.423 ± [0.332–0.539]). \*\*\*\*p<0.0001. OR, Odds ratio

## 2.3 Discussion

Interaction between Eph receptors and ephrin ligands can result in bidirectional signaling, meaning forward signaling in the Eph-bearing cell and reverse signaling in the cell that expresses the ephrin ligand. Deletion of one *Epha4* allele in the SOD1<sup>G93A</sup> mouse model abolishes both forward and reverse signaling, thereby increasing survival in these mice<sup>35</sup>. Furthermore *Epha4*<sup>-/-</sup> mice showed enhanced re-innervation capacity following axotomy of the sciatic nerve. To investigate whether the hazardous effect of *Epha4* on ALS and the re-innervation capacity after sciatic nerve axotomy is mediated through forward or reverse signaling, we used the *Epha4*<sup>eGFP/eGFP</sup> mouse in which the cytoplasmic domain has been replaced by an enhanced Green Fluorescent Protein (eGFP)<sup>206</sup>.

Replacement of one *Epha4* allele in the SOD1<sup>G93A</sup> mouse with an *Epha4*eGFP isoform, did not affect survival even though deletion of one *Epha4* allele did increase survival (Figure 2.7)<sup>35</sup>. Thus, it appears that reverse rather than forward signaling underlies the pathogenic contribution of *Epha4* in ALS. Although negative outcomes are always difficult to rely upon, we do think this conclusion is valid in view of the large number of mice that we used in these experiments. Furthermore, we excluded subtle effects on the disease by investigating the number of remaining motor neurons and neuromuscular innervation.

Still, our observation needs to be interpreted with caution. First, we only used heterozygous *Epha4*<sup>eGFP/+</sup> mice as homozygous *Epha4*<sup>eGFP/eGFP</sup> mice have a rabbit-like hopping gate making it difficult to assess motor performance<sup>206</sup>. Furthermore, we found that the replacement of the intracellular domain of *Epha4* by eGFP results in increased abundance of this hybrid molecule. This is also evident from the blots that have been published when this mouse was reported<sup>206</sup>. There may be several reasons for this. *Epha4* can be cleaved both by MMPs and by  $\gamma$ -secretases yielding *Epha4* extra- and intracellular domains<sup>201, 237</sup>. This cleavage of *Epha4* is important for the modulation of its expression and function<sup>238</sup>. Removal of the intracellular domain might impair proper cleavage of *Epha4* thereby altering its expression level, as we observed. In addition, complete removal of the intracellular domain also abolishes the SAM-domain, which is involved in receptor clustering, which may affect processing of the receptors. Finally, the Eph receptors are endocytosed resulting in breakdown of the receptor in lysosomes<sup>239</sup>. In this way the duration and intensity of downstream signaling can be regulated. It has been shown that *Epha4* can indeed be endocytosed<sup>240-241</sup>. Removal of the cytoplasmic domain in the *Epha4*eGFP isoform might interfere with this process of endocytosis and termination of signaling. Because of the increased abundance of the *Epha4*eGFP, it is possible that its reverse signaling is actually enhanced, in addition to its forward signaling being reduced.

That replacing the intracellular *Epha4* domain with eGFP may have effects other than just blocking the forward signaling is also suggested by the results of our axotomy experiments. It has been shown that *Epha4* plays a negative role in sprouting of neurons. *Epha4* is

upregulated in axonal stumps after injury<sup>212</sup> and in sprouting neurons of aged mice after stroke which contributes to reduced recovery<sup>217</sup>. Furthermore, blocking Epha4 induced more sprouting after spinal cord injury<sup>210</sup>. It is generally accepted that this negative effect on sprouting can be assessed *in vitro* by studying the inhibiting (collapsing) effect of ephrin ligands on the axonal growth cone. Growth cone collapse by stimulation with ephrin ligands is thought to be mediated by Epha4 forward signaling through the kinase function as this collapse could not be induced in Epha4<sup>eGFP/eGFP</sup> neurons and in Epha4<sup>KD/KD</sup> neurons in which the kinase domain has been mutated<sup>234</sup>. As these data indicate that Epha4 regulation of sprouting is mediated through forward signaling, we investigated the re-innervation capacity of Epha4<sup>eGFP/eGFP</sup> mice following sciatic nerve axotomy. Surprisingly, we found that Epha4<sup>eGFP/eGFP</sup> mice showed reduced re-innervation capacity following sciatic nerve axotomy while in Epha4<sup>-/-</sup> mice this re-innervation capacity was enhanced<sup>35</sup>. These data suggest that in the Epha4<sup>eGFP/eGFP</sup> mouse *in vivo*, the outgrowth enhancing effect of deleting the forward signaling, is abolished by the outgrowth inhibiting effect generated through the remaining reverse signaling, which is likely to be even further enhanced because of the increased abundance of the EphA4eGFP molecule as explained above.

Therefore, to confirm our conclusion that the hazardous effect of Epha4 on ALS is mediated through reverse signaling, it is of interest to investigate the effect of a more subtle inhibition of forward signaling on ALS. This can be done by studying the Epha4<sup>KD/KD</sup> mouse<sup>242</sup>. In this mouse model the kinase domain is not functional by the replacement of the critical lysine residue K653 by a methionine. So far all functions mediated through Epha4 forward signaling are thought to be mediated through the kinase domain, as no functions have been assigned to the SAM domain and the PDZ domain<sup>242-243</sup>. This Epha4<sup>KD/KD</sup> mouse model has some advantages over the Epha4<sup>eGFP/eGFP</sup> mouse. In the Epha4<sup>KD/KD</sup> mouse only one amino acid has been replaced, while in the Epha4<sup>eGFP/eGFP</sup> mouse the whole intracellular domain has been replaced. In this way no other domains involved in cleavage, clustering or endocytosis will be mutated. Crossbreeding of the Epha4<sup>KD/KD</sup> mouse with the mutant SOD1 mouse is being done in our lab. However, even in this experiment, we still have to be cautious to interpret these results as in the heterozygous Epha4<sup>KD/+</sup> mouse which will be used to cross with the mutant SOD1 mouse, the Epha4KD isoform can still be phosphorylated through crossphosphorylation of the *Epha4* wild type allele that is present. In the Epha4<sup>+/-</sup> and the Epha4<sup>eGFP/+</sup> mice this crossphosphorylation is not possible as there is less Epha4 receptor or less Epha4 intracellular domain respectively. Homozygous EphA4<sup>KD/KD</sup> transgenic mice may solve the problem but are almost impossible to obtain, as we also experienced with the homozygous epha4 knockout mice.





## Chapter 3. The role of ephrin ligands in ALS

All experiments performed by Lies Schoonaert. Vessel permeability assay in collaboration with Thomas Mathivet

### 3.1 Introduction

Epha4 is a promiscuous receptor, interacting with both ephrina and ephrinb ligands. Reverse signaling through interaction of Epha4 with both ephrin A and ephrin B ligands has been reported. The formation of the anterior commissure of the forebrain depends on Epha4 reverse signaling through ephrinb2<sup>242, 244</sup>. Furthermore, long-term potentiation is mediated through reverse signaling involving the interaction of Epha4 on the motor neurons and ephrina3 on the astrocytes<sup>205</sup>. Since our data suggest reverse signaling to be involved in the modifying effect of Epha4 on ALS pathogenesis, we intended to determine which Epha4 ligands might be involved in this process.

Reverse signaling can occur through interaction of Epha4 with ephrin ligands on surrounding cells such as muscle cells, astrocytes, microglia and oligodendrocytes<sup>245</sup>. At the neuromuscular junction, Epha4 can interact with ephrina1, ephrina2, ephrina5 and ephrinb1<sup>246-247</sup>. In the CNS, ephrina1, ephrina3, ephrina5, ephrinb1 and ephrinb2 have been identified in oligodendrocyte precursor cells and in mature oligodendrocytes<sup>248-250</sup>. Ephrina5 and ephrinb2 are upregulated during oligodendrocyte differentiation<sup>248</sup>. Astrocytes express ephrina2, ephrina3, ephrina5 and ephrinb2<sup>251-252</sup>. Ephrina3 has a crucial function in synaptic plasticity as it is involved the regulation of hippocampal dendritic spine morphology and regulates the abundance of glial glutamate transporters<sup>205, 253-255</sup>. Astrocytic ephrinb2 regulates adult hippocampal neurogenesis and is highly upregulated in reactive astrocytes after spinal cord lesions<sup>252, 256-257</sup>. Ephrina5 is highly upregulated in astrocytes at the perilesioned area after experimental stroke<sup>218</sup>. Since our data suggest reverse signaling to be involved in the modifying effect of Epha4 on ALS pathogenesis, we intended to study the Epha4 ligands which may be involved in this process.

## 3.2 Results

### 3.2.1 Expression profile of ephrin ligands in the SOD1<sup>G93A</sup> mouse

As EphA4 interacts with ephrina ligands as well as ephrinb ligands, we investigated expression of all ephrin ligands in spinal cord of SOD1<sup>G93A</sup> mice at different time points during the disease progression using qPCR. Different ligands showed different changes during disease progression. Expression of ephrina2, ephrina3, ephrina5 and ephrinb2 decreased at end stage (Figure 3.1B,C,E,G). Ephrina1, ephrina4, ephrinb1 and ephrinb3 did not change expression during disease course (Figure 3.1A,D,F,H).

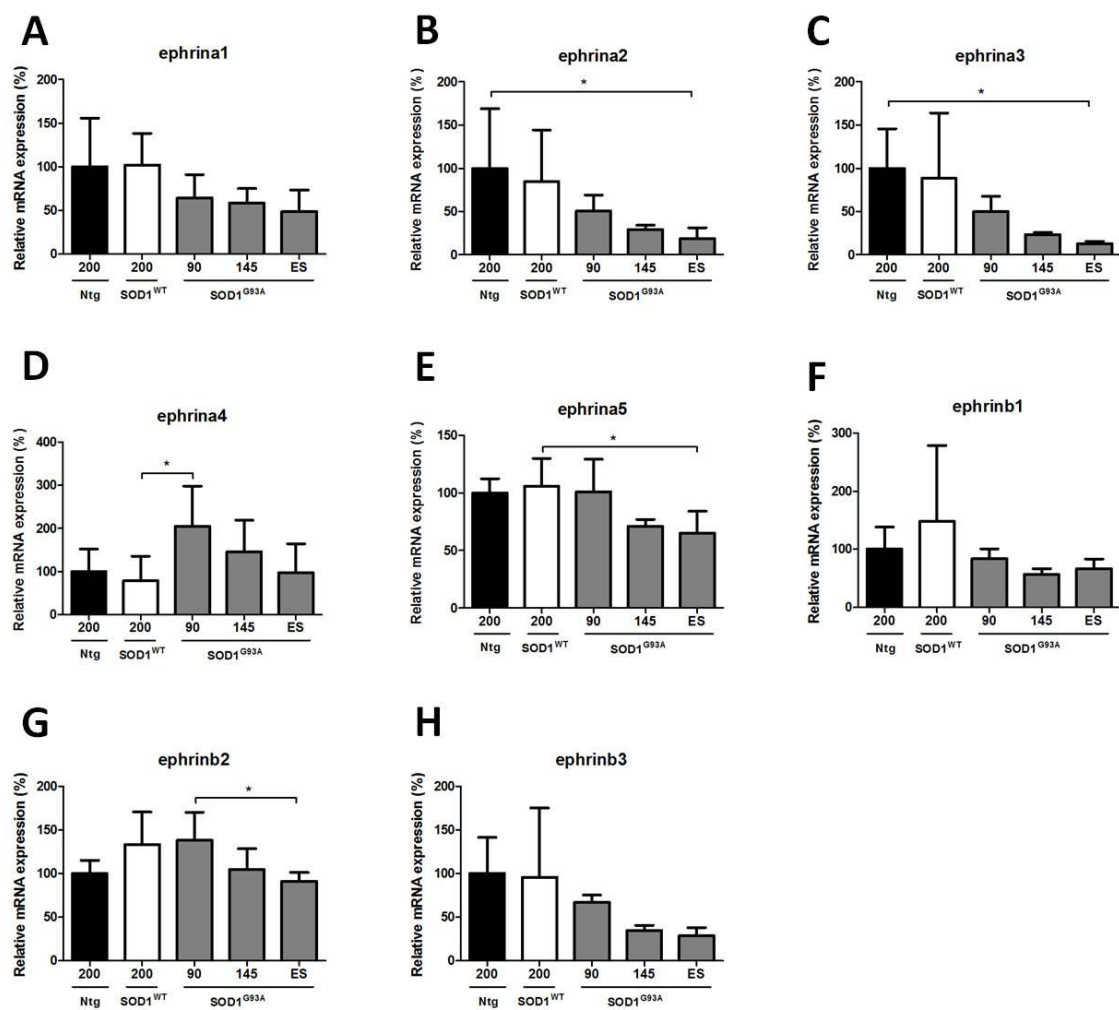


**Figure 3.1 Expression profile of ephrin ligands in the spinal cord of nontransgenic, SOD1<sup>WT</sup> and SOD1<sup>G93A</sup> mice.** (A) Quantitative RT-PCR of ephrina1 in ventral spinal cords of nontransgenic mice at P200 (n = 5, 100% expression), SOD1<sup>WT</sup> mice at P200 (n = 5, 102% expression) and SOD1<sup>G93A</sup> mice at P90 (n = 5, 64% expression), P145 (n = 5, 58% expression) and ES (n = 5, 49% expression). (B) Quantitative RT-PCR of ephrina2 in ventral spinal cords of nontransgenic mice at P200 (n = 5, 100% expression), SOD1<sup>WT</sup> mice at P200 (n = 5, 85% expression) and SOD1<sup>G93A</sup> mice at P90 (n = 5, 51% expression), P145 (n = 5, 29% expression) and ES (n = 5, 18% expression). (C) Quantitative RT-PCR of ephrina3 in ventral spinal cords of nontransgenic mice at P200 (n = 5, 100% expression), SOD1<sup>WT</sup> mice at P200 (n = 5, 88% expression) and SOD1<sup>G93A</sup> mice at P90 (n = 5, 50% expression), P145 (n = 5, 23% expression) and ES (n = 5, 13% expression). (D) Quantitative RT-PCR of ephrina4 in ventral spinal cords of nontransgenic mice at P200 (n = 6, 100% expression), SOD1<sup>WT</sup> mice at P200 (n = 6, 78% expression) and SOD1<sup>G93A</sup> mice at P90 (n = 6, 204% expression), P145 (n = 6, 146% expression) and ES (n = 6, 98% expression). (E) Quantitative RT-PCR of ephrina5 in ventral spinal cords of nontransgenic mice at P200 (n = 5, 100% expression), SOD1<sup>WT</sup> mice at P200 (n = 6, 106% expression) and SOD1<sup>G93A</sup> mice at P90 (n = 5, 101% expression), P145 (n = 4, 71% expression) and ES (n = 6, 65% expression). (F) Quantitative RT-PCR of ephrinb1 in ventral spinal cords of nontransgenic mice at P200 (n = 5, 100% expression), SOD1<sup>WT</sup> mice at P200 (n = 5, 148% expression) and SOD1<sup>G93A</sup> mice at P90 (n = 5, 84% expression), P145 (n = 5, 56% expression) and ES (n = 5, 67% expression). (G) Quantitative RT-PCR of ephrinb2 in ventral spinal cords of nontransgenic mice at P200 (n = 6, 100% expression), SOD1<sup>WT</sup> mice at P200 (n = 6, 133% expression) and SOD1<sup>G93A</sup> mice at P90 (n = 6, 138% expression), P145 (n = 6, 104% expression) and ES (n = 6, 91% expression). (H) Quantitative RT-PCR of ephrinb3 in ventral spinal cords of nontransgenic mice at P200 (n = 5, 100% expression), SOD1<sup>WT</sup> mice at P200 (n = 5, 96% expression) and SOD1<sup>G93A</sup> mice at P90 (n = 5, 67% expression), P145 (n = 5, 35% expression) and ES (n = 5, 29% expression). ANOVA tests were used for statistical analysis, \*p<0.05. Error bars denote standard deviation. RT-PCR, Real-Time Polymerase Chain Reaction; ES, End Stage

### 3.2.2 Expression profile of ephrinb2

In view of the pathogenic role of astrocytes in ALS and the fact that astrocytes are known to confer a hazardous effect in ALS, we focused on the ephrin ligands expressed by the astrocytes, and in particular on ephrinb2, as it is expressed both on resting and reactive astrocytes<sup>252, 256</sup>. Furthermore, there is evidence that astrocytic ephrinb2 affects recovery from spinal cord injury<sup>256-257</sup>. This improved recovery was correlated with an increased regenerative capacity of sprouting spinal cord axons<sup>212, 257</sup>.

To investigate the role of ephrinb2 in the pathogenesis of ALS, we first studied the ephrinb2 expression profile in spinal cords of wild type SOD1 and mutant SOD1 mice. Ephrinb2 immunoreactivity was present in neurons and oligodendrocytes in SOD1<sup>WT</sup> and SOD1<sup>G93A</sup>, as shown by its colocalisation with the neuronal marker Neuronal-specific nuclear protein (NeuN) and the oligodendrocytic marker Mouse Monoclonal APC antibody (cc1) (Figure 3.2 and 3.3). Ephrinb2 expression was not detected in microglia, as shown by absence of its colocalisation with the microglial marker Cluster of Differentiation Molecule 11B (cd11b) (Figure 3.4). Interestingly, in the spinal cord of end stage SOD1<sup>G93A</sup> mice, ephrinb2 expression was prominently present in reactive astrocytes, which is in accordance with high ephrinb2 expression in reactive astrocytes after spinal cord lesions (Figure 3.5)<sup>256-257</sup>.

In mutant SOD1<sup>G93A</sup> mice ephrinb2 was expressed in the nucleus of astrocytes at P60 and P90 (Figure 3.6A). From P120 on ephrinb2 was highly expressed in the nucleus and the processes of reactive astrocytes. Ephrinb2 was present in neurons at all stages (Figure 3.6B).

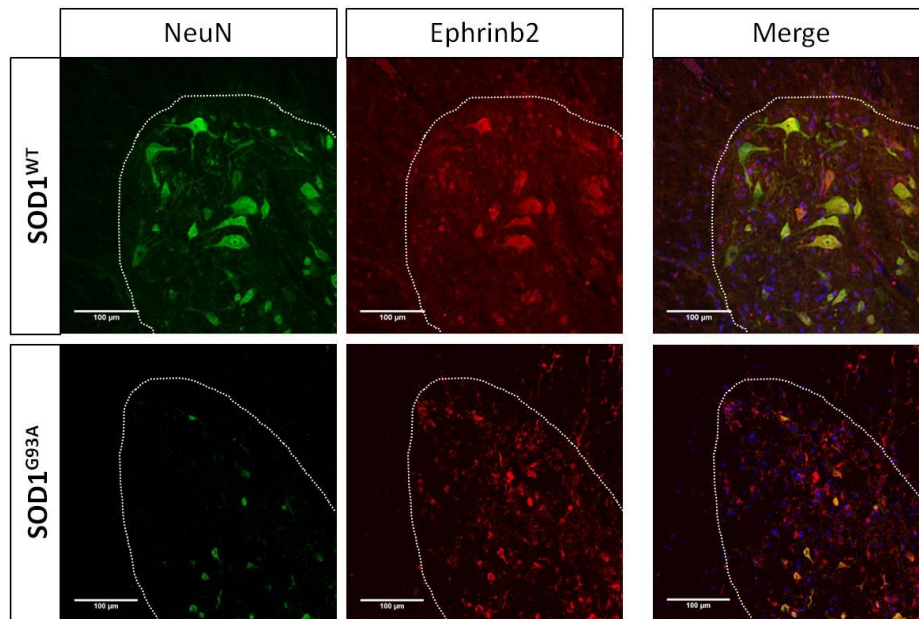


**Figure 3.2** Motor neurons in the spinal cord of end stage  $SOD1^{G93A}$  mice and age-matched  $SOD1^{WT}$  mice express ephrinb2. Ephrinb2 was co-stained with the neuronal marker, NeuN, in the spinal cord of  $SOD1^{WT}$  (150 d) and end stage  $SOD1^{G93A}$  mice.

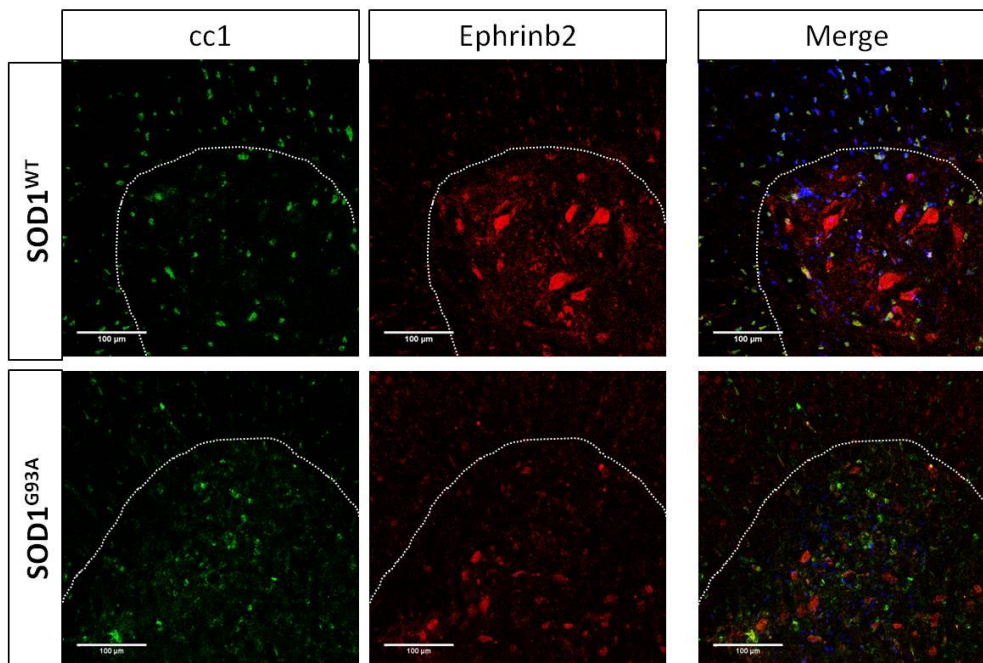


**Figure 3.3** Oligodendrocytes in the spinal cord of end stage  $SOD1^{G93A}$  mice and age-matched  $SOD1^{WT}$  mice express ephrinb2. Ephrinb2 was co-stained with the oligodendrocytic marker, cc1, in the spinal cord of  $SOD1^{WT}$  (150 d) and end stage  $SOD1^{G93A}$  mice.

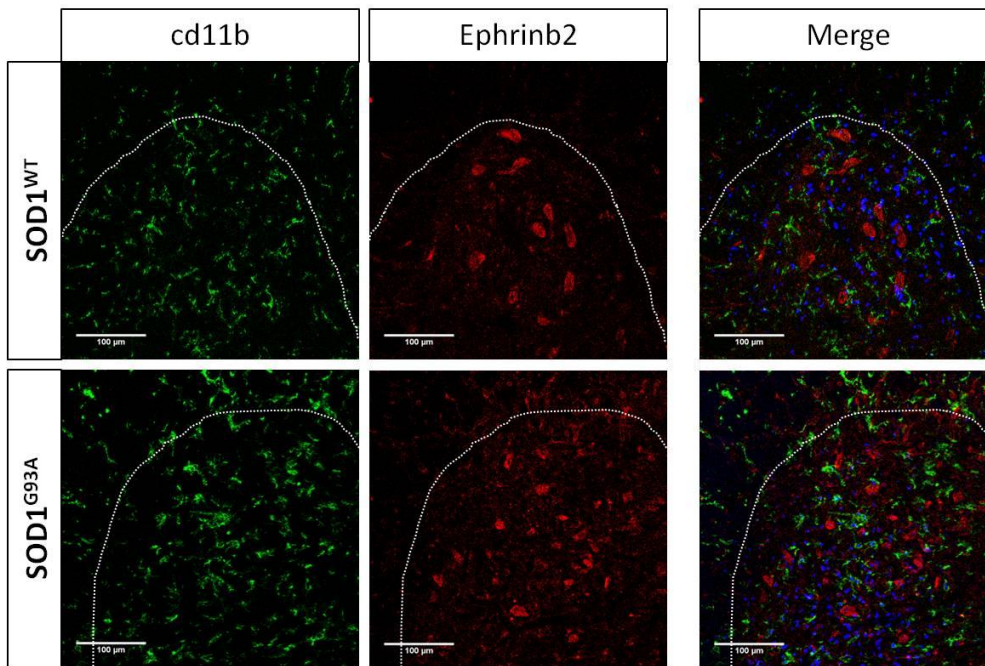


**Figure 3.4** Microglia in the spinal cord of end stage  $SOD1^{G93A}$  mice and age-matched  $SOD1^{WT}$  mice do not express ephrinb2. Ephrinb2 was co-stained with the microglial marker, cd11b, in the spinal cord of  $SOD1^{WT}$  (150 d) and end stage  $SOD1^{G93A}$  mice.

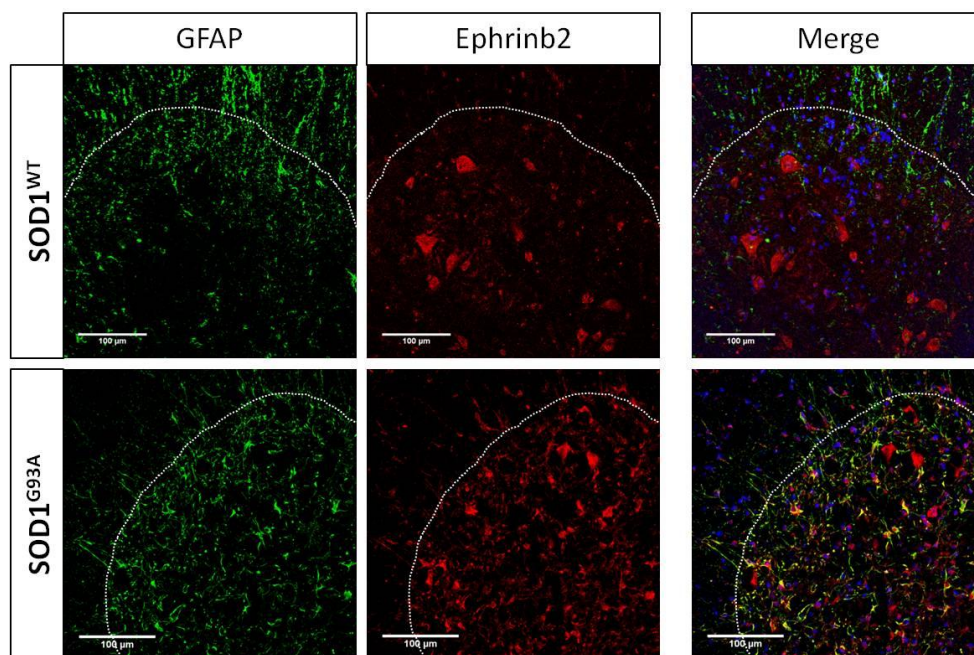


**Figure 3.5** Reactive astrocytes in the spinal cord of end stage  $SOD1^{G93A}$  mice ephrinb2. Ephrinb2 was co-stained with the neuronal marker, GFAP, in the spinal cord of  $SOD1^{WT}$  (150 d) and end stage  $SOD1^{G93A}$  mice. Resting astrocytes in the spinal cord of  $SOD1^{WT}$  mice only showed faint immunoreactivity in their nucleus, but reactive astrocytes in the spinal cord of end stage  $SOD1^{G93A}$  mice expressed ephrinb2 both in their cell bodies and their processes.

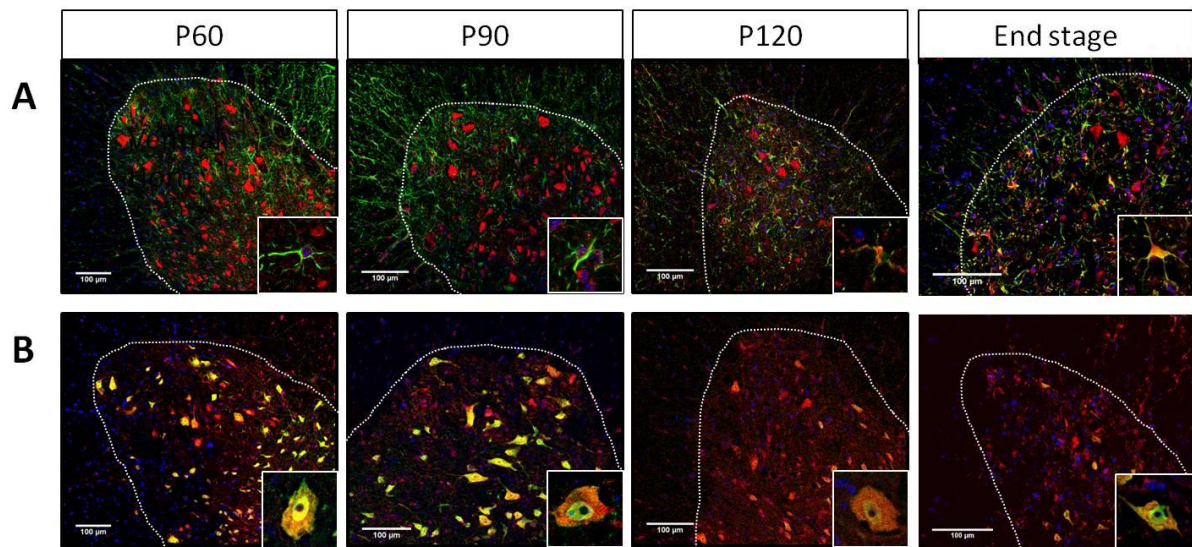


**Figure 3.6 Ephrinb2 expression in astrocytes and motor neurons over disease progression in the  $SOD1^{G93A}$  mouse model.** (A) At P60 and P90 ephrinb2 showed weak expression in the nucleus of astrocytes, while it was highly expressed in the nucleus and the processes of reactive astrocytes from P120 on. Co-labeling was performed with ephrinb2 (red) and the astrocytic marker GFAP (green). (B) Ephrinb2 was expressed in motor neurons during the disease course. Co-labeling was performed with ephrinb2 (red) and the neuronal marker NeuN (green).

In order to investigate whether these mice data are of relevance for human ALS, we studied ephrinB2 expression in the spinal cord of ALS patients and controls. As shown in figure 3.7, ephrinB2 expression was found to be present in motor neurons in the spinal cord of controls and of ALS patients. Interestingly, reactive astrocytes present in the spinal cord of ALS patients abundantly expressed ephrinB2 (Figure 3.7) much alike what we observed in the mutant SOD1 mouse model.



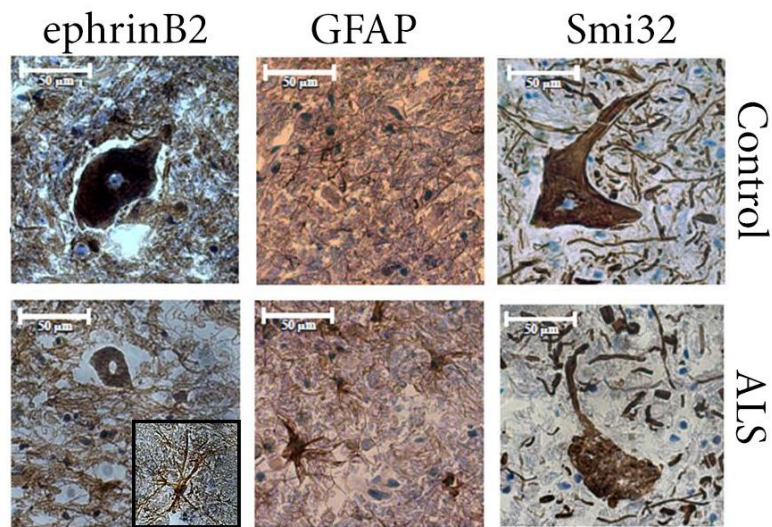


**Figure 3.7 EphrinB2 was expressed in motor neurons and reactive astrocytes in spinal cord of ALS-patients and controls.** Neuronal expression was shown by DAB-staining of the neuronal marker Smi32 in control and ALS spinal cord. GFAP expression was detected in resting astrocytes in control spinal cord and in reactive astrocytes in ALS spinal cord. EphrinB2 expression was observed in neurons in control and ALS spinal cord and in reactive astrocytes in ALS spinal cord. DAB, 3,3' diaminobenzidine tetrahydrochloride

In  $SOD1^{G93A}$  mice, ephrinb2 mRNA expression in the spinal cord was somewhat variable during the disease course; expression was lowest at P140, slightly increasing again during end stage disease (Figure 3.8C). These small fluctuations were not apparent at the protein level (Figure 3.9). mRNA and protein levels of ephrinb2 were unaltered in nontransgenic and  $SOD1^{WT}$  mice at similar time points (Figure 3.8A,B and figure 3.9).

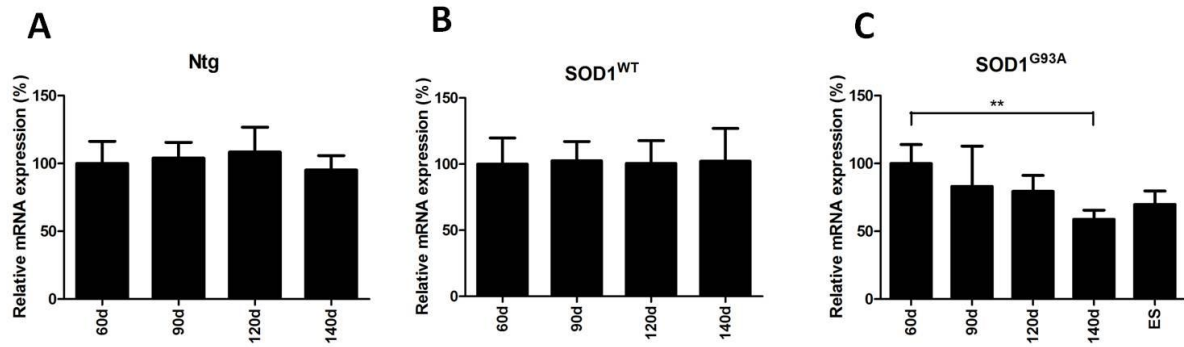


**Figure 3.8 Expression profile of ephrinb2 in the spinal cord of nontransgenic, SOD1<sup>WT</sup> and SOD1<sup>G93A</sup> mice.** (A) Quantitative RT-PCR of ephrinb2 in ventral spinal cords of nontransgenic mice at different ages: P60 (n = 5, 100% expression), P90 (n = 6, 104% expression), P120 (n = 6, 109% expression) and P140 (n = 9, 95% expression). (B) Quantitative RT-PCR of ephrinb2 in ventral spinal cords of SOD1<sup>WT</sup> mice at different ages: P60 (n = 4, 100% expression), P90 (n = 4, 103% expression), P120 (n = 5, 101% expression) and P140 (n = 5, 102% expression). (C) Quantitative RT-PCR of ephrinb2 in ventral spinal cords of SOD1<sup>G93A</sup> mice at different ages: P60 (n = 7, 100% expression), P90 (n = 5, 83% expression), P120 (n = 7, 79% expression), P140 (n = 4, 59% expression) and ES (n = 4, 70% expression). ANOVA tests were used for statistical analysis, \*p<0.05. Error bars denote standard deviation. RT-PCR, Real-Time Polymerase Chain Reaction; ES, End Stage

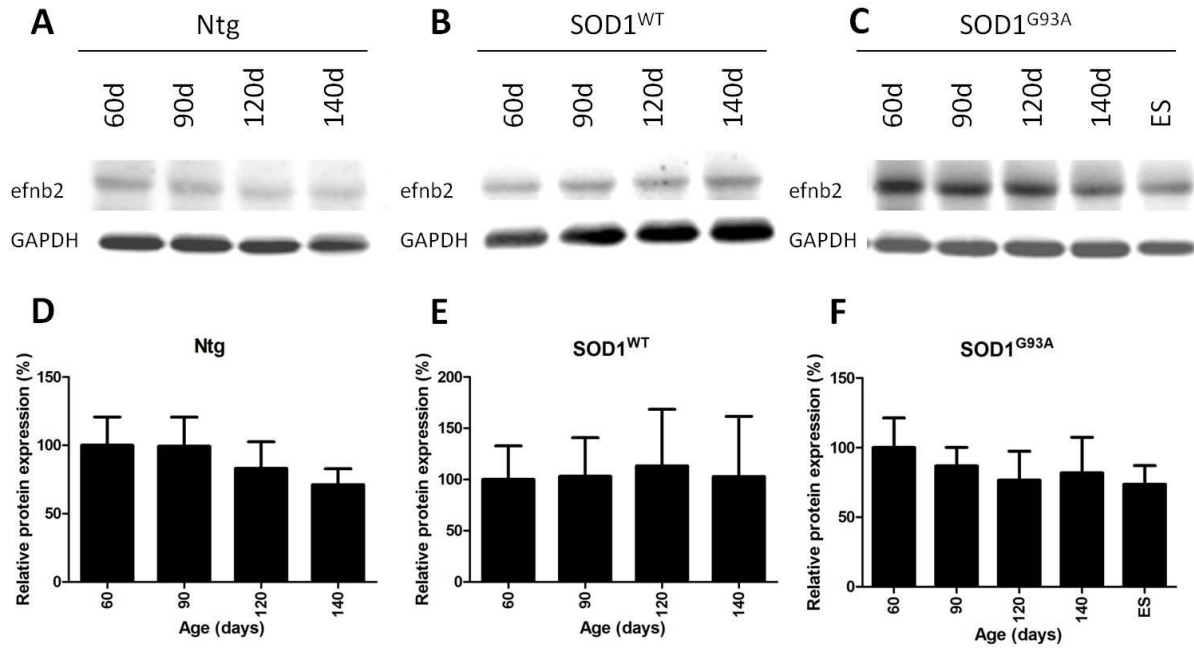


**Figure 3.9 Expression profile of ephrinb2 in the spinal cord of nontransgenic, SOD1<sup>WT</sup> and SOD1<sup>G93A</sup> mice.** (A,D) Western blot for ephrinb2 on ventral spinal cords of nontransgenic mice at different ages: P60 (n = 5, 100% expression), P90 (n = 5, 99% expression), P120 (n = 5, 83% expression), P140 (n = 5, 71% expression). (B,E) Western blot for ephrinb2 on ventral spinal cords of SOD1<sup>WT</sup> mice at different ages: P60 (n = 4, 100%) , P90 (n = 4, 103% expression), P120 (n = 4, 113% expression) and P140 (n = 3, 103% expression). (C,F) Western blot for ephrinb2 on ventral spinal cords of SOD1<sup>G93A</sup> mice at different ages: P60 (n = 4, 100% expression), P90 (n = 4, 87% expression), P120 (n = 4, 77% expression), P140 (n = 4, 82% expression) and ES (n = 4, 74% expression)) at different ages. GAPDH (37 kDa) was used as loading control (Figure A,B,C). Error bars denote standard deviation; ES, End Stage

### 3.2.3 Effect of ephrinb2 on ALS in the SOD1<sup>G93A</sup> mouse model

To assess the role of ephrinb2 in the pathogenesis of ALS, we studied the effect of deletion of ephrinb2 in the SOD1<sup>G93A</sup> mouse model. As the ephrinb2<sup>-/-</sup> mouse is embryonically lethal with major cardiovascular defects, we used the ephrinb2 conditional knockout mouse (Figure 3.10A)<sup>258</sup>. In this mouse model exon two of the *ephrinb2* gene is flanked by loxP sites and will be excised when the Cre enzyme is present and active (Figure 3.10A). To ascertain that ephrinb2 levels are not altered by the insertion of the loxP sites we performed quantitative real-time PCR on brain and spinal cord of efnb2<sup>+/+</sup>, efnb2<sup>fl/+</sup> and efnb2<sup>fl/fl</sup> mice; as expected no differences in ephrinb2 RNA levels were observed (Figure 3.10B,C).

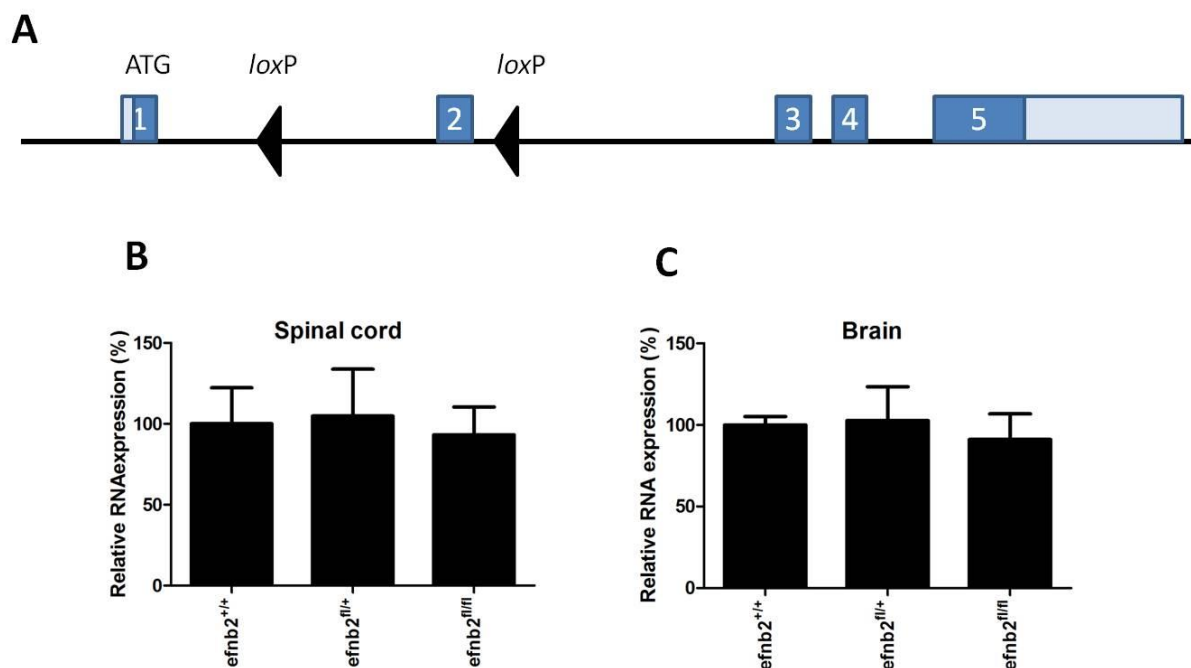


**Figure 3.10 The ephrinb2 conditional knockout mouse.** (A) Schematic representation of the ephrinb2 conditional knockout mouse (B) Quantitative RT-PCR of ephrinb2 in lumbar spinal cords of efnb2<sup>+/+</sup> mice (n = 3, 100% expression), efnb2<sup>fl/+</sup> mice (n = 4, 105% expression) and efnb2<sup>fl/fl</sup> mice (n = 4, 93% expression). (B) Quantitative RT-PCR of ephrinb2 in brains of efnb2<sup>+/+</sup> mice (n = 3, 100% expression), efnb2<sup>fl/+</sup> mice (n = 4, 103% expression) and efnb2<sup>fl/fl</sup> mice (n = 4, 91% expression). Error bars denote standard deviation. RT-PCR, Real-Time Polymerase Chain Reaction

### 3.2.4 Effect of selective deletion of ephrinb2 from astrocytes in the SOD1<sup>G93A</sup> mouse model

As ephrinb2 expression is upregulated in reactive astrocytes, we investigated whether deletion of ephrinb2 from reactive astrocytes influences disease progression in ALS. To this end, we used a GFAPCre mouse in which Cre is expressed in astrocytes from E14.5 on<sup>259</sup>. Therefore, our laboratory assessed the selectivity of the GFAPCre system by crossbreeding this GFAPCre mouse with an enhanced Yellow Fluorescent Protein (eYFP) reporter mouse<sup>260</sup>. In this reporter mouse the *eYFP* cDNA was preceded by a loxP-flanked stop sequence. YFP expression showed highest expression in astrocytes as expected, but was also expressed in neurons and oligodendrocytes (A. Nonneman et al. unpublished results). These findings suggest that in the *efnb2*<sup>fl/fl</sup>; GFAP mouse ephrinb2 expression is not exclusively reduced in astrocytes, but also in other cell types.

Therefore we used the Cx30CreER mouse which expresses the Cre enzyme in astrocytes only<sup>261</sup>. In the spinal cord of Cx30CreER mice crossed with the eYFP reporter mouse, YFP expression was present specifically in the astrocytes (A. Nonneman et al. unpublished results). High recombination efficiency was detected as almost all astrocytes showed YFP expression.

In the Cx30CreER mouse expression of the CreER fusion protein can be induced after administration of Tamoxifen (Tx). We crossbred the homozygous ephrinb2 conditional knockout mice with the Cx30CreER and the SOD1<sup>G93A</sup> mouse. All mice were treated with Tx 60 days after birth (P60). To assess deletion of ephrinb2, we compared the ephrinb2 protein expression in spinal cord lysates of *efnb2*<sup>fl/fl</sup>; Cx30; SOD1<sup>G93A</sup> and *efnb2*<sup>fl/fl</sup>; SOD1<sup>G93A</sup> 20 days after Tx administration (P80) and at end stage. No difference in ephrinb2 expression was detected between *efnb2*<sup>fl/fl</sup>; Cx30; SOD1<sup>G93A</sup> mice and *efnb2*<sup>fl/fl</sup>; SOD1<sup>G93A</sup> mice at P80, which is probably explained by the fact that astrocytes only weakly express ephrinb2 early in the disease (Figure 3.13A,B). However, at ES, when astrocytes abundantly express ephrinb2, a clear decrease in ephrinb2 protein expression was observed in *efnb2*<sup>fl/fl</sup>; Cx30; SOD1<sup>G93A</sup> mice (Figure 3.13C,D).

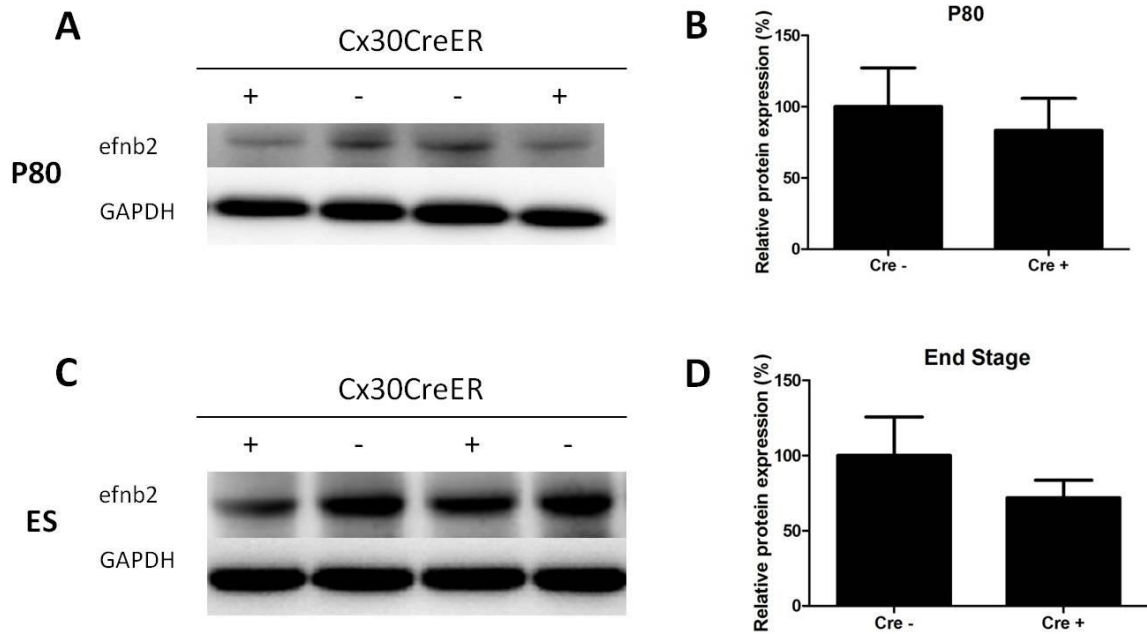


**Figure 3.13 Ephrinb2 excision in lumbar spinal cord in  $efnb2^{fl/fl}$ ;  $SOD1^{G93A}$  mice and  $efnb2^{fl/fl}$ ; Cx30;  $SOD1^{G93A}$  mice at P80 and end stage (A,B) Western blot of ephrinb2 in lumbar spinal cords of  $efnb2^{fl/fl}$ ;  $SOD1^{G93A}$  mice at P80 (n = 5, 100% expression) and  $efnb2^{fl/fl}$ ; Cx30;  $SOD1^{G93A}$  mice at P80 (n = 5, 83% expression, p = 0.3804). (C,D) Western blot of ephrinb2 in lumbar spinal cords of  $efnb2^{fl/fl}$ ;  $SOD1^{G93A}$  mice at ES (n = 5, 100% expression) and  $efnb2^{fl/fl}$ ; Cx30;  $SOD1^{G93A}$  mice at ES (n = 5, 72% expression, p = 0.0573). GAPDH was used as loading control. Error bars denote standard deviation; ES, End Stage**

We then investigated the effect of this selective deletion of ephrinb2 from the astrocytes on disease onset and survival in the  $SOD1^{G93A}$  mouse. Onset as assessed by hanging wire test was not different in  $efnb2^{fl/fl}$ ; Cx30;  $SOD1^{G93A}$  mice as compared to  $efnb2^{fl/fl}$ ;  $SOD1^{G93A}$  mice (Figure 3.14A). Unexpectedly, deletion of ephrinb2 from astrocytes worsened disease: disease duration was shortened by not less than 34% ( $efnb2^{fl/fl}$ ;  $SOD1^{G93A}$  (34d) and  $efnb2^{fl/fl}$ ; Cx30;  $SOD1^{G93A}$  (22.5 d) p = 0.0482) (Figure 3.14B) and survival was decreased (Average survival:  $efnb2^{fl/fl}$ ;  $SOD1^{G93A}$  (166d) and  $efnb2^{fl/fl}$ ; Cx30;  $SOD1^{G93A}$  (157 d) p = 0.0297) (Figure 3.14C,D). Overall, deleting ephrinb2 specifically from astrocytes aggravated the ALS phenotype.

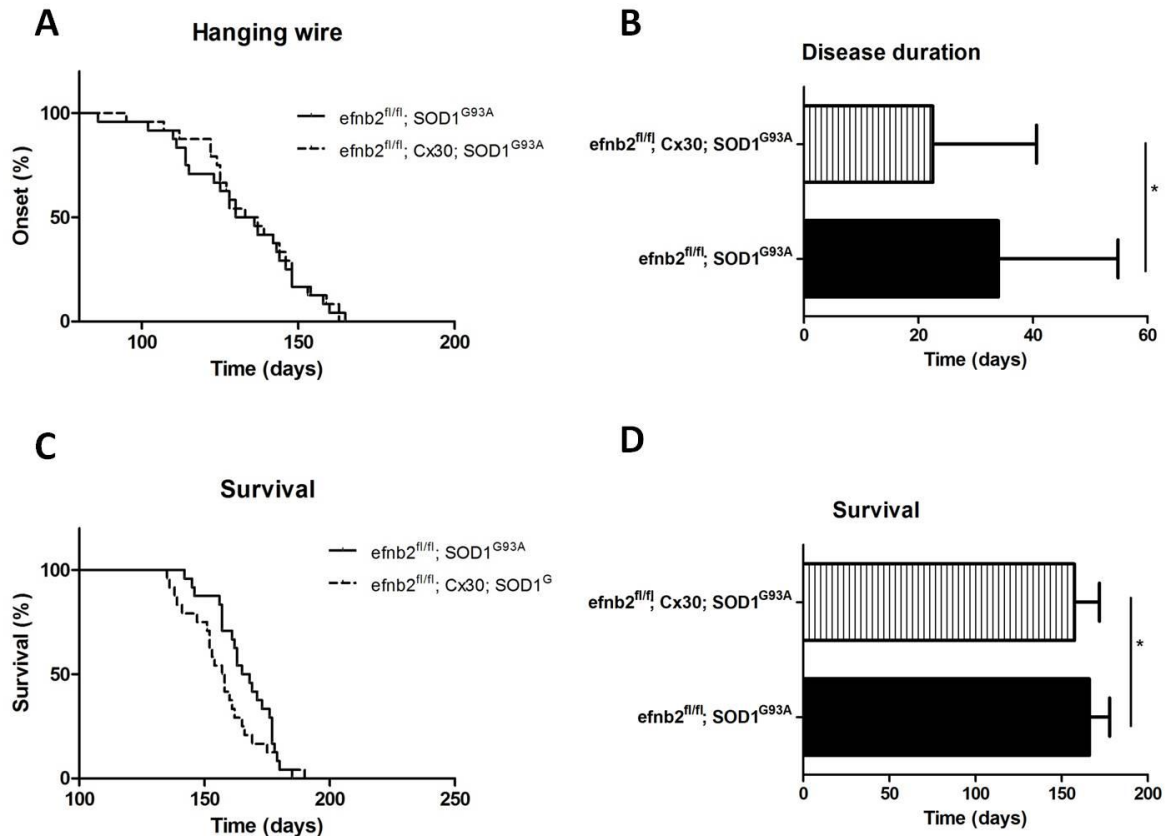


**Figure 3.14 Astrocytic deletion of ephrinb2 with the Cx30CreER mouse did not influence disease onset, but decreased the survival in  $SOD1^{G93A}$  mice.** (A) Disease onset as determined by hanging wire. Median disease onset: 133 d ( $efnb2^{fl/fl}; SOD1^{G93A}$ ,  $n = 24$ ) and 135 d ( $efnb2^{fl/fl}; Cx30; SOD1^{G93A}$ ,  $n = 24$ ). (B) Average disease duration as determined by hanging wire: 34 d ( $efnb2^{fl/fl}; SOD1^{G93A}$ ,  $n = 24$ ), 23 d ( $efnb2^{fl/fl}; Cx30; SOD1^{G93A}$ ,  $n = 24$ ,  $p = 0.0482$ ). (C,D) Average survival: 166 d ( $efnb2^{fl/fl}; SOD1^{G93A}$ ,  $n = 24$ ) and 157 d ( $efnb2^{fl/fl}; Cx30; SOD1^{G93A}$ ,  $n = 24$ )  $p = 0.0297$ . \* $p < 0.05$ . Error bars denote standard deviation.

To better understand this unexpected result, we investigated whether deleting ephrinb2 from astrocytes affects the glial population: astrocytes, microglia, NG2 glia and oligodendrocytes, all known to play a role in ALS. To do so, we studied the mRNA levels of several glial markers in whole spinal cord lysates of  $efnb2^{fl/fl}; Cx30; SOD1^{G93A}$  and  $efnb2^{fl/fl}; SOD1^{G93A}$  mice at P80 and at ES. As expected, the mRNA levels of astrocytic (Glial Fibrillary Acid Protein (GFAP) and 10-formyltetrahydrofolate dehydrogenase (Aldh1l1)), microglial (CX3C Chemokine Receptor 1 (CX3CR1)) and oligodendrocyte precursor (Neural/glial antigen 2 (NG2)) markers were increased and the oligodendrocytic marker Myelin Basic Protein (MBP) was significantly decreased at end stage compared to P80 mice (Figure 3.15). Interestingly,  $efnb2^{fl/fl}; Cx30; SOD1^{G93A}$  mice at end stage showed decreased levels of GFAP mRNA, a reactive astrocyte marker, compared to  $efnb2^{fl/fl}; SOD1^{G93A}$  mice (Figure 3.15A). This difference was not seen for Aldh1l1, a general astrocyte marker (Figure 3.15B). Surprisingly, the mRNA level of the microglial marker CX3CR1 was highly upregulated in  $efnb2^{fl/fl}; Cx30; SOD1^{G93A}$  mice compared to  $efnb2^{fl/fl}; SOD1^{G93A}$  mice (Figure 3.15C). The

mRNA level of NG2 was not different between  $efnb2^{fl/fl}$ ; Cx30; SOD1<sup>G93A</sup> and  $efnb2^{fl/fl}$ ; Cx30; SOD1<sup>G93A</sup> mice (Figure 3.15D). MBP expression was decreased in  $efnb2^{fl/fl}$ ; Cx30; SOD1<sup>G93A</sup> mice at end stage compared to  $efnb2^{fl/fl}$ ; SOD1<sup>G93A</sup> mice (Figure 3.15E). Thus, reduced astrocytic ephrinb2 expression resulted in a decrease expression of GFAP, a marker for reactive astrocytes expression, and MBP, an oligodendrocyte marker, and an increase in CX3CR1, a marker for microglia.

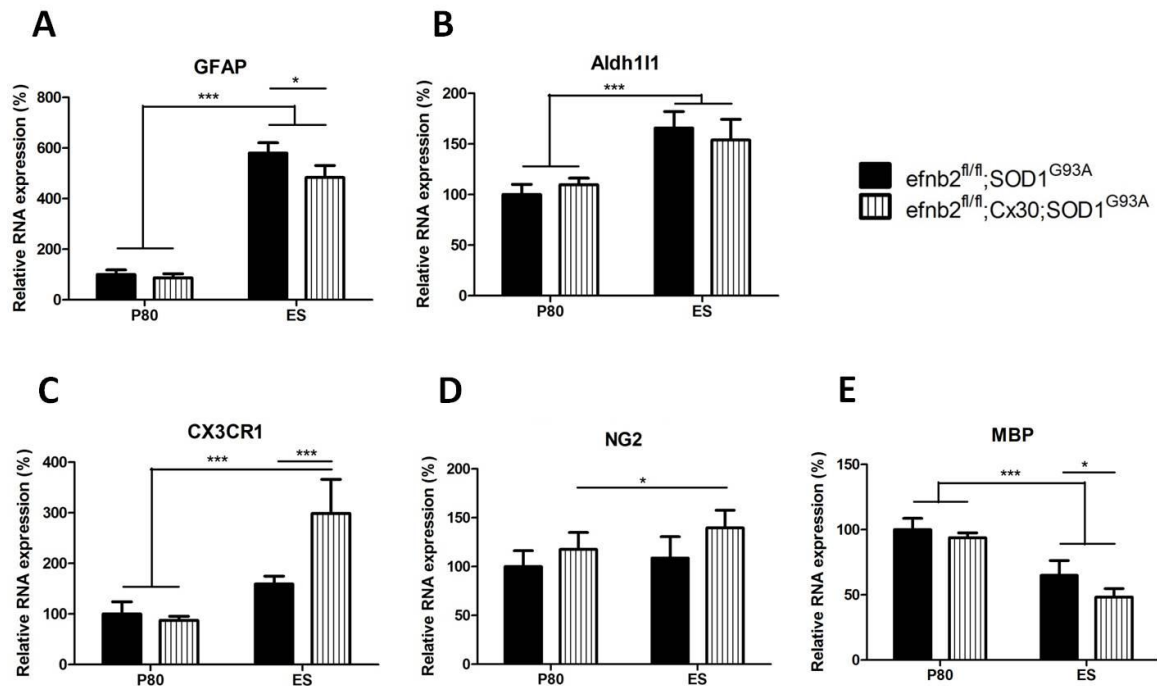


**Figure 3.15 Quantitative RT-PCR analyses of gli-related molecules in the lumbar spinal cord of  $efnb2^{fl/fl}$ ; SOD1<sup>G93A</sup> and  $efnb2^{fl/fl}$ ; Cx30; SOD1<sup>G93A</sup> mice.** (A) Quantitative RT-PCR of GFAP in lumbar spinal cords of  $efnb2^{fl/fl}$ ; SOD1<sup>G93A</sup> mice at P80 (n = 4, 100% expression) and ES (n = 4, 580% expression), and  $efnb2^{fl/fl}$ ; Cx30; SOD1<sup>G93A</sup> mice at P80 (n = 4, 87% expression) and ES (n = 4, 484% expression); two-way ANOVA, both age and genotype factor are statistically significant, t-test age p = 0.0215. (B) Quantitative RT-PCR of Aldh11l1 in lumbar spinal cords of  $efnb2^{fl/fl}$ ; SOD1<sup>G93A</sup> mice at P80 (n = 4, 100% expression) and ES (n = 4, 166% expression), and  $efnb2^{fl/fl}$ ; Cx30; SOD1<sup>G93A</sup> mice at P80 (n = 4, 110% expression) and ES (n = 4, 154% expression); two-way ANOVA, only age factor is statistically different. (C) Quantitative RT-PCR of CX3CR1 in lumbar spinal cords of  $efnb2^{fl/fl}$ ; SOD1<sup>G93A</sup> mice at P80 (n = 4, 100% expression) and ES (n = 4, 159% expression), and  $efnb2^{fl/fl}$ ; Cx30; SOD1<sup>G93A</sup> mice at P80 (n = 4, 87% expression) and ES (n = 4, 191% expression); two-way ANOVA, both age and genotype are statistically significant, t-test ES p = 0.0069. (D) Quantitative RT-PCR of NG2 in lumbar spinal cords of  $efnb2^{fl/fl}$ ; SOD1<sup>G93A</sup> mice at P80 (n = 4, 100% expression) and ES (n = 4, 109% expression), and  $efnb2^{fl/fl}$ ; Cx30; SOD1<sup>G93A</sup> mice at P80 (n = 4, 118% expression) and ES (n = 4, 140% expression); two-way ANOVA, only genotype factor is statistically significant. (E) Quantitative RT-PCR of MBP in lumbar spinal cords of  $efnb2^{fl/fl}$ ; SOD1<sup>G93A</sup> mice at P80 (n = 4, 100% expression) and ES (n = 4, 65% expression), and  $efnb2^{fl/fl}$ ; Cx30; SOD1<sup>G93A</sup> mice at P80 (n = 4, 94% expression) and ES (n = 4, 48% expression); two-way ANOVA, both age and genotype factor are statistically significant, t-test ES p = 0.0434. Each result was normalized with qBase to 18s, GAPDH and polr2a. \*p < 0.05, \*\*p < 0.01, \*\*\*p < 0.001. Error bars denote standard deviation. RT-PCR, Real-Time Polymerase Chain Reaction; ES, End Stage



To explain how impairing astrocyte function through astrocyte-specific deletion of ephrinb2 worsens ALS, we considered the role ephrinb2 plays in the sprouting of endothelial cells<sup>262-263</sup>. Ephrinb2 might have a similar effect in astrocytes on the motility and morphology of its processes. As one functions of the astrocytes is the establishment and maintenance of the BBB with their so-called endfeet, we hypothesized that loss of ephrinb2 from astrocytes may impair the integrity of the blood brain barrier, which then may contribute to worsening of the disease. BBB integrity was assessed by perfusing *efnb2<sup>fl/fl</sup>*; Cx30CreER and *efnb2<sup>fl/fl</sup>* mice two to three months after tamoxifen administration with Evans blue fluorescent dye. Leakage of the dye into the parenchyma was used as a measure for BBB leakiness. Extravasation of dye in the brain of *efnb2<sup>fl/fl</sup>*; Cx30CreER mice clearly exceeded that in *efnb2<sup>fl/fl</sup>* mice (Figure 3.16). These data suggest that deletion of ephrinb2 from the astrocytes impairs the integrity of the BBB.

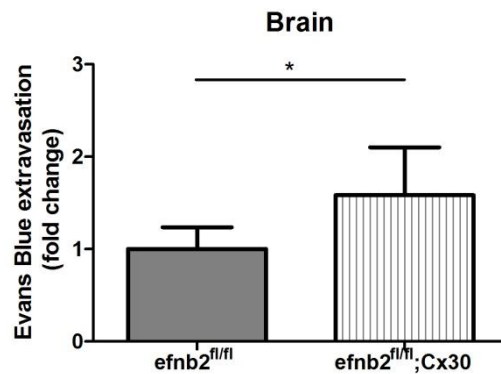


**Figure 3.16 Evans blue quantification in the brain of *efnb2<sup>fl/fl</sup>* and *efnb2<sup>fl/fl</sup>; Cx30* mice.** Two hours after Evans blue intravenous injection *efnb2<sup>fl/fl</sup>* (n = 5) and *efnb2<sup>fl/fl</sup>; Cx30* (n = 8) mice were sacrificed and intracardially perfused with 2% PFA solution. Evans blue quantity was calculated using a standard curve. A significant increase was detected in the brain of *efnb2<sup>fl/fl</sup>; Cx30* mice. \*p < 0.05. Error bars denote standard deviation. PFA, paraformaldehyde

To further elucidate this in the context of ALS, we investigated the BBB integrity in *SOD1<sup>G93A</sup>* mice at different time points during the disease progression. Increased BBB leakage and Blood Spinal Cord Barrier (BSCB) leakage was detected in brain and in spinal cord in *SOD1<sup>G93A</sup>* mice during disease progression while no leakage was detected in age-matched *SOD1<sup>WT</sup>* mice (Figure 3.17A,B). Deletion of ephrinb2 from astrocytes in *SOD1<sup>G93A</sup>* mice further increased BBB leakiness in brain as well as in spinal cord (Figure 3.17C,D). The increased leakage was already detectable at P100-110, to further increase at P140.

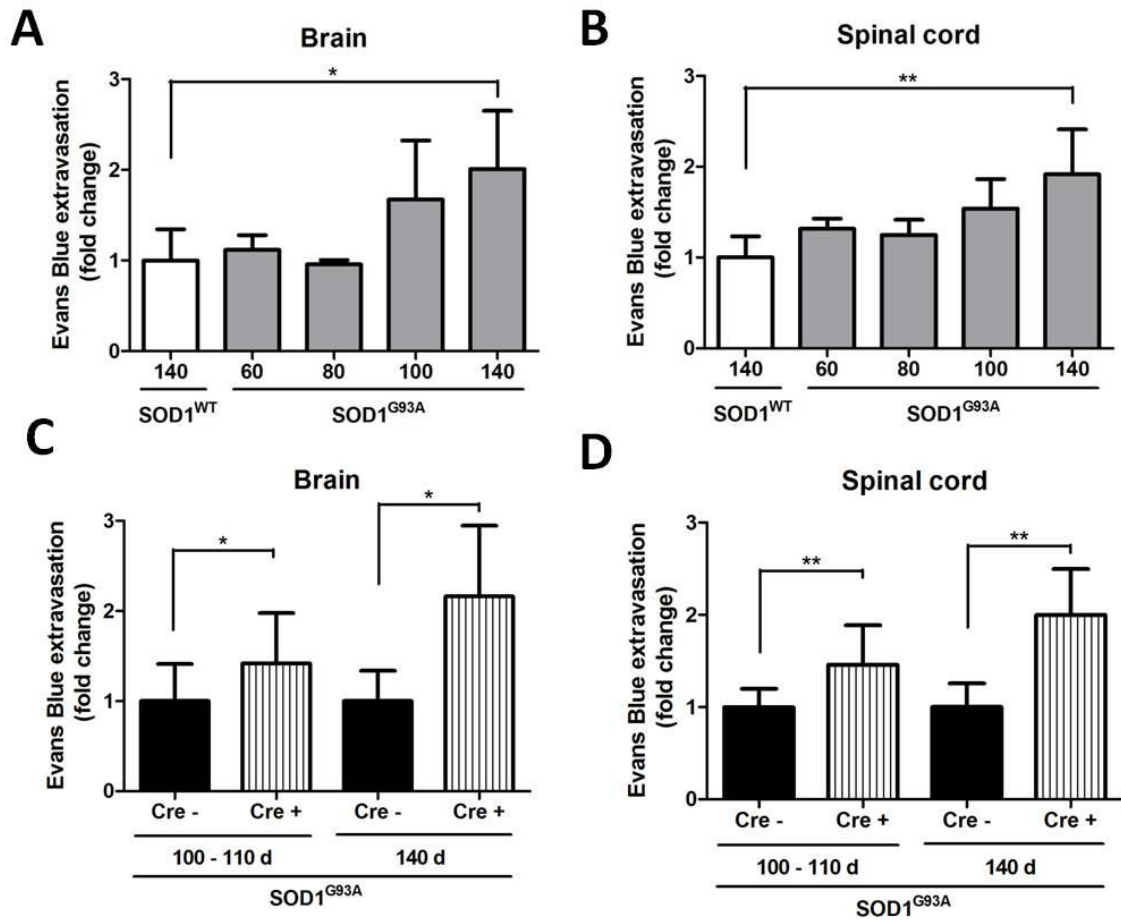


**Figure 3.17 Evans blue quantification in brain and spinal cord.** Two hours after Evans blue intravenous injection mice were sacrificed and intracardially perfused with 2% PFA solution. Evans blue quantity was calculated using a standard curve. (A) Evans blue extravasation in brain of SOD1<sup>WT</sup> mice at P140 (n = 5, mean = 1.00) and SOD1<sup>G93A</sup> mice at P60 (n = 4, mean = 1.12), P80 (n = 3, mean = 0.96), P100 (n = 6, mean = 1.67) and P140 (n = 4, mean = 2.01). (B) Evans blue extravasation in spinal cord of SOD1<sup>WT</sup> mice at P140 (n = 5, mean = 1.00) and SOD1<sup>G93A</sup> mice at P60 (n = 4, mean = 1.32), P80 (n = 3, mean = 1.25), P100 (n = 6, mean = 1.54) and P140 (n = 4, mean = 1.92). (C) Evans blue extravasation in brain of efnb2<sup>fl/fl</sup>; SOD1<sup>G93A</sup> mice at P100 – 110 Cx30Cre negative (n = 4, mean = 1.00) and Cx30Cre positive (n = 5; mean = 1.42) and efnb2<sup>fl/fl</sup>; SOD1<sup>G93A</sup> mice at P140 Cx30Cre negative (n = 4, mean = 1.00) and Cx30Cre positive (n = 5; mean = 2.16). (D) Evans blue extravasation in spinal cord of efnb2<sup>fl/fl</sup>; SOD1<sup>G93A</sup> mice at P100 – 110 Cx30Cre negative (n = 4, mean = 1.00) and Cx30Cre positive (n = 5; mean = 1.46) and efnb2<sup>fl/fl</sup>; SOD1<sup>G93A</sup> mice at P140 Cx30Cre negative (n = 4, mean = 1.00) and Cx30Cre positive (n = 5; mean = 2.00). p < 0.05; \*\*p < 0.01. Error bars denote standard deviation. PFA, paraformaldehyde

### 3.3 Discussion

In this chapter, we explored the potential role of ephrin ligands in the pathogenesis of ALS. We quantified all ephrins in the spinal cord of the SOD1<sup>G93A</sup> mouse, and although the expression of some ephrins temporarily increased with disease progression, no consistent pattern emerged. We therefore concentrated on astrocytic ephrins, more specifically on ephrinb2. We found ephrinb2 to be expressed in neurons, oligodendrocytes and astrocytes. We detected high ephrinb2 expression in the neurons in the spinal cord of adult SOD1<sup>WT</sup> and SOD1<sup>G93A</sup> mice which is in agreement with high ephrinb2 RNA expression in isolated cortical neurons of P7 mice<sup>264</sup>. This neuronal expression decreased during disease progression as motor neurons degenerate. The astrocytic ephrinb2 expression also changed with disease progression in the SOD1<sup>G93A</sup> mouse model. At P60 and P90 ephrinb2 showed weak nuclear expression in astrocytes while from P120 on ephrinb2 was detected throughout the astrocytes, including its processes. The expression of ephrinb2 in reactive astrocytes has already been reported<sup>256-257</sup>. mRNA and protein levels of ephrinb2 did not show major changes over disease progression in the SOD1<sup>G93A</sup> mouse model, which can be explained by a decreased neuronal expression as neurons degenerate and an upregulated expression in reactive astrocytes.

To delete ephrinb2 from reactive astrocytes we intended to use the GFAPCre mouse in which Cre is expressed in astrocytes from E14.5 on<sup>259</sup>. However, as previously reported in the CNS GFAP is not only expressed in astrocytes, but also in ependymal cells<sup>265</sup>. In our laboratory we showed GFAP to be present mainly in astrocytes, but also in neurons and oligodendrocytes (A. Nonneman et al., unpublished results). In addition, outside the central nervous system GFAP could also be detected in kidney, testis, skin, bone, pancreas and liver<sup>266-269</sup>. Therefore we used the Cx30CreER mouse which expresses the Cre enzyme only in astrocytes<sup>261</sup>. In the spinal cord Cx30 was present specifically in astrocytes (A. Nonneman et al., unpublished results). Outside the CNS, expression of Cx30 has also been detected in the ear and in the skin, but deletion of Cx30 did not affect hearing and did not cause skin disorders<sup>270-271</sup>. Thus, the Cx30CreER mouse is a suitable mouse model to study the effect of astrocyte specific deletion of ephrinb2 on the disease progression in ALS.

Astrocyte-specific deletion of ephrinb2 in the SOD1<sup>G93A</sup> mouse did not affect disease onset, but aggravated the disease. Current experiments are being done to support this worsening in terms of motor neuron counts and neuromuscular innervation. This worsening of the clinical disease progression was associated with evidence for increased severity at the molecular level, as shown by increased microglial activation and oligodendrocytic dysfunction. Although it is possible that increased CX3CR1 and decreased MBP reflect faster progression of the disease, it is possible that these molecular changes are directly induced by the lack of ephrinb2 in astrocytes and thus the cause of the faster progression. Indeed, astrocytes affect microglial activation, and are a supplier of lactate providing metabolic

support to the oligodendrocytes. Thus, clinical as well as biochemical analysis demonstrate that astrocyte-specific deletion of ephrinb2 worsens ALS.

Previously we showed that Epha4 reverse signaling through ephrin ligands at least partially contributes to the effect of Epha4 in ALS. As Epha4 is mainly expressed on motor neurons, it interacts with ephrin ligands on surrounding cells including astrocytes, microglia and oligodendrocytes<sup>35</sup>. As ephrinb2 is highly expressed on reactive astrocytes, which play an important role in the pathogenesis of ALS, we hypothesized that the effect of Epha4 in ALS is at least partially mediated through its interaction with astrocytic ephrinb2. We expected that reducing astrocytic ephrinb2 levels thereby abolishing its interaction with neuronal Epha4 would result in a protective effect. Counterintuitively we found a decrease in survival when ephrinb2 is deleted in the astrocytes, suggesting that the effect of Epha4 in ALS is not mediated through astrocytic ephrinb2 signaling. However, we have to be cautious when interpreting these results. Next to Epha4, ephrinb2 interacts with several EphB receptors of which EphB4 is the most important one<sup>149</sup>. Deleting ephrinb2 from the astrocytes will abolish the interaction with Epha4, but also with other Eph receptors which might negatively influence the pathogenesis of ALS. To elucidate whether ephrinb2 reverse signaling is involved in the effect of Epha4 in the pathogenesis of ALS, we would have to block specifically the interaction between Epha4 and ephrinb2, which is difficult to accomplish because of the presence of other interaction partners for both Epha4 and ephrinb2.

Absence of ephrinb2 can obviously affect multiple functions of the astrocyte. One such function is the establishment of the blood brain barrier. The BBB consists of endothelial cells surrounded by pericytes and astrocytes. Astrocytes are important regulators in the development and maintenance of the BBB through their so-called their endfeet<sup>272</sup>. Astrocyte-specific deletion of ephrinb2 induced BBB leakage in adult mice. In the mouse ALS model as well as in humans, a leaky BBB has been demonstrated before and astrocytic endfeet are known to be swollen and dissociated from the endothelium<sup>273-275</sup>. We found that deleting ephrinb2 from astrocytes enhanced the existing BBB leakiness in mutant SOD1 mice. The finding that this increase is evident already early in the disease, and that leakiness is also found in the absence of mutant SOD1, suggests that the increased BBB permeability in the astrocytic ephrinb2 deleted mice is not just a reflection of enhanced disease progression. However, further investigation is needed to elucidate whether BBB impairment is a direct consequence of astrocytic ephrinb2 deletion or a secondary phenomenon. The morphological basis for this abnormality requires electronmicroscopic evaluation of the endothelial-pericytic-astrocytic tripartite and is currently being carried out in our laboratory.

These data show that the BBB plays a role in the pathogenesis of ALS. BBB impairment has been observed in mutant SOD1 animal models as well as in ALS patients<sup>276</sup>. In mutant SOD1 mice the BBB breakdown can be detected prior to motor neuron degeneration and inflammation. Furthermore, reduced levels of tight junction proteins and microhemorrhages were observed before alterations in inflammation could be detected<sup>277</sup>. However, the

specific cause of BBB in the pathogenesis of ALS has not been identified and further investigation is needed to elucidate whether BBB impairment is a initial factor or a secondary phenomenon.

In conclusion, deletion of ephrinb2 from astrocytes worsens ALS. Thus, ephrinb2 is unlikely to be the ligand through which Eph4 contributes to ALS. Our findings demonstrate that loss of ephrinb2 from astrocytes impairs BBB function and enhanced BBB leakiness at least partially contributes to the hazardous effect of astrocytic ephrinb2 deletion on ALS.

# Materials and methods

## 1. Animal housing, breeding, evaluation and experiments

### Animal housing and ethics statement

Mice were housed in the 'KU Leuven' animal facilities with a 12 h light-dark cycle at a temperature of 20 °C. Animals were given free access to standard rodent chow and water and were helped with their food and fluid intake at the end of their disease. All animals received care in accordance to The Principles of Laboratory Animal Care formulated by the National Society for Medical Research and the Guide for the Care and Use of Laboratory Animals published by the National Institutes of Health (NIH publication no. 86-23, revised 1996). Protocols were designed to minimize animal discomfort and all experiments were approved by the Ethical Committee for Animal Research of the University of Leuven, Belgium.

### Animals

Epha4<sup>-/-</sup> mice (C57/Bl6J background) were generated as previously described<sup>236</sup> and were kindly provided by Professor A.M. Turnley (University of Melbourne, Victoria, Australia). Both the EphA4<sup>eGFP/eGFP</sup> mouse (C57/Bl6J background) as well as the conditional ephrinb2 knockout mouse (efnb2<sup>fl/fl</sup>, official name: Efnb2<tm4Kln>, C57/Bl6J background) were generated as previously described<sup>206</sup> and were kindly provided by Professor R. Klein (Max-Planck-Institute of Neurology, Munich, Germany). The Cx30CreER mouse (Tg(Gjb6-cre/ERT2), C57/Bl6J background) was generated as previously described<sup>261</sup> and was kindly provided by Professor Dr. F.W. Pfrieger (European Neuroscience Institute, Strasbourg, France). Transgenic mice overexpressing wild type human SOD1 [B6SJL-Tg(SOD1)2Gur/J; stock number: 002297] and mutant human SOD1 [B6SJL-Tg(SOD1\*G93A)1Gur/J; stock number: 002726] as well as the CAGGCreER mouse (B6.Cg-Tg(CAG-cre/Esr1\*)5Amc/J; stock number: 004682) were purchased from Jackson Laboratory. GFAPCre mice (B6.Cg-Tg(GFAP-cre)8Gtm/Nci; stock number: 01XN3) were purchased from the Mouse Repository.

### Evaluation of mice

Three times a week motor performance was evaluated with the rotarod test and the hanging wire test. For the rotarod test, a rotarod treadmill (Ugo Basile, Varese, Italy) rotating at 15 rpm during 300 s was used. Each mouse was given three trials of 300 s, three times a week starting at 60 days after birth. Disease onset was defined as the time point when rotarod performance was reduced with more than 50%. Disease onset by the hanging wire test was

defined as the time point at which the mouse failed to hang upside down for at least one min on a grid one meter above a soft surface. End stage of the disease was determined as the inability to turn around within 30 s after placement on their back. At this moment the mouse was scarified and this time point was considered as the time of death. Late-symptomatic stage was considered as the time point when mice could not sustain the hanging wire test for more than 2 s. At this time point all littermates were sacrificed for pathology.

### **Sciatic nerve axotomy.**

Sciatic nerve axotomy was performed on  $Epha4^{+/+}$ ,  $Epha4^{+/-}$  and  $Epha4^{-/-}$  mice. After anesthesia with 3% isoflurane, a small incision was made unilaterally at midhigh level. Muscles were separated to visualize and transect the sciatic nerve. Afterwards, muscle and skin were sutured separately. Twenty days after sciatic nerve axotomy, the gastrocnemius muscle was instantly frozen in cooled isopentane (VWR, Paris, France) upon dissection and stored at  $-80^{\circ}\text{C}$  for further analysis.

### **Vessel permeability assay (BBB leakage)**

Mice were anesthetized and injected intravenously with 100  $\mu\text{l}$  1% Evan's blue solution (Sigma-Aldrich, St. Louis, USA). Two h after injection, mice were sacrificed and intracardially perfused with a 2% paraformaldehyde (PFA) (VWR, Paris, France) solution. Dissected brains were weighed and incubated in a formamide (Sigma-Aldrich, St. Louis, USA) solution at  $56^{\circ}\text{C}$  for 24 h to extract the dye. The absorbance of the solution was measured with the Victor Multilabel Plate Reader (PerkinElmer, Zaventem, Belgium) at 620 nm. The amount of Evans Blue is calculated using a standard curve. Data were expressed as fold increase compared to wild type animals with weight normalization.

## **2. Histopathology**

### **Neuromuscular junction staining**

After embedding the muscles in Tissue-Tek O.C.T compound (Sakura, Antwerp, Belgium), 20  $\mu\text{m}$  thick longitudinal sections were made. Sections were washed twice with 1X Phosphate Buffered Saline (PBS) (Sigma-Aldrich, St. Louis, USA) for 5 min and blocked with 5 % normal donkey serum (Sigma- Aldrich, St. Louis, USA) in PBST (PBS with 0.1% Triton X-100(Sigma-Aldrich, St. Louis, USA, T8787)) for 1 h at room temperature. To visualize neuromuscular junctions, sections were simultaneously incubated with Alexa-555-conjugated

$\alpha$ -bungarotoxin (1/5,000, Invitrogen, Carlsbad, CA, B35451) and Alexa-488-conjugated NF-200 (1/500, Cell Signaling Technologies, Danvers, MA, USA, #80245) diluted in PBST for 2 h at room temperature. Sections were washed twice with PBST for 5 min and mounted with 4',6-diamidino-2-phenylindole (DAPI)-containing Vectashield (Vectorlabs Inc., Burlingame, CA). Fluorescent stains were visualized with a Zeiss Axio Imager M1 microscope (Carl Zeiss, Jena, Germany), using the monochrome AxioCam Mrm camera. At least 200 neuromuscular junctions were analysed for each mouse.

### **Cresyl violet staining**

Spinal cords were dissected, fixed in 4% paraformaldehyde (PFA, VWR, Paris, France) and cryoprotected in 30% sucrose (Sigma-Aldrich, St. Louis, USA, S0389) in 1x PBS (Sigma-Aldrich, St. Louis, USA). After embedding the spinal cords in Tissue-Tek O.C.T compound (Sakura, Antwerp, Belgium), fresh frozen sections (20 $\mu$ m) were cut on a cryostat (Leica, Wetzlar, Germany) and every tenth slide was captured, in total 10 slides per animal. First, sections were hydrated for 3 min in 100% EtOH (VWR, Paris, France), 3 min in 95% EtOH, 3 min in 70% EtOH and immersed with cresyl violet acetate for 5 min (0.5%, Sigma-Aldrich, St. Louis, USA), followed by rehydration for 20s in 70% EtOH with 0.1% acetic acid, 3 min in 95% EtOH, 3 min in 100% EtOH and three times 3 min in 100% HistoClear (National Diagnostics, Georgia, USA, HS-200). Motor neurons were visualized with a Zeiss Axio Imager M1 microscope (Carl Zeiss, Jena, Germany) using the monochrome AxioCam Mrc5 camera. The number of neurons in different size groups was calculated using Axiovision 4 software (Zeiss, Jena Germany) thereby normalizing to the area of normal appearing neurons in the ventral horn. Neurons with a cell body area >250  $\mu$ m<sup>2</sup> were considered motor neurons.

## **3. Laser capture microdissection**

### **Cresyl violet staining**

Mice were anesthetized with 10 % Nembutal (Ceva chemicals, Hornsby, NSW, Australia) and were transcardially perfused with 1X PBS (Sigma-Aldrich, St. Louis, USA). The lumbar spinal cord was dissected and embedded in Tissue-Tek OCT compound (Sakura, Antwerp, Belgium). Frozen sections (20 $\mu$ m) were cut on a cryostat (Leica, Wetzlar, Germany) and mounted on 1.0 PEN membrane slides (Zeiss, Göttingen, Germany). First, sections were hydrated for 3 min in 100% EtOH (VWR, Paris, France), 3 min in 95% EtOH, 3 min in 70% EtOH and immersed with cresyl violet acetate for 5 min (0.5%, Sigma-Aldrich, St. Louis, USA), followed by rehydration for 20s in 70% EtOH with 0.1% acetic acid, 3 min in 95% EtOH and 3 min in 100% EtOH.



## **Laser capture microdissection**

Laser capture microdissection is a method to isolate the cells of interest under direct microscopic visualization<sup>278</sup>. A laser is coupled to the microscope and focuses on the spinal cords mounted on 1.0 PEN membrane slides (Zeiss, Göttingen, Germany). Ventral horn neurons of the lumbar spinal cord with a cell body area larger than 250  $\mu\text{m}^2$  were considered as motor neurons and microdissected using a laser capture microdissection system (Zeiss, Göttingen, Germany). The outline of the motor neurons was predefined by the user and cut out with the laser after which the sample is sucked up and captured in adhesive caps (Adhesive Cap 500 opaque, Zeiss, Göttingen, Germany). At least 1,500 motor neurons were collected for each condition.

## **Quantitative real-time PCR**

Total RNA was extracted from the captured motor neurons using the TRIPURE method<sup>13</sup>. RNA concentrations were determined by a NanoDrop ND-1000 spectrophotometer (NanoDrop Technologies, DE, USA). cDNA was synthesized from 1  $\mu\text{g}$  of total RNA using the Superscript III polymerase according to manufacturer's instructions (Invitrogen, Carlsbad, CA). Quantitative Real-Time PCR reactions were performed using TaqMan Universal PCR master mix (Applied Biosystems, Foster city, CA, USA, 4305719) and commercially available TaqMan gene expression assays against EphA4 (Invitrogen, Carlsbad, CA, Mm01256005\_m1) and Polr2a (Invitrogen, Carlsbad, CA, USA, Mm00839502\_m1). Thermal cycling was performed on the 7900HT Fast and the Step One Plus (AB) Real-time PCR system (Applied Biosystems, Foster city, CA, USA) using a standard amplification protocol.

## **4. Molecular Biology**

### **Western Blot**

All mice were anesthetized with 10 % Nembutal (Ceva chemicals, Hornsby, NSW, Australia). Mouse spinal cords, hippocampi and cortices were dissected and homogenised in RIPA lysis buffer (Sigma-Aldrich, St. Louis, USA) with proteinase (cOmplete; Roche, Vilvoorde, Belgium) and phosphatase inhibitors (phosphostop; Roche, Vilvoorde, Belgium) using the MagnNaLyser (Roche, Vilvoorde, Belgium). Protein concentration was determined using the Micro-BCA assay (Thermo Scientific, Breda, Nederland, 23235). Freshly made 8% SDS-PAGE gels (GFP blots) or 10% SDS-PAGE gels (ephrinb2 blots) were used for electrophoresis. Fifteen or twenty microgram was loaded for each sample. After SDS-PAGE the gel was transferred to Immobilon-P membrane (Millipore, Overijse, Belgium, IPVH00010) and subsequently blocked with 10% Bovine Serum Albumin (Serva, Heidelberg, Germany, 11930)

for 1 h at room temperature. As primary antibodies N-terminal mouse anti-EphA4 (1/1,000; ECM Biosciences, Lexington, USA, EM2801), chicken anti-GFP (1/1,000; Aves labs, Tigard, USA, GFP-1020), mouse C-terminal EphA4 (1/500; Invitrogen, Carlsbad, CA, 37-1600), mouse  $\beta$ -actin (1/10,000; Sigma-Aldrich, St. Louis, USA, A2228), goat anti-ephrinb2 (1/500, R&D, Abingdon, UK, AF496), rat anti-GFAP (1/1,000; Invitrogen, Carlsbad, CA, 13-0300) and mouse anti-GAPDH (1/5,000, Thermo Scientific, Breda, Nederland, AM4300) were used. As secondary antibodies anti-mouse-HRP (horse radish peroxidase), anti-rabbit-HRP, anti-goat-HRP (all 1/5,000; DAKO, Heverlee, Belgium) were used. FEMTO ECL (Thermo Scientific, Breda, Nederland, 34095) was used as substrate and the signal was detected using LAS4000 (GE Healthcare, Diegem, Belgium).

### **Immunoprecipitation**

Mouse spinal cords were dissected and homogenized in RIPA lysis buffer (Sigma-Aldrich, St. Louis, USA) supplemented with proteinase (cOmplete; Roche, Vilvoorde, Belgium) and phosphatase inhibitors (phosphostop; Roche, Vilvoorde, Belgium) using the MagnaLyser (Roche, Vilvoorde, Belgium). Protein concentration was determined using the Micro-BCA assay (Thermo Scientific, Breda, Nederland, 23235). Five  $\mu$ g of mouse anti-EphA4 antibody (Invitrogen, Carlsbad, CA, 37-1600) was incubated with 1.5 mg protein G Dynabeads (Life Technologies, Merelbeke, Belgium, 10004D) for 10 min at room temperature. One mg of CNS lysate was added and samples were rotated for 2h at 4°C. After washing the beads with 1x PBS, the target antigen was eluted with 20  $\mu$ l of elution buffer (Life Technologies, Merelbeke, Belgium, 10007D) by heating 10 min at 70°C. The eluate was separated on a Novex Nupage 4-12% bis tris gel (Life Technologies, Merelbeke, Belgium, NP0321BOX). After SDS-PAGE the gel was transferred to Immobilon-P membrane (Millipore, Overijse, Belgium, IPVH00010) and subsequently blocked with 10% Bovine Serum Albumin (Serva, Heidelberg, Germany, 11930) for 1 h at room temperature. Rabbit phospho-EphA4 (Tyr-799) (1/500; ECM Biosciences, Lexington, USA, EP2751) and mouse C-terminal EphA4 (1/500; Invitrogen, Carlsbad, CA, 37-1600) were used as primary antibodies and secondary antibodies anti-mouse-HRP and anti-rabbit-HRP (all 1/5,000; DAKO, Heverlee, Belgium) were used. Femto ECL (Thermo Scientific, Breda, Nederland, 34095) was used as a substrate and the signal was detected using LAS4000 (GE Healthcare, Diegem, Belgium).

### **Digital droplet PCR**

Spinal cord RNA was extracted using the TRIPURE method<sup>13</sup>. RNA was quantified and reverse-transcribed using random hexamer and oligodT priming and Superscript III polymerase (Invitrogen, Carlsbad, CA, 18080051). Gene expression assays for ephrinb2 covering exon 1-2 (IDT, Leuven, Belgium Mm.PT.58.29108694) and  $\beta$ -actin (Applied Biosystems, Foster city, CA, USA, 4351315,) and the ddPCR<sup>TM</sup> Supermix for Probes (no dUTP)

(Bio-Rad, Hercules, CA, USA, 186-3025) were used. Samples were subsequently placed into the QX200 Droplet Generator (Bio-Rad, Hercules, CA, USA), which uses proprietary reagents and microfluidics to partition the samples into 20.000 nanoliter-sized droplets. The droplets are transferred to a 96-well plate for PCR-amplification using the T100™ Thermal Cycler (Bio-Rad, Hercules, CA, USA). Following PCR amplification of the nucleic acid target in the droplets, the samples are placed in the QX200 Droplet Reader (Bio-Rad, Hercules, CA, USA), which analyzed each droplet individually. With the QuantaSoft™ software the PCR-positive and PCR-negative droplets are counted and analyzed.

### **Quantitative real-time PCR**

Spinal cord RNA was extracted using the TRIPURE method<sup>13</sup>. RNA was quantified and reverse-transcribed using random hexamer and oligodT priming and Superscript III polymerase (Invitrogen, Carlsbad, CA, 18080051). For quantitative real-time PCR TaqMan gene expression assays for ephrinb2 covering exon 1-2 (IDT, Leuven, Belgium, Mm.PT.58.29108694), ephrinb2 covering exon 4-5 (IDT, Leuven, Belgium, Mm.PT.58.7363143), 18s (Invitrogen, Carlsbad, CA, USA, Mm04277571\_s1), polr2a (IDT, Leuven, Belgium, Mm.PT.39a.22214849), GAPDH (IDT, Leuven, Belgium, Mm.PT.39a.1), GFAP (IDT, Leuven, Belgium, Mm.PT.58.10570926) and the TaqMan Fast Universal PCR Master Mix (Applied Biosystems, Foster city, CA, USA, 4352042) were used. SYBR Green assays were run for Aldh111 (Fw primer GCAGGTACTTCTGGGTTGCT, Rv primer GGAAGGCACCCAAGGTCAAA), NG2 (Fw primer AGGCTGAGGTAATGCTGGG, Rv primer GCAGGTGGTGAGGACAGTAG), CX3CR1 (Fw primer CGTGAGACTGGGTGAGTGAC, Rv primer GGACATGGTGAGGTCCTGAG) and MBP (Fw primer CATCCTTGACTCCATCGGGC, Rv primer CAGGGTACCTTGCCAGAGC), using the Fast SYBR Green Master Mix (Applied Biosystems, Foster city, CA, USA, 4385618). All primers are ordered at IDT, Leuven, Belgium. Expression levels were normalised to polr2a, GAPDH and 18s using qBase. Thermal cycling was performed on the Step One Plus (AB) Real-time PCR systems (Applied Biosystems, Foster city, CA, USA). Each reaction was done in triplicate.

## **5. Stainings**

### **Immunostaining**

Spinal cords were dissected, fixed in 4% paraformaldehyde (PFA, VWR, Paris, France) and cryoprotected in 30% sucrose (Sigma-Aldrich, St. Louis, USA, S0389) in 1x PBS (Sigma-Aldrich, St. Louis, USA). After embedding the spinal cords in Tissue-Tek O.C.T compound (Sakura, Antwerp, Belgium), fresh frozen sections (20µm) were cut on a cryostat (Leica, Wetzlar, Germany). Co-labeling was established by immunostaining for goat anti-ephrinb2 (1/75

overnight at 4°C, Neuromics, Edina, Minnesota, USA, GT15026-100), mouse anti-NeuN (1/200 1h room at temperature (RT), Millipore, Overijse, Belgium, MAB377), mouse anti-GFAP (1/500 1h at RT, Invitrogen, Carlsbad, CA, USA, A-21282), anti-cc1 (1/200 1h at RT, Abcam, Cambridge, Massachusetts, USA, Ab16794), rat anti-cd11b (1/200 1h at RT, AbD Serotec, Bio-rad, Hercules, CA, USA, MCA618R) and anti-iba1 (1/200 1h at RT, WAKO, Richmond, USA, 019-19741). After incubation with primary antibodies, the slides were washed three times with PBST and consequently incubated with Alexa-488/555 labeled secondary antibodies (1/500 1h at RT, Invitrogen, Carlsbad, CA, USA). All slides were washed twice with PBST for 5 min and once with PBS for five min, and mounted with Prolong® Gold Antifade Mountant with DAPI (Thermo Scientific, Breda, Nederland, P36935). Pictures were taken with the Leica SP8x confocal microscope (Leica, Diegem, Belgium).

### **DAB staining**

After embedding the human spinal cords in Tissue-Tek O.C.T compound (Sakura, Antwerp, Belgium), fresh frozen sections (20µm) were cut on a cryostat (Leica, Wetzlar, Germany). Tissue was fixed for 15 min with 4% paraformaldehyde (PFA, VWR, Paris, France). Endogenous peroxidases were blocked by incubating the slides for 30 min with 0.3% H<sub>2</sub>O<sub>2</sub> (VWR, Paris, France) in 50% MeOH (VWR, Paris, France). Samples were incubated with goat anti-ephrinb2 (1/75 overnight 4°C, Neuromics, Edina, Minnesota, USA, GT15026-100), mouse anti-smi32 (1/200, Covance, Princeton, NJ, USA, SMI-32R) and sheep anti-GFAP (1/500 1h at RT, Abcam, Cambridge, Massachusetts, USA, ab90601). After incubation with primary antibodies, the slides were washed three times with PBST and consequently incubated with biotinylated secondary antibodies (1/500 1h RT, DAKO, Heverlee, Belgium). The signal is amplified using an avidin-biotin peroxidase complex and visualised with 3,3'-diaminobenzidine tetrahydrochloride (DAB) (Vectastain ABC kit, Vectorlabs Inc., Burlingame, CA). Pictures were taken with a Zeiss Axio Imager M1 microscope (Carl Zeiss, Jena, Germany) using the monochrome AxioCam Mrc5 camera.



## Part 2. Exploration of the therapeutic potential of EphA4 inhibitors

### Introduction

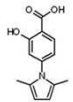
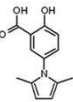

EphA4 has been found to play a role in cancer biology and in the pathogenesis of several neurological disorders<sup>279</sup>. It is upregulated in spinal cord injury, traumatic brain injury and stroke, and blocking the receptor increases functional recovery in models for these conditions<sup>208, 210, 219</sup>. Interestingly, inhibition of EphA4 improves LTP defects in a mouse model for AD and improves outcome in animal models for ALS<sup>228, 280-281</sup>. The finding that EphA4 expression is inversely correlated with survival in ALS patients, suggests that EphA4 is involved in human pathology as well<sup>281</sup>. These findings suggest that EphA4 inhibition opens perspectives for treatment of neurological disorders.

Inhibition of EphA4 signaling can be obtained through targeting the adenosine triphosphate (ATP)-binding pocket in the kinase domain or by blocking the interaction with ephrin ligands<sup>282-283</sup>. Because the ATP-binding pocket is highly conserved among tyrosine kinases, it is very difficult to develop specific inhibitors. Targeting the ligand-binding domain on the other hand allows the development of more selective compounds, but poses several problems. One of these is the large protein interaction surface to be covered (for EphA4 more than 900 Å<sup>2</sup>)<sup>284-285</sup>, and the dynamic nature of the ligand-binding domain, as EphA4 adapts a conformation like other EphA receptors to interact with ephrina ligands and like EphB receptors to interact with ephrinb ligands<sup>144, 146, 286</sup>.

So far, two classes of EphA4 binding site antagonists have been described (Table 1): a family of benzoic acid derivatives, of which the so-called C1 compound is the most studied one, and peptidergic antagonists. Of the peptidergic antagonists, the dodecapeptide KYL (named after its first three amino acids) has been extensively studied *in vitro* and *in vivo*<sup>222</sup>. It has been reported to have beneficial effects in spinal cord injury and in ALS models similar to that seen when EphA4 is knocked down genetically<sup>213, 222, 281, 287</sup>. However, peptidergic inhibitors have limited potency and/or are not stable<sup>283</sup>. The KYL peptide has a K<sub>D</sub> value of approximately 1 μM and a very short half-life in serum (11 min in mouse serum)<sup>222, 287</sup>. An EphA4 inhibitor with higher potency, the cyclic peptide APY-βAla8.am has been reported recently, but is awaiting further characterization<sup>284</sup>. All other EphA4 inhibitors lack specificity and block EphA4 activation at higher concentrations only (micromolar range) (Table 1)<sup>282, 288-289</sup>.

In the present chapter, we first have explored the potential of the small compound C1, an antagonist that targets both EphA4 and EphA2<sup>290</sup>, and of which we previously showed that it corrects the phenotype in the zebrafish ALS model. Second, we have used Nanobody technology in order to generate selective and stable EphA4 antagonists<sup>291-292</sup>. Nanobodies

(Nbs) are small antigen-binding fragments derived from camelid heavy-chain antibodies that are devoid of light chains. They are superior to conventional antibodies in terms of stability, solubility and immunogenicity<sup>291</sup>. Furthermore, they are much smaller than conventional antibodies (12-15 kDa vs. 150-160 kDa) and can penetrate small clefts and cavities<sup>293</sup>. We generated Nbs against the ligand-binding domain of the EphA4 receptor.

Structure	Compounds	Eph receptors inhibited	K <sub>D</sub> (ITC)( $\mu$ M)	ephrin binding to EphA4 inhibited	IC <sub>50</sub> inhibit ephrin binding ( $\mu$ M)	IC <sub>50</sub> inhibit phosphorylation ( $\mu$ M)	Efficacy (half-life)	Reference
<b>Small compounds</b>								
	Compound 1	A2 A4	ND	A1 A2 A3 A5 B3	(A4) 13	>100	ND	290
	Compound 2	A2 A4	ND	A1 A2 A3 A5 B3	(A4) 10	>100	ND	290
	Compound 22	A4	3.77	ND	3.4	ND	30h in mouse serum	288
<b>peptide</b>								
KYLPYWVLSL	KYL	A4	0.8	ND	2.7	5.1	11 min in mouse serum	222
APYCVYRGSWSC	APY	A4	1.4	ND	7.3	20	16 min in mouse serum	287
c[APY- $\beta$ Ala8.am]	c[APY- $\beta$ Ala8.am]	A4	0.03	ND	0.031	0.5	ND	284
VTMEAINLAFPG	VTM	A4	4.7	ND	22	50	36 min in mouse serum	222
c[CTYYWPLPC]	TYY	A4	ND	ND	11.7	ND	ND	289

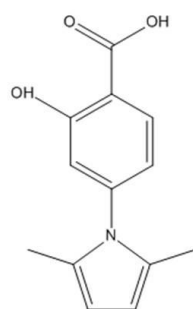
**Table 1. Overview of known EphA4 inhibitors.** ND = not determined. For all compounds and peptides all properties concerning specificity, interaction and activity are indicated. Three compounds are able to inhibit EphA4 in the micromolar range. Five peptides can inhibit EphA4 in micromolar range with cAPY peptide in nanomolar range.

## Chapter 4. Exploring the use of existing EphA4 inhibitors in ALS

Experiments in collaboration with Division of Pharmaceutical Analysis, KU Leuven

### 4.1 Introduction

We aimed to explore the use of existing EphA4 inhibitors in animal models for ALS. Several EphA4 inhibitors have been published in literature, but many of them are not very selective (Table 1). We explored the *in vivo* use of compound 1 (C1), a 2-hydroxy-4-(2,5-dimethyl-1-pyrrol-1-yl)benzoic acid derivative (Figure 4.1).



**Compound 1 (C1)**

**Figure 4.1 Structure of compound 1 (C1).**

In a high throughput screen 10,000 compounds from the DIVERSet™ library (ChemBridge, Inc.) were tested and 43 compounds were able to inhibit the binding between the KYL-peptide and the EphA4 receptor<sup>290</sup>. One compound was also able to inhibit the binding of EphA4 to ephrina5. Fourty-nine additional compounds belonging to the same class of 2,5-dimethylpyrrolyl benzene derivatives were tested of which two were able to inhibit the binding of EphA4 both to the KYL-peptide and to ephrina5. Compound 1 binds into the high affinity ephrin-binding channel of the EphA4 ligand-binding domain, thereby inhibiting the binding of ephrin ligands, except for ephrina4 and ephrinb2<sup>290, 294</sup>. Stimulation of the hippocampal cell line HT22 with preclustered ephrina5 induces EphA4 phosphorylation, which can be inhibited in a dose-dependent way by C1<sup>290</sup>. Furthermore, the ephrin system has inhibitory effects on axonal outgrowth, which can be assessed *in vitro* by studying their inhibiting (collapsing) effect on the axonal growth cone. Neuronal stimulation with ephrin ligands induces this growth cone collapse, which can be inhibited by C1<sup>290</sup>. The usefulness of this compound has already been shown in previous zebrafish work in our laboratory, in which we showed that blocking the EphA4 receptor with C1 could completely rescue the axonal phenotype in the zebrafish model of ALS<sup>35</sup>.

Newly synthesized C1 is not active, but when exposed to air and light, C1 undergoes spontaneous oxidation forming an active form of C1 thereby acquiring a dark brown color<sup>295</sup>. However, to date the active form of the compound has not been identified<sup>295</sup>.



## 4.2 Results

To validate the protective effect of EphA4 inhibition by C1 in other animal models, the feasibility of treating SOD1<sup>G93A</sup> mice with this compound was investigated. A bioanalytical method using High Performance Liquid Chromatography (HPLC) with UV detection (HPLC-UV) was developed to detect and quantify the drug in biological samples. This work was performed by Yan Xu, under supervision of Hui Chen, in collaboration with Prof. Dr. A. Van Schepdael (Division of Pharmaceutical Analysis, KU Leuven).

First, the method was validated using spiked cerebrospinal fluid (CSF) samples (Figure 4.2). There was no interference in the chromatogram of CSF matrix at the retention time of C1. The retention time of C1 corresponded with the oxidation product of the compound. Next, the method was validated for other biological samples (blood, kidney, liver, brain and spinal cord), by comparing control samples to spiked samples (data not shown).

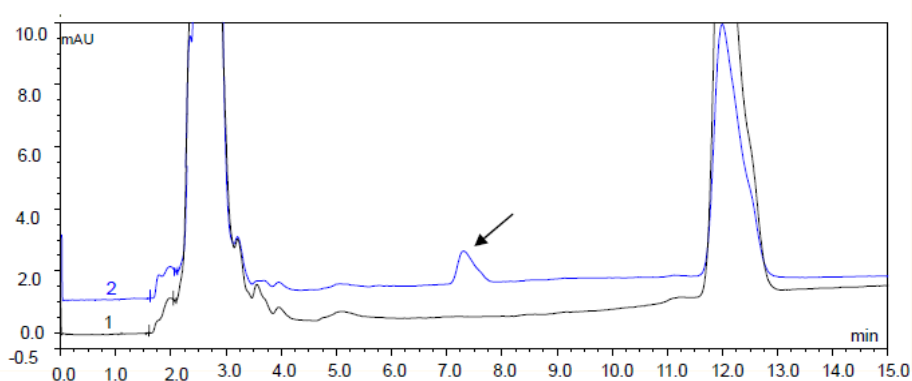


**Figure 4.2. Chromatogram of a spiked CSF sample (2) versus control CSF sample (1).**

The pharmacokinetics of C1 were determined for nontransgenic mice injected intraperitoneally with the compound (50 mg/kg mouse) or the control solution. The concentration of C1 decreased very rapidly over time in all tissues evaluated and could no longer be detected eight hours after injection (Table 4.1).

Time after injection (h)	Blood ( $\mu\text{g/ml}$ )	Kidney ( $\mu\text{g/ml}$ )	Liver ( $\mu\text{g/ml}$ )	Brain ( $\mu\text{g/ml}$ )	Spinal Cord ( $\mu\text{g/ml}$ )
1	75.7	2.13	0.7	0.362	0.437
4	14.65	<LOQ = 0.589	<LOQ = 0.589	<LOQ = 0.589	<LOQ = 0.589
8	<LOD = 0.178	<LOD = 0.178	<LOD = 0.178	<LOD = 0.123	<LOD = 0.178

**Table 4.1. Detection of compound 1 at different time points after injection in nontransgenic mice.** One hour after injection the concentration of the compound could be determined in all tissues. Four hours after injection the compound could still be detected, but not quantified. Eight hours after injection the concentration of the compound was below the detection limit. (LOD = limit of detection, LOQ = limit of quantification)

In a second approach we explored the possibility of continuous administration of C1 into the lateral ventricle using mini-osmotic pumps. We determined the stability of C1 in PBS at 37°C which revealed rapid degradation of the compound over a few days (Figure 4.3). These data indicate that the compound lacks the stability for continuous administration with mini-osmotic pumps.

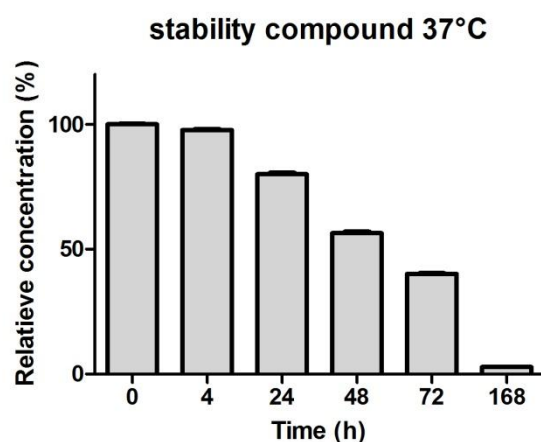


**Figure 4.3. Stability of C1 in PBS.** Concentration of C1 in PBS over time at 37°C as determined with HPLC-UV. Error bars denote standard deviation.

### 4.3 Discussion

Here we investigated the feasibility to treat SOD1<sup>G93A</sup> ALS mice with the C1-compound, a somewhat selective EphA4 inhibitor. We determined the pharmacokinetics for C1 in different tissues after intraperitoneal injection in nontransgenic mice. The concentration of C1 rapidly declined over time and was undetectable eight hours after injection, greatly limiting the therapeutic potential of C1-IP injection for the treatment of rodent ALS models.

An alternative approach by delivering the compound directly into the CSF through mini-osmotic pumps was explored. When treating ALS rodents with mini-osmotic pumps, preferentially pumps with long duration (4 weeks) are used to avoid repetitive surgeries, requiring the drug administered to be stable over a period of 4 weeks. The concentration of C1 in PBS solution at body temperature (37°C) was shown to decline over several days precluding the possibility of using it in mini-osmotic pumps.

The instability of C1 has also been reported elsewhere<sup>295-296</sup>. Not only this compound, but the whole class of 2,5-dimethyl-pyrrol-1-yl-benzoic acid inhibitors is potentially unstable during long-term storage<sup>297</sup>. Thus, although C1 is a useful antagonist for certain short-term experiments, its chemical instability limits its potential for use *in vivo*<sup>297</sup>.

## Chapter 5. Identification and characterization of Nanobodies specific for the Ephrin A4 receptor

Submitted: Schoonaert et al.

EphA4 and Nanobody expression in collaboration with the Protein Service Facility (VIB). Nanobody generation in collaboration with the Nanobody Service Facility (VIB). Surface Plasmon Resonance in collaboration with Bart Roucourt. EphA4 phosphorylation assay in collaboration with Vertex Pharmaceuticals. All other experiments performed by Lies Schoonaert with assistance of Mieke Timmers.

### 5.1 Introduction

We explored the potential of Nanobody technology to specifically and potently block EphA4 signaling<sup>291-292</sup>. Nanobodies were discovered more than two decades ago at the Vrije Universiteit Brussel<sup>298</sup>. Camelids among which camels, llamas and alpacas contain both conventional antibodies as well as heavy-chain antibodies (Figure 5.1)<sup>291</sup>. Conventional antibodies consist of two identical heavy chains and two identical light chains. The N-terminal variable domain of the heavy chain (VH) and the variable domain of the light chain (VL) interact with each other forming the antigen binding site (Figure 5.1). Heavy-chain antibodies lack the light chain and the first constant domain, and have some differences in the variable domain of the heavy chain (VHH) which are responsible for the association with the light chain in conventional antibodies<sup>291</sup>. Nanobodies (Nbs) are the isolated VHH domains responsible for antigen binding.

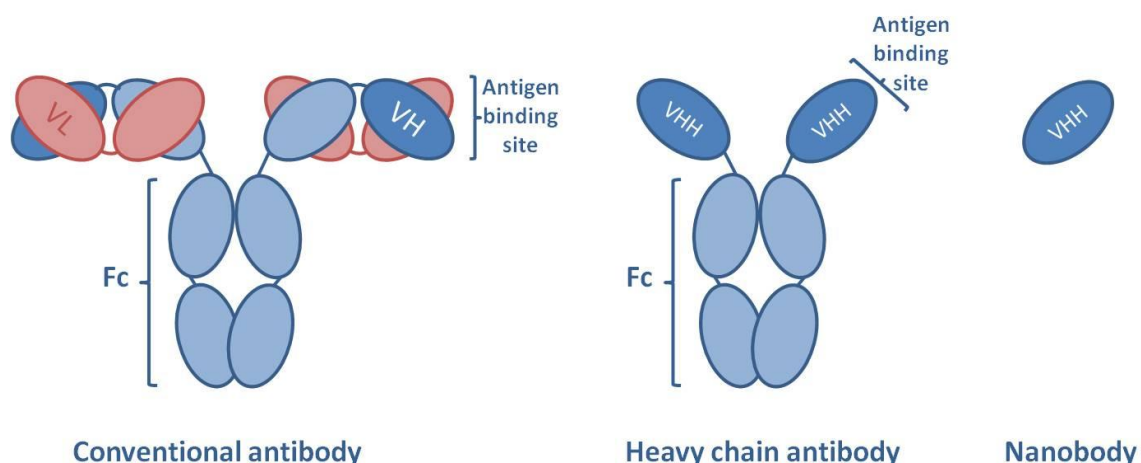


**Figure 5.1 Antibodies and Nanobodies.** The antigen binding sites of conventional antibodies are formed by the fusion of VH and VL domains with a flexible linker. Heavy-chain antibodies lack the light chain and the first constant domain of conventional antibodies. Their antigen binding site consists of an autonomous single variable domain (VHH). VH, variable domain of heavy chain; VL, variable domain of light chain.

Nanobodies have many advantages over conventional antibodies. They are much smaller than conventional antibodies (12-15 kDa vs. 150-160 kDa) and are superior to conventional antibodies in terms of stability, solubility and immunogenicity<sup>291, 293</sup>. Nbs are extremely stable with a long shelf-life of several months at 4°C, and even longer at -20°C and resistance to thermal and chemical denaturation<sup>291</sup>. High solubility of Nbs is achieved by the presence of hydrophilic amino acids in one of the framework regions<sup>299</sup>. Furthermore, Nbs lack the Fragment crystallizable (Fc) region, which is important for the recruitment of immune cells and for effector functions, explaining their limited immunogenicity, to which also their small size and their high sequence similarity to human VH contribute<sup>291</sup>. Of interest, 12 out of 14 amino acids that differ between Nanobody and human VH can be humanized thereby diminishing its immunogenicity, a necessary step to be accepted as human therapeutics<sup>300</sup>. In general, conventional antibodies bind proteins with a flat interface, while Nbs can bind and penetrate into small clefts and cavities using their long Complementarity Determining Region 3 (CDR3), one of the regions responsible for the recognition of the antigen<sup>301</sup>.

Nbs are rapidly cleared from the blood (half-life of 1.5 h or less), and poorly penetrate the blood-brain barrier and cell membrane. Of notice, these drawbacks can be overcome through chemical modifications (see below). Furthermore, several methods have been tested to cross the blood-brain barrier<sup>302</sup>.

## 5.2 Results

### 5.2.1 Generation of anti-EphA4 LBD Nbs

An alpaca was immunized with recombinant human EphA4 ligand-binding domain (LBD) according to standard procedures<sup>303</sup>. In addition to conventional antibodies, alpacas also produce heavy chain only antibodies in response to the recombinant protein. A phagemid library was constructed from the RNA from peripheral blood lymphocytes and transformed in *E. coli* TG1 cells. A library of about  $2 \times 10^8$  independent transformants was obtained and about 87% of transformants harbored the vector with the right insert size. The library was subjected to four consecutive rounds of panning, performed on solid-phase coated EphA4 LBD. The phage population was enriched for antigen-specific phages after 3<sup>rd</sup> and 4<sup>th</sup> rounds of panning. In total, 190 individual colonies from 3<sup>rd</sup> and 4<sup>th</sup> rounds (95 from each round) were randomly selected and analyzed by ELISA for the presence of antigen-specific VHs in their periplasmic extracts. In total, 41 colonies (14 and 27 from 3<sup>rd</sup> and 4<sup>th</sup>, respectively) scored positive in this assay. Sequencing of the VHH genes from 41 positive colonies resulted in 15 different Nbs, belonging to 9 different clonally-unrelated B-cell clones based on sequence homology in the complementarity determining region 3 (CDR3) (Figure 5.2). Nbs belonging to the same group show very high sequence similarity suggesting they are from clonally-related B-cells as a result of hypermutation. Nbs 39, 16, 71, 28 and 22 most likely belong to unrelated B-cell clones. Their amino acid sequences are shown in Figure 5.2. Nbs are characterized by three complementarity determining regions (CDRs), all contributing to antigen binding specificity. The most important differences between clones are mainly located in the CDRs (Figure 5.2).

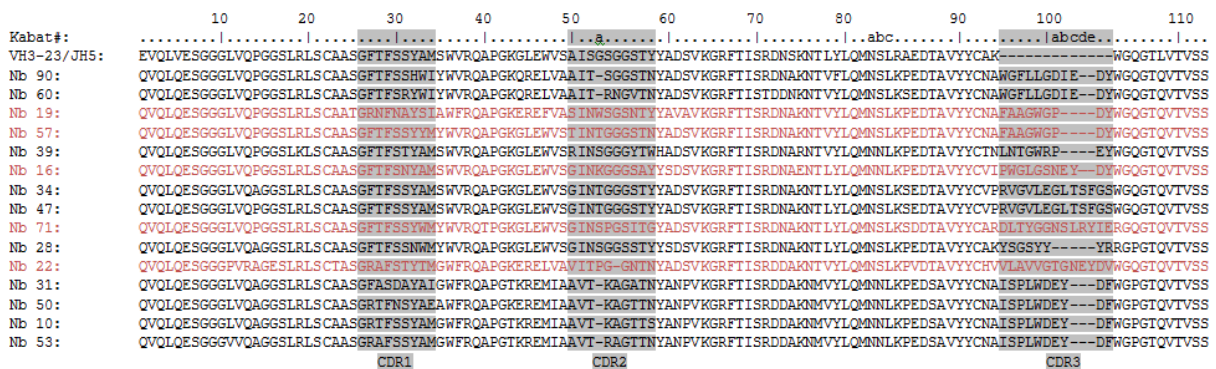


**Figure 5.2** Amino acid sequence of fifteen different anti-EphA4 LBD Nbs. The Nbs have been numbered according to Kabat numbering with reference sequence VH3-23/JH5 on top. The complementarity determining regions (CDRs) have been assigned according to the AbM definitions and are shown with a grey background. The Nbs belong to nine, clonally-unrelated B-cell clones and the different groups are shown alternatively in black and purple. According to the amino acid sequences Nb 90 and 60, Nb 19 and 57, Nb 34 and 47, Nb 31, 50, 10 and 53 belong to the same group. Nb 39, 16, 71, 28, 22 belong to unrelated B-cell clones.

### 5.2.2 Cloning and expression of the anti-EphA4 LBD Nbs

To express and purify the selected Nbs, their genes were subcloned into the pHEN6c expression vector, in fusion with a PelB signal leader sequence and a C-terminal His<sub>6</sub>-tag. The pHEN6c vectors were transformed into WK6 *E. coli* cells enabling the expression of the Nbs as a fusion protein with the PelB peptide, directing the expressed protein to the bacterial periplasm. The expressed Nbs were extracted from the periplasm by osmotic shock, purified using immobilized metal-ion affinity chromatography (IMAC) and gel filtration chromatography. The purity of the fractions was analyzed with Coomassie-stained SDS-polyacrylamide gels and western blot detection using His<sub>6</sub>-tag (data not shown). All Nbs could be detected at a position corresponding to about 15 kDa. There was no contamination with other proteins or Lipopolysaccharide (LPS), but there were obvious differences in expression levels of the Nbs (Table 5.1) and concentrating the poorly expressed ones resulted in protein aggregation. We therefore eliminated Nbs 90, 16, 71, 28 and 10 from the screen. The remaining 10 were used for further screening.

	mg Nb per liter of culture
Nb 90	0.22725
Nb 60	1.14
Nb 19	0.6204
Nb 57	2.33
Nb 39	3.2
Nb 16	0.14
Nb 34	7.29
Nb 47	0.7812
Nb 71	0.0945
Nb 28	0.0585
Nb 22	18.855
Nb 31	21.7125
Nb 50	3.59
Nb 10	0
Nb 53	7.7

**Table 5.1 Concentration of Nbs expressed in and purified from *E. coli*.** Nb 90, 16, 71, 28 and 10 did not yield high concentration and concentrating them led to aggregation.

### 5.2.3 Analysis of EphA4 binding

We next determined whether the Nbs recognised EphA4 under reducing conditions. None of them bound recombinant EphA4 (data not shown) on Western Blot; an EphA4 monoclonal antibody was used as a positive control and readily bound the recombinant protein. These data suggest that the Nbs target a conformational epitope on the EphA4 LBD.

To test whether the Nbs were indeed able to bind native EphA4, we performed immunoprecipitation experiments (Figure 5.3). Nbs 31, 50, 57, 53 and 39 precipitated EphA4 protein and EphA4 in turn precipitated these Nbs (data shown for Nbs 53 and 39 in Figure 5.3A,B). In contrast to the other Nbs, Nanobody 22 showed lower binding to mouse EphA4 compared to human EphA4 (Figure 5.3C). This is unexpected as the amino acid similarity between the LBD of human and mouse EphA4 is over 98%. Nbs 19, 34 and 47 showed non-specific binding to the beads and to recombinant ephrinb2 (data shown for Nanobody 19 and 47 in Figure 5.3D,E). Nanobody 60 did not show non-specific binding to the beads, but precipitated with recombinant ephrinb2 indicating non-specific binding (Figure 5.3F).

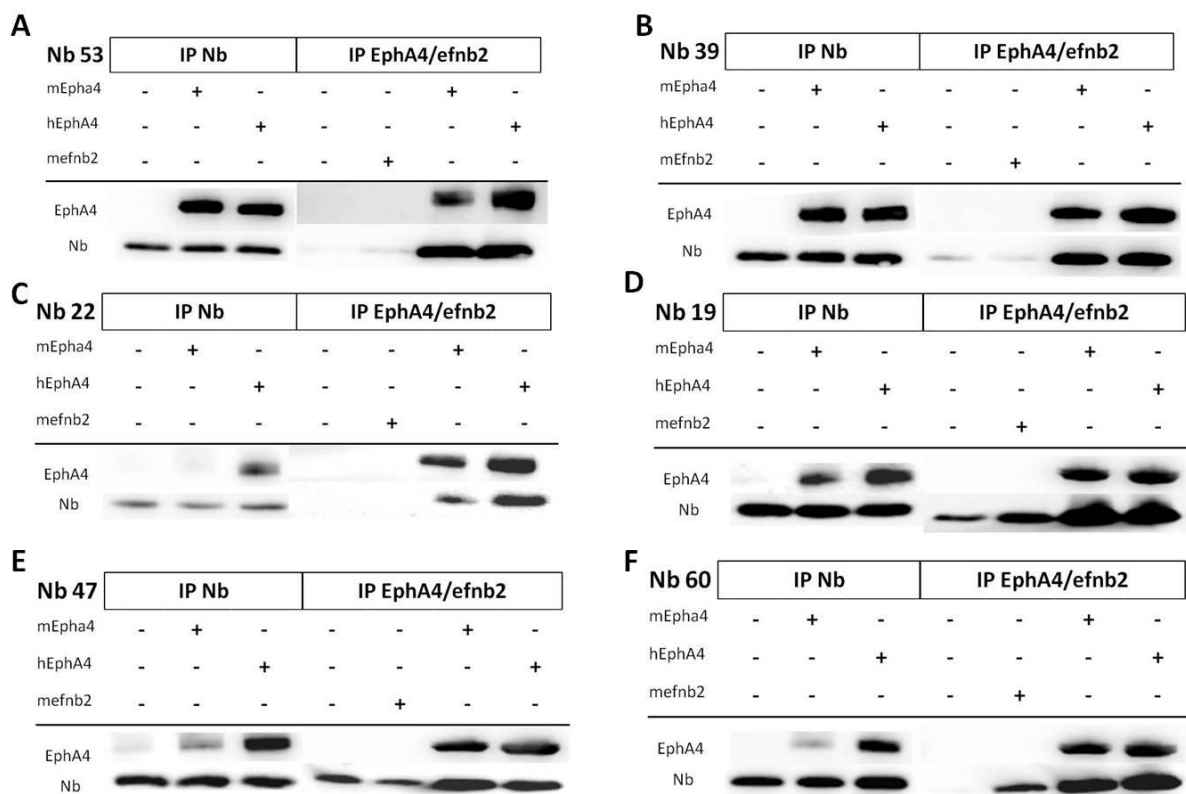


**Figure 5.3 Immunoprecipitation of EphA4 with different Nbs (left panel). Immunoprecipitation of Nb with EphA4 (right panel).** (A,B) Nb 53 and 39 could capture EphA4 and could be captured by EphA4. (C) Nb 22 showed lower affinity for mouse EphA4 compared to human EphA4. (D,E) Nb 19 and 47 showed aspecific binding to the beads. (F) Nb 60 showed aspecific binding to ephrinb2. Immunoprecipitation with ephrinb2 (Efnb2) was performed as a control experiment.



To identify the Nbs with the highest affinity we determined their binding kinetics to EphA4 using Surface Plasmon Resonance (SPR). The EphA4 ligand-binding domain (LBD) was immobilized onto the chip and Nbs (1 nM to 300 nM) were used as analyte. SPR analysis revealed that Nbs 34 and 47 did not bind to the EphA4 LBD (Table 5.2). Nbs (60, 57, 39, 22, 31, 50) showed binding in low nanomolar range, while Nanobody 19 showed binding in the higher nanomolar range only.

We next investigated the affinity of the Nbs for the EphA4 LBD, their affinity for full-length recombinant human and for the mouse EphA4 receptor. Most Nbs showed similar binding to the full-length receptor as to the EphA4 LBD. Nanobody 31 showed somewhat higher binding to the EphA4 LBD than to full length EphA4. Nanobody 22 showed a twofold difference in binding affinity between human and mouse EphA4, in agreement with what we found in the immunoprecipitation experiments described above (Figure 5.3C).

Based on these results, we selected seven Nbs (60, 57, 39, 22, 31, 50 and 53) with affinity in the nanomolar range for both the EphA4 LBD and the full-length receptor. Nbs 34, 47 and 19 showed low affinity for EphA4 and were omitted from further analysis.

	EphA4LBD					Human EphA4					Mouse EphA4				
	$k_{on}$ (1/Ms)	$k_{off}$ (1/s)	$k_{az}$ (1/s)	$k_{dz}$ (1/s)	$K_D$ (nM)	$k_{on}$ (1/Ms)	$k_{off}$ (1/s)	$k_{az}$ (1/s)	$k_{dz}$ (1/s)	$K_D$ (nM)	$k_{on}$ (1/Ms)	$k_{off}$ (1/s)	$k_{az}$ (1/s)	$k_{dz}$ (1/s)	$K_D$ (nM)
Nb 60	$1.73 \times 10^6$	0.11484	0.00014	0.00018	36.96	$1.23 \times 10^6$	0.04885			39.58	$2.70 \times 10^9$	74.05041			27.41
Nb 19	$1.82 \times 10^5$	0.10771	0.00480	0.02886	506.9	$1.07 \times 10^5$	0.09097			851.6	$1.18 \times 10^5$	0.13456			1143
Nb 57	$3.85 \times 10^6$	0.25686	0.00021	0.00133	57.52	$5.97 \times 10^6$	0.22869			38.31	$7.63 \times 10^6$	0.28821			37.79
Nb 39	$1.01 \times 10^6$	0.06067	0.00011	0.00186	56.56	$9.65 \times 10^5$	0.02906			30.13	$6.71 \times 10^5$	0.01582			23.59
Nb 34	/	/	/	/	/	5807.55	0.16824	0.00734	0.01209	18030	8245.13	0.34532	0.01260	0.02262	26900
Nb 47	Hardly any signal above background														
Nb 22	$2.32 \times 10^5$	0.01433	0.00036	0.00255	54.1	$3.14 \times 10^5$	0.01477			47.1	$2.21 \times 10^5$	0.02299			104.1
Nb 31	$3.47 \times 10^5$	0.15483	0.00355	0.00676	29.3	$7.08 \times 10^5$	0.20028	0.00647	0.01046	175	$4.22 \times 10^5$	0.15132	0.00447	0.01155	258.5
Nb 50	$1.61 \times 10^6$	0.19233	0.00023	0.00062	87.33	$2.41 \times 10^6$	0.16758	0.00018	0.00220	64.21	$1.10 \times 10^6$	0.11397			103.7
Nb 53	$1.24 \times 10^6$	0.05942	0.00011	0.00213	45.74	$6.91 \times 10^5$	0.01563			22.6	$1.07 \times 10^6$	0.02445			22.8

**Kinetic model**



**Table 5.2. Overview of the EphA4-Nanobody binding constants.** Association constants ( $k_a$ ), dissociation constants ( $k_d$ ) and equilibration constants ( $K_D$ ) determined by Surface Plasmon Resonance (SPR) through kinetics analysis. The models used for the analysis are shown under the table. Alternating red and black colour indicates different Nb groups.

### 5.2.3 Cross-reactivity with other Eph receptors

The homology between the different Eph receptors is very high. We therefore used Alphascreen technology to study the specificity of the Nbs generated. All Eph receptors tested showed binding with ephrina5 and/or ephrinb2 indicating that all receptors adapt their correct conformation. Ephrina5 interacted with all EphA receptors and with EphB2 as has been previously shown (Figure 5.4A)<sup>145</sup>. Ephrinb2 interacted with all EphB receptors and EphA4, but not with EphB6 for which no ligands have been identified so far (Figure 5.4B)<sup>146, 304</sup>. The control Nanobody did not bind to any of the Eph receptors as expected (data not shown).

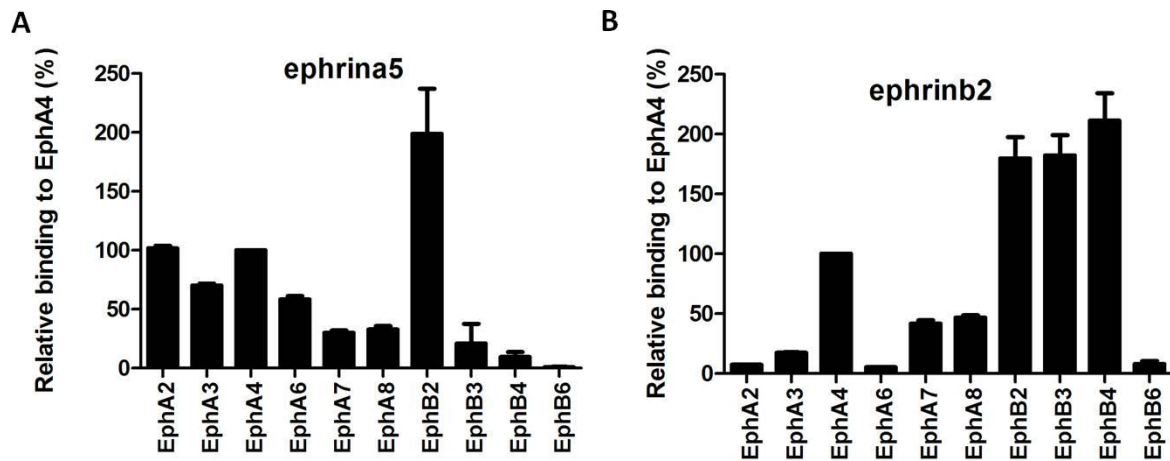


**Figure 5.4 Interaction of ephrina5 and ephrinb2 with different Eph receptors.** (A) Ephrina5 interacted with different EphA receptors and with EphB2. (B) Ephrinb2 interacted with different EphB receptors and EphA4. Values indicated represent mean with SD

Alphascreen analysis showed that Nanobody 60 interacted with several Eph receptors other than EphA4 (Figure 5.5A), in agreement with the immunoprecipitation results obtained with Nanobody 60 (Figure 5.3F). Nanobody 57 bound EphA4, but also EphA3 and EphA7, and Nanobody 50 bound EphA4 but also EphA3, EphA6, EphA7 and EphA8 (Figure 5.5B,F). Nbs 22, 39, 31 and 53 were almost completely selective for EphA4, although some binding to EphA7 was noted (Figure 5.5C, D, E, G). We therefore selected the latter four for further screening.

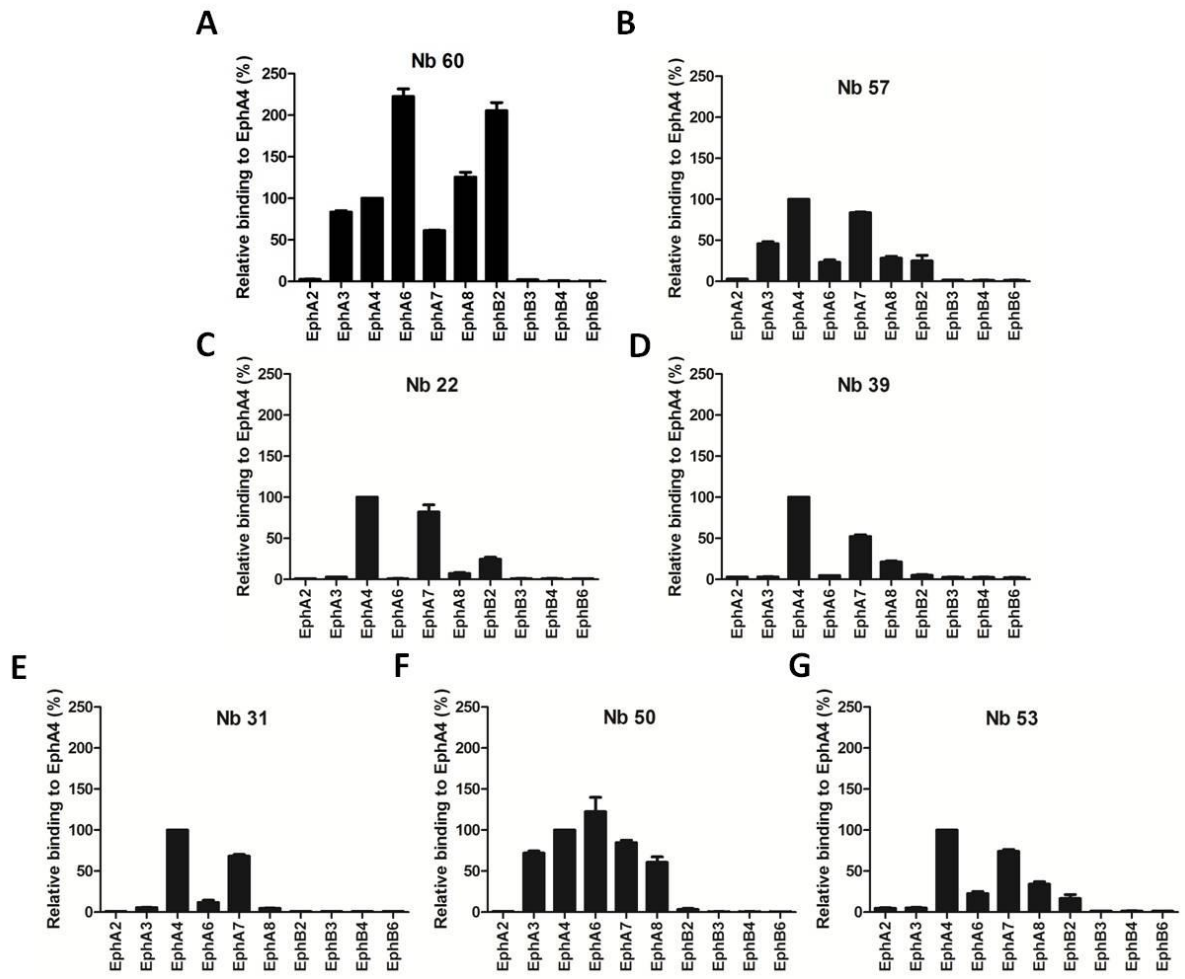


**Figure 5.5 Cross-reactivity with other Eph receptors (Alphascreen).** (A) Next to EphA4 Nb 60 also interacted with many other different Eph receptors. (B,C,D,E,F) Nb 57, 22, 39, 31 and 53 had highest selectivity to the EphA4 receptor. (F) Nb 50 had low selectivity for EphA4 as it also interacts with EphA3, EphA6, EphA7 and EphA8. Error bars denote standard deviation.

#### 5.2.4 Competition with ephrin ligands for the interaction with EphA4

EphA4 interacts with most of the ephrins<sup>144, 146</sup>. We therefore investigated whether the Nbs selected were able to displace these ligands from the EphA4 receptor. We determined the optimal concentration for the different ephrin ligands for a fixed concentration of the EphA4 LBD to avoid the hooking effect (oversaturation of donor and acceptor beads inhibiting their association) and added increasing concentrations of the Nbs. The control Nanobody did not show any interaction with the different Eph receptors, as expected (data not shown). The KYL peptide, a known EphA4 inhibitor was used as a positive control.

Nb 39 and Nb 53 completely displaced all ephrin ligands from EphA4 binding in a concentration range lower than the KYL-peptide (Figure 5.6A-H). Nbs 22 and 31 were less potent. Nb 22 completely displaced ephrina3 (Figure 5.6C) and almost completely displaced ephrinb ligands (Figure 5.6F, G, H) from EphA4 binding, but no full displacement of the other ephrina ligands was obtained with the concentrations tested (Figure 5.6A, B, D, E). Its potency was comparable to that of the KYL peptide. Nanobody 31 completely displaced ephrina1, ephrinb1 and ephrinb2 at lower concentrations than the KYL-peptide (Figure 5.6A, F, G), completely displaced ephrina3 in concentrations similar to the KYL-peptide (Figure 5.6C), but ephrina2, ephrina4, ephrina5 and ephrinb3 could not be completely displaced with the concentrations tested (Figure 5.6B, D, E). These data show that Nbs 39 and 53 are able to block the interaction of all ephrin ligands with the EphA4 ligand-binding domain.

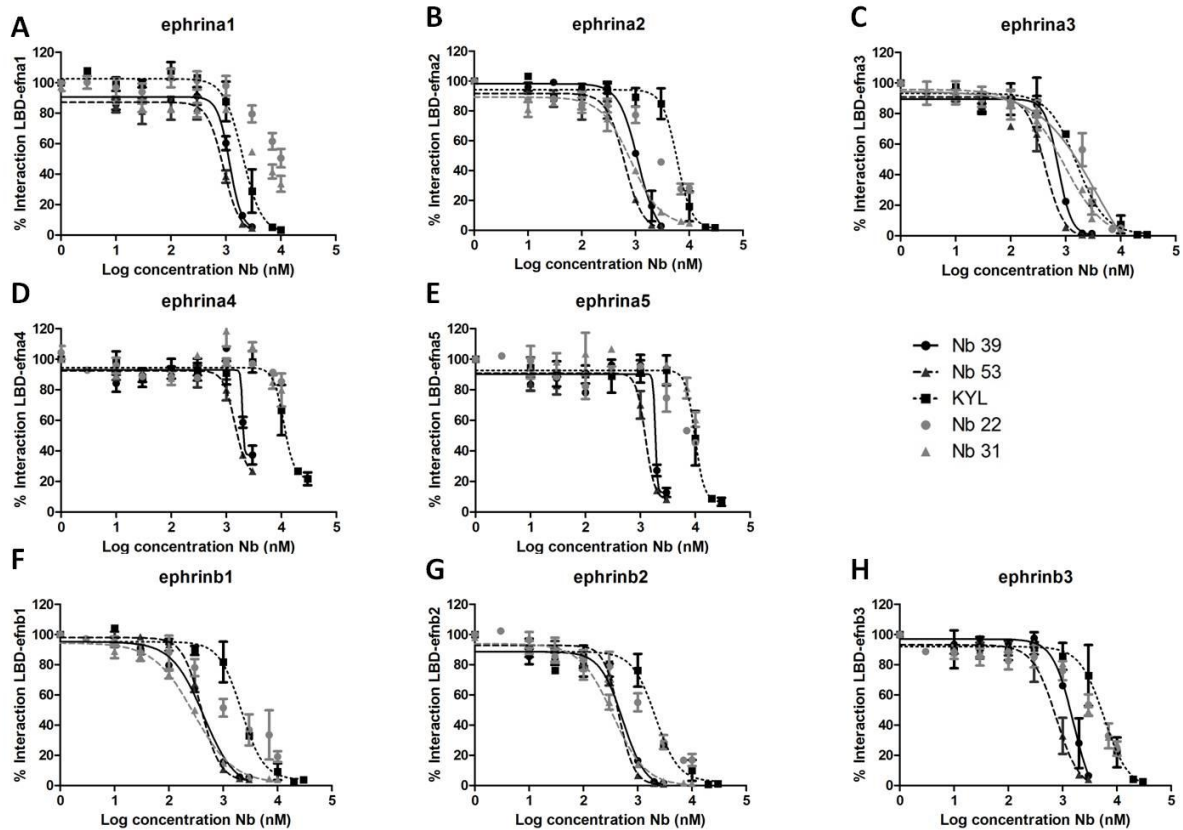


**Figure 5.6 Inhibition of ligand-binding.** (A,D,E,H) Nb 22 and 31 did not show complete inhibition. Nb 39 and Nb 53 showed complete inhibition of ligand-binding at a lower concentration than the KYL-peptide. (B,F,G) Nb 22 did not show complete inhibition. Nb 39, Nb 53 and Nb 31 showed complete inhibition of ligand-binding at a lower concentration than the KYL-peptide. (C) Nb 39 and 53 showed complete inhibition of ligand-binding at a lower concentration than Nb 22, Nb 31 and the KYL-peptide. Error bars denote standard deviation.

### 5.2.5 Inhibition of ephrin-induced EphA4 activation

To assess the antagonistic properties of the Nbs, we tested their effect on ephrin-induced phosphorylation. Ephrin-induced phosphorylation was examined using the PathHunter assay in U2OS cells. All cells are stimulated with ephrina1 with or without the presence of an EphA4 antagonist and the resulting phosphorylation of EphA4 is measured. The control Nanobody did not have any effect on receptor phosphorylation (data not shown). The KYL peptide showed complete inhibition of ephrina1-induced phosphorylation with an  $IC_{50}$  value of  $52.96 \mu\text{M}$  (Figure 5.7). Nbs 39 and 53 also reached complete inhibition of ephrina1-induced phosphorylation, but at lower concentrations than the KYL-peptide with an  $IC_{50}$  of  $170 \text{ nM}$  and  $261 \text{ nM}$  respectively (Figure 5.7). These data indicate that Nbs 39 and 53 are at least ten times more potent than the KYL peptide in ephrina1-induced phosphorylation of the EphA4 receptor.

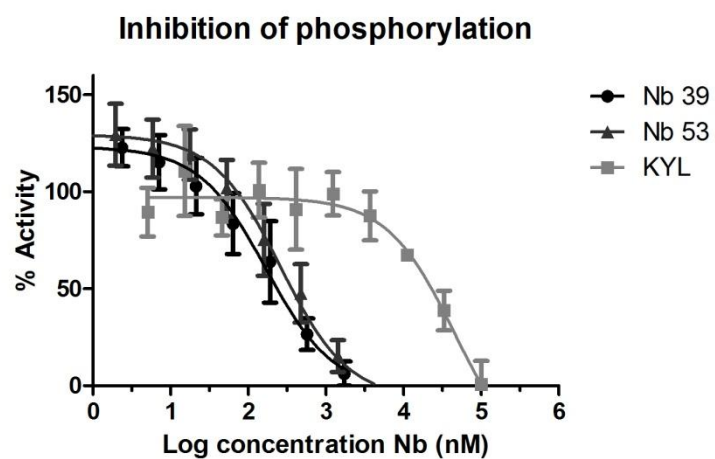


**Figure 5.7 Inhibition of phosphorylation.** Nb 39 and Nb 53 showed complete inhibition of phosphorylation at a lower concentration than the KYL-peptide. Error bars denote standard deviation.

### 5.3 Discussion

One EphA4 inhibitor, the KYL peptide, has been studied extensively in models for several neurological disorders such as acute injuries including spinal cord injury and stroke, and neurodegenerative disorders such as ALS and AD<sup>280-281</sup>. Unfortunately, this peptide has a  $K_D$  value of approximately 1  $\mu$ M and a very short half-life in serum (11 min in mouse serum)<sup>222, 287</sup>. Only one very recent study has reported an EphA4 inhibitor with higher potency, the cyclic peptide APY- $\beta$ Ala8.am<sup>284</sup>, which is yet to be characterized biologically. All other EphA4 inhibitors lack specificity and need higher concentration (in the micromolar range) to block EphA4 activation (Table 1).

As Nbs are known to be very specific, we used this approach to develop a selective EphA4 inhibitor targeting the ligand-binding domain. Here, we describe the generation and screening of EphA4 inhibitors targeting the LBD based on the Nanobody (Nb) technology. We immunized alpacas with the human EphA4 LBD and identified 15 different Nbs against this LBD. In a series of experiments, we found Nb 39 and 53 to be at least ten times more potent than the KYL peptide with potencies in the nanomolar range. Nb 39 and Nb 53 were most selective for EphA4, but still showed considerable binding to EphA7. Interestingly, EphA7 KO mice as well as rats treated with EphA7 antisense oligonucleotides show enhanced recovery after SCI compared to control mice<sup>305-306</sup>. Therefore, targeting EphA7 in addition to EphA4, may be of benefit rather than detrimental. This obviously needs further study.

Conventional antibodies (about 150 kDa) have limited tissue penetration and bind to small receptor pockets because of their large size and preference for concave epitopes. Nbs on the other hand prefer clefts and small pockets and show higher tissue penetration. However, their small size limits their half-life to about 1.5 hours<sup>307</sup>. This low half-life can be overcome by linking the Nb to a Nb that binds serum albumin which can increase the half-life to 20-30 h in mice. In humans this strategy was shown to extend the half-life of Nbs to 19 days<sup>308-309</sup>. Another strategy to increase the half-life is adding polyethyleenglycol (PEG) groups to the Nbs, taking care that the PEG groups do not influence the binding to EphA4<sup>310</sup>. The addition of PEG groups increases the apparent molecular weight above the glomerular filtration limit avoiding renal clearance and/or evades cellular clearance mechanisms<sup>311</sup>.

We here describe Nbs targeting the EphA4 ligand-binding domain. Two Nbs were most selective for EphA4 and had  $K_D$  and  $IC_{50}$  values in the nanomolar range. Both Nbs were able to block the interaction of EphA4 with all ephrin ligands and inhibit phosphorylation of EphA4. Future studies need to investigate whether these promising results can be translated in *in vitro* and *in vivo* functional models. In addition, the affinity of these Nbs can be further increased through error-prone PCR mutagenesis and/or making bispecific Nbs<sup>312-313</sup>.





## **Material and Methods**

### **1. Pharmacokinetics compound 1**

#### **Animal housing and ethics statement**

Nontransgenic mice with a C57/Bl6J background were purchased from the animal facility. Mice were housed in the 'KU Leuven' animal facilities with a 12 h light-dark cycle at a temperature of 20 °C. Animals were given free access to standard rodent chow and water and were helped with their food and fluid intake at the end of their disease. All animals received care in accordance to The Principles of Laboratory Animal Care formulated by the National Society for Medical Research and the Guide for the Care and Use of Laboratory Animals published by the National Institutes of Health (NIH publication no. 86-23, revised 1996). Protocols were designed to minimize animal discomfort and all experiments were approved by the Ethical Committee for Animal Research of the University of Leuven, Belgium.

#### **Biodistribution of C1**

Nontransgenic mice were injected intraperitoneally (IP) with C1 (1 mg dissolved in DMSO, with 200 µl extra physiological water). Blood sample was saved in a heparin solution (1/10 in water) to prevent coagulation. Before organ samples were collected, the mice were perfused by 1x PBS (Sigma-Aldrich, St. Louis, USA) to remove all blood from the organs. Each organ sample was saved in 2 ml distilled water and homogenized. Sample preparation methods and the detection of C1 were optimised and validated in collaboration with the Division of Pharmaceutical Analysis, KU Leuven. The work was performed by Yan Xu, under supervision of Hui Chen and Prof. Dr. A. Van Schepdael. Briefly, for different samples, different sample preparation methods were applied. As the CSF sample has a very low protein content, it can be analyzed directly. For blood, liver and kidney samples, protein precipitation was needed. For spinal cord and brain samples, Solid Phase Extraction (SPE) was performed, to remove interfering matrix components and selectively concentrate the analyte. After sample preparation, all samples were analyzed with HPLC-UV.

### **2. Nanobody screening**

#### **Expression and purification of the EphA4 ligand-binding domain**

The EphA4 ligand-binding domain (AA 22 – AA 203 according to *Singla et al., 2010*<sup>286</sup>) was cloned from the EphA4 Human cDNA ORF clone (Origene) and expressed in the *E. coli* strain

BL21 codon + pICA2 transformed with the pLH36Epha plasmid. Expression is induced by isopropyl b-D-1-thiogalactopyranoside under control of a pL-promotor developed by the Protein Service Facility of VIB. The pLH36 plasmid is provided with a His<sub>6</sub>-tag followed by a murine caspase-3 site. The murine caspase-3 site can be used for the removal of the His<sub>6</sub>-tag attached at the N terminus of the protein of interest during purification. The transformed bacteria were grown in Luria Bertani medium supplemented with ampicillin (100 µg/mL) and kanamycin (50 µg/mL) overnight at 28°C before 1/100 inoculation in a 20 liter fermenter provided with Luria Bertani medium supplemented with ampicillin (100 µg/mL) and 1% glycerol. The initial stirring and airflow was 200 rpm and 1.5 L/min, respectively. Further, this was automatically adapted to keep the pO<sub>2</sub> at 30 %. The temperature was kept at 28°C. The cells were grown to an optical density of A<sub>600nm</sub> = 1.0, transferred at 20°C, and expression was induced by addition of 1 mM isopropyl b-D-1-thiogalactopyranoside overnight. Cells were then harvested and frozen at -20°C. After thawing, the cells were resuspended at 3 mL/g in 20 mM NaH<sub>2</sub>PO<sub>4</sub> pH 7.5, 500 mM NaCl, 20 mM imidazole and 1 mM phenylmethylsulfonyl fluoride. The cytoplasmic fraction was prepared by sonication of the cells followed by centrifugation at 18,000g for 30 min. All steps were conducted at 4°C. The clear supernatant was applied to a 74 mL Ni-Sepharose 6 FF column (GE Healthcare, Diegem, Leuven), equilibrated with 20 mM NaH<sub>2</sub>PO<sub>4</sub> pH 7.5, 500 mM NaCl, 20 mM imidazole and 0.1% CHAPS. The column was eluted with 20 mM NaH<sub>2</sub>PO<sub>4</sub> pH7.4, 20mM NaCl, 400mM imidazole and 0.1% CHAPS after an extra wash step with 50 mM imidazole. The elution fraction was diluted 1/20 with 20 mM Tris pH 8.0 and 0.1% CHAPS and loaded on a 20-mL Source 15Q column (GE Healthcare, Diegem, Leuven) to remove contaminants. After equilibration, the protein of interest was eluted by a linear gradient over 20 column volumes of NaCl from 0 to 1 M in 20 mM Tris pH 8.0 and 0.1% CHAPS. To the EphA4-containing fractions, activated murine caspase-3 (1/100 % m/m murine caspase-3/EphA4) with 10 mM DTT was added to remove the His<sub>6</sub>-tag. After 1 h incubation at 37°C, the reaction solution was injected on a HiLoad 26/60 Superdex 75 prep grade with PBS as running solution for formulation and to remove minor contaminants, His<sub>6</sub>-tag and murine caspase-3. The obtained fractions were analyzed by SDS-PAGE and the concentration was determined using the Micro-BCA assay (Thermo Scientific, Breda, Nederland, 23235).

### **Construction of a VHH library**

Nbs targeting the EphA4 ligand-binding domain (LBD) were obtained in collaboration with the VIB Nanobody Service Facility. An alpaca was injected subcutaneously on days 0, 7, 14, 21, 28 and 35, each time with about 250 µg of human Ephrin A4 LBD. On day 39, anticoagulated blood was collected for lymphocyte preparation. A variable domain of heavy-chain antibodies (VHH) library was constructed and screened for the presence of antigen-specific Nbs. To this end, total RNA from peripheral blood lymphocytes was used as template for first strand cDNA synthesis with oligo(dT) primer. Using this cDNA, the VHH encoding sequences were amplified by PCR, digested with PstI and NotI, and cloned into the PstI and

NotI sites of the phagemid vector pMECS. A VHH library of about  $2 \times 10^8$  independent transformants was obtained. About 87% of transformants harbored the vector with the right insert size.

### **Isolation of hEphA4 LBD-specific Nbs**

To screen for the presence of EphA4-specific Nbs, the library was subjected to 4 consecutive rounds of panning, performed on solid-phase coated EphA4 LBD (concentration:  $\sim 200 \mu\text{g/ml}$ ,  $\sim 20 \mu\text{g/well}$ ). The enrichment for antigen-specific phages after each round of panning was assessed by comparing the number of phages eluted from antigen-coated wells with the number of phages eluted from negative control (only-blocked) wells. These experiments suggested that the phage population was enriched for antigen-specific phages after 3<sup>rd</sup> and 4<sup>th</sup> rounds of panning. In total, 190 individual colonies from 3<sup>rd</sup> and 4<sup>th</sup> rounds (95 from each round) were randomly selected and analyzed by ELISA for the presence of antigen-specific Nbs in their periplasmic extracts (ELISA using crude periplasmic extracts including soluble Nbs). Of 190 colonies, 41 colonies (14 and 27 from 3<sup>rd</sup> and 4<sup>th</sup>, respectively) scored positive in this assay. The selected clones were analysed and their VHH genes were sequenced to identify the different Nbs.

### **Expression and purification of recombinant Nbs**

The Nanobody genes were subcloned into the pHEN6c expression vector, in fusion with a C-terminal His<sub>6</sub>-tag. The pHEN6c vectors were transformed into WK6 E. coli cells and grown in Luria Bertani medium supplemented with ampicillin (100  $\mu\text{g/mL}$ ) and 0.1 % glucose at 37°C overnight. Further, the cultures were inoculated 1/100 to have 1 liter productions in Terrific Broth medium supplemented with ampicillin (100  $\mu\text{g/mL}$ ) and 0.1 % glucose in baffles shake flasks. The temperature was kept at 37°C. The cells were grown to an optical density of  $A_{600\text{nm}} = 1.0$ , transferred at 28°C, and expression was induced by addition of 1 mM isopropyl b-D-1-thiogalactopyranoside overnight. Cells were then harvested and frozen at -20°C. The expressed Nbs were extracted from the periplasm by osmotic shock and purified using His GraviTrap (GE Healthcare, Diegem, Belgium) in parallel, equilibrated with 20 mM NaH<sub>2</sub>PO<sub>4</sub>, pH 7.5, 300 mM NaCl, 20 mM imidazole, and 1 mM PMSF. After loading, the columns were washed with 20 column volumes of the same buffer. The Nanobody was first eluted with 20 mM NaH<sub>2</sub>PO<sub>4</sub>, pH 7.5, 20 mM NaCl, 50 mM imidazole, 1 mM PMSF and then with 400 mM imidazole in the same buffer. Finally, the Nbs were desalted to PBS on sephadex G25 (GE Healthcare, Diegem, Belgium). The obtained fractions were analyzed with Coomassie-stained SDS-polyacrylamide gels. Protein concentration was measured by the Micro-BCA assay (Thermo Scientific, Breda, Nederland, 23235).

## Immunoprecipitation experiments

One and a half mg protein G Dynabeads (Life Technologies, Merelbeke, Belgium, 10004D) were preblocked with 1% BSA for 1 h at room temperature, washed four times with PBS and incubated with 2.5 µg of recombinant mouse or human EphA4 protein (R&D, Abingdon, UK, 641-A4-200 and 6827-A4-050) for 10 min at room temperature. After washing four times with PBS the beads were incubated with 1 µg Nanobody overnight at 4°C. The beads were washed four times with PBS, boiled for 10 min in reducing sample buffer (Thermo Scientific, Breda, Nederland, 39000) and proteins were fractionated with a Novex Nupage 4-12% bis tris gel (Life Technologies, Merelbeke, Belgium, NP0321BOX). After SDS-PAGE the gel was transferred to Immobilon-P membrane (Millipore, Overijse, Belgium, IPVH00010) and subsequently blocked with 10% Blotting-grade blocker (Bio-Rad, Hercules, CA, USA, 1706404) for 1 h at room temperature. Mouse anti-EphA4 antibody 1/1,000 (ECM Biosciences, Lexington, USA, EM2801) and mouse anti-HA antibody 1/1,000 (Covance, Princeton, NJ, USA, MMS-101P) were used to detect EphA4 and Nanobody respectively. EphA4 was captured with Nanobody anti-HA magnetic Dynabeads (Life Technologies, Merelbeke, Belgium, 88837) were used and all following steps were performed as described above.

## Surface Plasmon Resonance

The equilibrium dissociation constant ( $K_D$ ) and the association ( $k_a$ ) and dissociation rates ( $k_d$ ) were determined using surface plasmon resonance detection on a BIAcore T200 (GE Healthcare). Two approaches were used. First, the extracellular N-terminal domain of human EphA4 was immobilized directly onto a CM5 S series sensor chip (GE Healthcare, Diegem, Belgium, BR100530) using standard amine coupling. After activation of the carboxyl moieties on the matrix on the chip surface with a 7-min injection of a 1:1 mixture of 0.4 M EDC and 0.1 M NHS, the N-terminal domain of human EphA4 (50 µg/ml in 10 mM acetate, pH 4.5) was immobilized to a predefined level of response units (RU). Approximately 300 RU of N-terminal domain of human EphA4 was bound onto flow channels. The remaining activated carboxyl groups were blocked by injecting 1 M ethanolamine (pH 8.5) for 7 minutes. Flow rate was kept constant at 10 µl/min. A flow channel activated with EDC/NHS and immediately afterwards blocked by ethanolamine served as reference channel. Throughout the analysis 10 mM Hepes, 150 mM NaCl, 3 mM EDTA, 0.01 mM Surfactant P-20 pH 7.35 was used as running buffer. 20 mM glycine pH 2.5 was used to regenerate the channels (remove all bound proteins). The second approach used the anti-human Fc capture kit as described by the manufacturer. Briefly, approximately 8000 RU anti-human Fc antibody was capture on the surface of the channels using amine coupling as described above. In a next step, EphA4-hFc (both human and mouse EphA4 (R&D, Abingdon, UK, 641-A4-200 and 6827-A4-050) fusion protein (2 µg /ml diluted in running buffer) was injected (10 µl/min for 6 minutes) over de the channel resulting in the capture of approximately 500 RU of EphA4-hFc fusion

protein on the surface of the channel. In this approach, a channel with only anti-human Fc antibody served as reference. 3M MgCl<sub>2</sub> was used as regeneration buffers. The Nbs were diluted to the indicated concentrations in running buffer and injected (60 µl/min) over the channel with immobilized EphA4 and the reference channel. After correction of the response using the responses from the reference channel and a blank injection of running buffer over the Eph4A-immobilized channel (double referencing), kinetic parameters were determined using Biacore T200 evaluation software (GE Healthcare, Diegem, Belgium).

### **Phosphorylation assay**

The amount of phosphorylation of EphA4 was determined using the PathHunter assay (DiscoverX Corporation, Birmingham, UK) with U2OS cells adapted for the EphA4 receptor according to manufacturers instructions. In short, a small peptide epitope is expressed recombinantly on the intracellular C-terminus of the EphA4 receptor tyrosine kinase. An interaction partner containing SH2 domains is co-expressed with a larger sequence, termed enzyme activator (EA). Ephrina1-induced activation causes dimerisation leading to crossphosphorylation. The SH2-EA fusion protein binds the phosphorylated receptor forcing the complementation of EA and the peptide epitope, yielding an active β-galactosidase enzyme. This interaction can be visualised with a chemiluminescent substrate. Increasing concentrations of the Nbs are added to the medium before ephrina1 stimulation.

EphA4 U2OS cells were plated into white opaque 384-well plates at a volume of 20 µl containing 5,000 cells. After short centrifugation to ensure contact with the bottom of the plate, the plate is incubated for 24h at 37°C 5% CO<sub>2</sub>. Five µl Nb dilutions or vehicle are added per well followed by short centrifugation of the plate and incubation for 1h at 37°C. Five µl of ephrina1 (1.2 µg/ml) or vehicle is added to each well followed by short centrifugation of the plate and incubation for 3h at room temperature. Twelve µl of detection reagent (Galacton Star, Emerald II solution, PathHunter cell assay buffer in relative volumes of 1:5:19 respectively) is added followed by short centrifugation ensuring contact with media. After one hour incubation at room temperature the plate can be read on a Pherastar (BMG Labtech, Ortenberg, Germany). Percentage activity is calculated as (signal – positive control)/(negative control– positive control)\*100. The positive control is background without any ephrin added. The negative control is maximum signal with ephrin stimulation without any Nanobody added.

### **AlphaScreen**

To test the specificity of the Nbs for the different Eph receptors all Nbs were biotinylated with a five times molar excess of EZ link NHS biotin (Thermo Scientific, Breda, Nederland, 21217). The Nbs were incubated with the biotin for two hours on ice allowing the interaction of the biotin with the primary amines on the surface of the protein. Ten µl of biotinylated

Nbs (100 nM) were incubated with 10 µl of a subhooking concentration of mouse recombinant Eph receptor (R&D, Abingdon, UK, 641-A4-200) for one hour in standard buffer (50 mM Hepes, 100 mM NaCl, 0.1% Triton and 0.1% BSA). The determined subhooking concentrations are 3 nM for EphB4, 10 nM for EphA2, A4, B2 and B3, 30 nM for EphA3, A6, A7 and B6, and 100 nM for EphA8. Ten µl of anti-IgG AlphaLISA acceptor beads (20 µg/ml; Perkin Elmer, Zaventem, Belgium, AL103M and AL105M) and 10 µl streptavidin donor beads (20 µg/ml; Perkin Elmer, Zaventem, Belgium, 6760002) were subsequently incubated for one hour and 30 minutes respectively at room temperature, protected from light. The plate was read on the Envision Multilabel Reader (Perkin Elmer, Zaventem, Belgium). A Nanobody targeting the Superoxide Dismutase 1 protein (SOD1) was used as a negative control.

To test the inhibition of interaction between EphA4 and its different ligands, the EphA4 LBD (2mg/ml) was biotinylated with a two and a half times molar excess of EZ link NHS biotin (Thermo Scientific, Breda, Nederland, 21217) for two hours on ice allowing the interaction of the biotin with primary amines on the surface of the protein. Five µl of a subhooking concentration of biotinylated EphA4 LBD (10 nM) was incubated with five µl of different concentrations of Nb for one hour in standard buffer (50 mM Hepes, 100 mM NaCl, 0.1% Triton and 0.1% BSA). Subsequently five µl of subhooking concentration of ephrin ligand was added and incubated for one hour at room temperature. The determined subhooking concentrations are 3 nM for efna1 and efna4, and 10 nM for efna2-3, efna5 and efnb1-3. Next five µl of anti-IgG AlphaLISA acceptor beads (20 µg/ml, Perkin Elmer, Zaventem, Belgium, AL103M and AL105M) and five µl streptavidin donor beads (10 µg/ml, Perkin Elmer, Zaventem, Belgium, 6760002) were added and incubated for one hour and 30 minutes respectively at room temperature, protected from light. The plate was read on the Envision Multilabel Reader (Perkin Elmer, Zaventem, Belgium). A Nanobody targeting the Superoxide Dismutase 1 protein (SOD1) was used as a negative control.

## General discussion

Epha4 plays an important role in embryonic development as an axonal guidance repellent<sup>151, 314</sup>. The role of Epha4 in the adult central nervous system has been addressed only recently. It has been found to play a role in synaptic plasticity, and has been implicated in the pathogenesis of several disorders such as cancer and several neurological disorders such as trauma, neuroinflammatory and neurodegenerative diseases<sup>219, 221, 227</sup>. We have previously shown Epha4 to be a modifier of ALS, in animal models as well as in patients<sup>35</sup>. Reduced Epha4 expression increased motor performance and survival of the SOD1<sup>G93A</sup> mouse model and EphA4 expression inversely correlated with disease severity in ALS patients. However, the mechanism through which Epha4 reduction/inhibition attenuated ALS pathogenesis is unclear. In this present work, we addressed several aspects of Epha4 biology in ALS and developed Nanobodies against EphA4 as a tool for future mechanistic or therapeutic studies.

### **Epha4 contributes to the vulnerability of motor neurons and determines re-innervation capacity**

Epha4 is mainly expressed in motor neurons in the spinal cord of SOD1<sup>WT</sup> and SOD1<sup>G93A</sup> mice. We confirmed that large motor neurons are more vulnerable in ALS, and demonstrated that these are preferentially rescued when Epha4 is reduced. Thus, vulnerability and regeneration capacity seem to be somehow interrelated or may even be two characteristics of the same biological reality. Of interest, we showed that Epha4 at least partially determines sprouting capacity of motor neurons. Mice with decreased Epha4 expression showed a dose-dependent improvement in neuromuscular junctions re-innervation after sciatic nerve injury<sup>35</sup>. This enhanced sprouting was also detected in rats after corticospinal tract injury when treated with an Epha4 antagonist<sup>213</sup>. It is tempting to speculate that this is also reflected in what is well known to occur in the growth cone of embryonic motor neurons. Epha4 expressed on the growth cone interacts with ephrin ligands on adjacent cells leading to the reorganization of the cytoskeleton through RhoGTPases and induces growth cone collapse<sup>212, 315-317</sup>. This sprouting capacity can be restored by treatment with Epha4 antagonists as shown by the rescue of the growth cone collapse in cultured neurons<sup>213, 284</sup>.



## **Epha4 reverse signaling in the biology of ALS**

Interaction between Eph receptors and ephrin ligands can result in forward signaling in the Eph-bearing cell and reverse signaling in the ephrin-bearing cell. We found that partial replacement of Epha4 by an Epha4 molecule in which the cytoplasmic domain of Epha4 has been replaced by an eGFP cassette, did not influence ALS in the SOD1<sup>G93A</sup> mouse model. This indicates that it is the reverse signaling of Epha4 that is hazardous in ALS and explains the modifying effect of Epha4 in ALS. Some caution is needed for the interpretation of this observation. Indeed, in the Epha4 molecule, the entire intracellular domain is absent, which affects expression of the Epha4eGFP isoform, receptor clustering, and endocytosis. Thus, more than reverse signaling may be affected in this Epha4eGFP molecule. This is indeed evident from the axotomy experiments in which reduced regeneration was seen, indicating that the replacement of the intracellular domain with eGFP results in more than silencing the reverse signaling. Therefore, it may be of interest to repeat this experiment with a mouse in which the kinase activity is silenced through a point mutation rather than through the replacement of the entire domain. These experiments are being performed in the lab.

In spite of these considerations, it can be concluded that reverse signaling at least partially contributes to the effect of Epha4 in ALS. This can occur through interaction with ephrin ligands on muscle cells, astrocytes, oligodendrocytes, microglial cells or motor neurons themselves (through *cis* interaction), as all these cells are known to express ligands for Epha4.

## **Ephrins in ALS**

We quantified all ephrins in the spinal cord of the SOD1<sup>G93A</sup> mouse, and concentrated on astrocytic ephrins as no consistent pattern emerged. Ephrina2, ephrina3 and ephrinb2 are expressed on astrocytes<sup>251-252</sup>. The role of ephrina2 in astrocytes has not yet been elucidated. Ephrina3 on the other hand is a crucial regulator of synaptic function and plasticity<sup>205</sup>. Astrocytic ephrina3 is critical in the regulation of hippocampal dendritic spine morphology and it regulates the abundance of glial glutamate transporters which is crucial to prevent glutamate toxicity under pathological conditions<sup>205, 253-255</sup>. Under normal physiological conditions, ephrinb2 signaling in astrocytes regulates adult hippocampal neurogenesis<sup>252</sup>. After spinal cord injury, its expression is highly upregulated in the astrocytes of the glial scar after spinal cord lesions<sup>256</sup>. Furthermore, the deletion of ephrinb2 from reactive astrocytes reduced glial scar formation and improved recovery after spinal cord injury<sup>256-257</sup>. This improved recovery was correlated with an increased regenerative capacity of sprouting spinal cord axons<sup>212, 257</sup>. Ephrina5 has not been detected on resting astrocytes, but its expression is highly upregulated in astrocytes at the peri-lesioned area after experimental stroke<sup>218</sup>. In this model, high astrocytic ephrina5 expression inhibited

axonal sprouting and motor recovery<sup>218</sup>. Both ephrinA5 and ephrinB2 are interesting interaction candidates of Epha4 in the pathogenesis of ALS, as their expression is upregulated in reactive astrocytes which is a hallmark of ALS. Here, we explored the role of ephrinB2 during ALS pathogenesis.

### **EphrinB2 in ALS**

In normal conditions, ephrinB2 is highly expressed in motor neurons. In ALS, the declined ephrinB2 expression due to motor neuron loss is accompanied by an obvious ephrinB2 expression in reactive astrocytes, which may explain why total spinal cord levels barely change. Transgenically deleting ephrinB2 from the astrocytes worsened disease in the SOD1<sup>G93A</sup> mouse. EphrinB2 therefore unlikely is involved in the Epha4 reverse signaling, which mediates the hazardous reverse signaling explaining the beneficial effect of Epha4 inhibition. Two of our findings, likely to be related, may explain the hazardous effect of the deletion of ephrinB2 from the ALS mouse. First the expression of CX3CR1, a marker for CNS microglia and inflammatory cells from the circulation, was greatly increased, indicating increased inflammation in the spinal cord, which may enhance motor neuron degeneration. Second, we found evidence for disruption of the BBB upon deletion of ephrinB2 from astrocytes. The BBB consists of endothelial cells, pericytes and astrocytes creating a neurovascular unit with the adjacent neurons<sup>318</sup>. Evidence for abnormalities of the BBB and BSCB has been found in animal models of ALS and in ALS patients<sup>276, 319-320</sup>. Barrier impairment has even been detected in mutant SOD1 mice and rats before motor neuron degeneration and inflammation<sup>277, 320</sup>. Reduction of tight junction proteins and swollen astrocyte-endfeet that dissociate from the endothelium has been found<sup>273, 276, 321</sup>. We found that astrocyte-specific deletion of ephrinB2 worsened the BBB leakage in mutant SOD1 mice, an effect that became more pronounced when disease progressed. Further investigation is needed to investigate the role of astrocytic ephrinB2 on tight junction expression and the association of its astrocyte-endfeet with the endothelium, but already, our data suggest that alterations in the BBB and BSCB enhance motor neuron degeneration<sup>276</sup> and that understanding the BBB pathophysiology may implicate therapeutic options.

Furthermore, the question arises which receptor astrocytic ephrinB2 interacts with to have its effect in ALS and on the BBB. Obvious candidates are EphB2 and EphB4 on endothelial cells, which have been studied extensively, especially during development<sup>322-324</sup>. However, as VEGFR1 and VEGFR2 have been detected in astrocytes, it is also possible that ephrinB2 interacts *in cis* with a VEGFR thereby regulating its internalization and signaling<sup>262-263, 325-326</sup>. Of interest is the notion that ephrinB2 and VEGF have been shown to be very tightly linked during angiogenesis and lymphangiogenesis<sup>263, 327</sup>. More specifically, ephrinB2 regulates the internalization and signaling of VEGFR2 and VEGFR3<sup>262-263</sup>. VEGF is upstream of ephrinB2

and controls its expression<sup>328-329</sup>. We have previously found that VEGF may be involved in the biology of ALS, as decreasing VEGF expression enhances ALS and treatment of ALS rats with VEGF attenuates their disease<sup>330-331</sup>. Similarly astrocyte-specific deletion of ephrinb2 worsened the disease progression, suggesting that reducing ephrinb2 levels might interfere with VEGF signaling at play in the astrocytes. However, further investigation is needed to elucidate whether reducing ephrinb2 levels in astrocytes impairs VEGFR internalization and VEGF signaling in this way contributing to the worsened disease progression. VEGF is neurotrophic factor and it protects motor neurons from insults such as glutamate-mediated excitotoxicity<sup>332</sup>. However, VEGF might also affect motor neurons through an indirect effect on glial cells such as astrocytes. VEGF might influence the release of neurotrophic factors and they might protect motor neurons from excitotoxicity by inducing GluR2 expression and/or regulating glial glutamate transporter expression<sup>333</sup>. Further investigation is needed to elucidate whether these mechanisms are at play in the worsened disease progression of efnb2<sup>fl/fl</sup>; Cx30; SOD1<sup>G93A</sup> mice.

### **Developing a specific EphA4 inhibitor**

Blocking the EphA4 receptor attenuates motor neuron degeneration. However, EphA4 antagonists have major shortcomings as discussed above. We therefore set out to develop better tools. As it is the reverse signaling, which likely underlies the effects of EphA4 in ALS, inhibitors of its forward (kinase-dependent) signaling, if specific ones could be generated, are less attractive. We therefore took the challenge of generating blockers of the extracellular, ligand-binding domain through the development of Nanobodies. So far, no conventional antibodies are available that target the EphA4 ligand-binding domain, most likely due to the dynamic nature of this domain<sup>144, 146, 286</sup>. However, Nanobodies have been used to fix receptors in one conformation, thereby facilitating the development of crystal structures to determine its structure<sup>293, 334</sup>. This property of Nbs is useful for the development of a Nb targeting a dynamic structure such as the EphA4 ligand-binding domain.

From the fifteen Nbs initially identified in the screen, we found two Nanobodies (Nb 39 and Nb 53) with high affinity for EphA4. These Nbs were most selective for EphA4, though they also show binding to EphA7. Furthermore, they blocked the interaction with all ephrin ligands and inhibited ephrin-induced phosphorylation. Nb 39 and Nb 53 are at least 10 times more potent than the KYL-peptide. EphA7 has not as extensively been studied as EphA4, but similar results as EphA4 have been shown in spinal cord injury<sup>305, 335</sup>. This suggests that blocking both EphA4 and EphA7 might result in an even better outcome. However, this will need further investigation.

Among existing EphA4 antagonists, both Nb39 and 53 are good inhibitors with  $K_D$  values in the high nanomolar range. However, most Nanobodies published so far have  $K_D$  values in the low nanomolar, even picomolar range<sup>336</sup>. The affinity of these Nbs can be further increased through error-prone PCR mutagenesis and/or making bispecific Nbs<sup>312-313</sup>. Nbs are easily engineered into multivalent and multispecific formats<sup>312</sup>. Bivalent or bispecific Nbs can be obtained by connecting two identical or two different Nbs with a linker thereby improving the avidity. However, dimerisation of Eph receptors induces clustering and subsequently activation, which can be obtained with a preclustered antibody<sup>337</sup>. Therefore we have to be cautious how to design multivalent Nbs. As linking two Nbs targeting the ligand-binding domain is likely to induce clustering, another option would be to link a Nb targeting the ligand-binding domain with a second Nb targeting another region of the EphA4 extracellular domain. However, further investigation is needed to elucidate which would be the best option.

Overall, further studies are needed to investigate whether the promising results of the can be translated in *in vitro* and *in vivo* functional models. We will investigate whether Nb 39 and 53 are able to rescue ephrin-induced growth cone collapse, which has been shown for known EphA4 antagonists<sup>213, 284</sup>. The best Nb will be tested in *in vivo* functional models. As EphA4 plays a role in acute injuries as well as in neurodegenerative disorders, the usefulness of the Nb can be tested in different models.

## **Future perspectives**

We have previously shown Epha4 to be a modifier of ALS in animal models and in patients. We tried to unravel the mechanism of action of the hazardous effect of EphA4 in ALS. We found Epha4 to contribute to the vulnerability of motor neurons in the SOD1<sup>G93A</sup> mouse model. Future experiments are needed to elucidate whether this also holds true in ALS patients. Next to vulnerability, we also investigated the role of the signaling direction of the ephrin system in ALS. Experiments with the Epha4<sup>eGFP/eGFP</sup> mouse model showed that Epha4 reverse signaling at least partially contributes to the hazardous effect of Epha4 in ALS. However, as we have to be cautious when interpreting these results, we are currently repeating this experiments with a mouse in which the kinase activity is silenced through a point mutation rather than through the replacement of an entire domain. Comparing all results together will give us more insight in the complex signaling of the ephrin system and which signaling contributes to the hazardous effect of Epha4 in ALS.

Epha4 interacts with different ephrin ligands. In this PhD thesis we focused on the role of ephrinb2 in the pathogenesis of ALS. We found reduction of astrocytic ephrinb2 to have a detrimental role in ALS pathogenesis. Further research is currently being performed in our

laboratory to elucidate the mechanism of action. As ephrinb2 is not likely to be the interaction partner of EphA4 in its hazardous effect on ALS, the role of another ephrin ligands will be investigated. Recent data in our laboratory showed ephrina5 to be upregulated in reactive astrocytes (data not shown). We are currently elucidating the role of ephrina5 in the pathogenesis of ALS.

We also explored the therapeutic potential of EphA4 inhibitors in the pathogenesis of ALS. We found C1 to be chemically unstable thereby limiting its potential for *in vivo* use. We are currently testing the therapeutic potential of new EphA4 inhibitors such as APY- $\beta$ Ala8.am in the pathogenesis of ALS. In addition, we tried to develop specific EphA4 inhibitors using Nanobody technology. We found two Nanobodies, Nb 39 and Nb 53 to be good EphA4 inhibitors. Future experiments are needed to investigate its therapeutic potential both *in vitro* and *in vivo* in the pathogenesis of ALS. In addition, we will try to improve the specificity and affinity of Nb39 and 53.

### **EphA4 as therapeutic target?**

In this first part of PhD thesis we tried to unravel the mechanism of action of EphA4 in the pathogenesis of ALS. Using different transgenic mouse models, we revealed new aspects of the ephrin system on a molecular level. However, the experiments with these mouse models showed that we have to be cautious when interpreting these results. Influencing the system has led to surprising results, showing again the complexity of this system. The hazardous effect of EphA4 has also been shown in other neurological disorders, but the mechanism of action and the best way to target EphA4 awaits further investigation and could vary between different disorders.

In the second part of this PhD thesis we explored the therapeutic potential of EphA4 inhibitors of ALS and developed new EphA4 inhibitors using Nanobody technology. Several EphA4 inhibitors have been developed, but many of them have major shortcomings as discussed above. Improved inhibitors have been developed (Nb 39 and Nb 53, APY- $\beta$ Ala8.am), but further refinement is needed to increase its affinity, selectivity and pharmacokinetic properties. In addition, EphA4 inhibitors must be able to reach their target which is prevented by the BBB. In acute injuries this barrier is impaired, but in neurodegenerative diseases such as ALS getting drugs across the BBB still remains a major challenge.

To conclude, improvements in EphA4 inhibitors and unraveling the ephrin system might open new possibilities to treat several neurological disorders.

## Summary

Amyotrophic Lateral Sclerosis (ALS) is a dramatic neurodegenerative disease due to its progressive character, the short survival of the patient and the enormous impact on his/her quality of life and that of his/her caretaker. Interestingly, ALS patients, even carrying the same mutation in *SOD1*, have great variations in clinical characteristics as age of onset, disease duration and severity of the disease. This indicates that ALS is a multifactorial disease influenced by modifying genes and environmental factors. Epha4 is such a genetic factor that modifies ALS both in animal models as well as in patients. We investigated the mechanism in which Epha4 is modifying the disease pathogenesis in ALS. We found that vulnerable motor neurons have high Epha4 expression and that Epha4 reduced the re-innervating capacity of motor neurons, possibly contributing to the higher vulnerability of Epha4 expressing motor neurons in ALS. Furthermore, deleting the Epha4 cytoplasmic domain did not affect disease onset and survival in the *SOD1*<sup>G93A</sup> mouse model indicating that Epha4 forward signaling in the Eph-bearing cell does not play a role in the modifying effect of Epha4 in ALS. We therefore suggest that the reverse pathway in the ephrin-bearing cell should be modified in order to alter ALS pathology. We studied ephrinb2 as a possible ligand for the Epha4-mediated effect in ALS. It was highly expressed in motor neurons and in reactive astrocytes. However, deletion of ephrinb2 enhanced disease rather than attenuating it. Interestingly, deleting ephrinb2 from the astrocytes impaired the blood brain barrier integrity which possibly contributed to the reduced disease duration and survival in the *SOD1*<sup>G93A</sup> mouse model.

To inhibit Epha4 reverse signaling we developed Nanobodies targeting the EphA4 ligand-binding domain. Nb 39 and Nb 53 were selective for EphA4, and had  $K_D$  and  $IC_{50}$  values in the nanomolar range. Both Nanobodies were able to block the interaction of EphA4 with all ephrin ligands and they inhibited ephrin-induced phosphorylation. In conclusion, blocking the interaction of EphA4 and its ephrin ligands will be the most efficient way to block EphA4 reverse signaling and to develop a specific EphA4 antagonist.



## Samenvatting

Amyotrofe Laterale Sclerose (ALS) is een dramatische neurodegeneratieve aandoening door het progressieve karakter van de ziekte, de korte overleving van de patiënt en de grote impact op zijn levenskwaliteit en die van zijn omgeving. ALS-patiënten met dezelfde mutatie in SOD1 vertonen grote variabiliteit in klinische manifestatie van de ziekte zoals de leeftijd waarop de eerste symptomen voorkomen, de ziekteprogressie en de agressiviteit waarmee de ziekte evolueert. Dit toont aan dat ALS een multifactoriële ziekte is die beïnvloed wordt door modifierende genen en omgevingsfactoren. Epha4 is zo'n genetische factor die de ziekte beïnvloedt zowel in diermodellen als bij patiënten. We onderzochten het mechanisme van Epha4 dat het verloop van de ziekte beïnvloedt. Hoge Epha4-expressie verminderde het reïnnervatiepotentieel van grote motorneuronen, wat bijdraagt aan de hogere gevoeligheid van deze motorneuronen in ALS. Bovendien had de verwijdering van het intracellulaire domein van Epha4 geen invloed op het tijdstip van aanvang van de ziekte en de overleving van de SOD1<sup>G93A</sup> muis, wat er op duidt dat de voorwaartse signalisatie in de cel die EphA4 bevat, geen rol speelt in het modifierende effect van Epha4 in ALS. Dit suggereert dat er geïnterfereerd moet worden met de terugwaartse signalisatie in de cel met de efrineliganden om de ziekte te beïnvloeden. Efrineb2, één van de EphA4-liganden, was duidelijk aanwezig in motorneuronen en reactieve astrocyten. Het verwijderen van efrineb2 van de astrocyten tastte de bloedhersenbarrière aan, wat onder meer zorgde voor een verminderde duur van de ziekte in de SOD1<sup>G93A</sup> muis. Om de terugwaartse signalisatie van EphA4 te blokkeren, ontwikkelden we Nanobodies gericht tegen het ligand-bindende domein van EphA4. Nanobody 39 en 53 interageerden selectief met EphA4 en hadden K<sub>D</sub> en IC<sub>50</sub> waardes in het nanomolaire bereik. Beide Nanobodies konden de interactie van EphA4 met alle efrineliganden blokkeren en inhibeerden EphA4-fosforylatie geïnduceerd door efrinea1. Dit werk toont aan dat het blokkeren van de interactie tussen EphA4 en zijn efrineliganden de meest efficiënte manier zal zijn om de terugwaartse signalisatie van EphA4 te blokkeren en om een specifieke EphA4-inhibitor te ontwikkelen.





## References

1. Cleveland DW, Rothstein JD. From Charcot to Lou Gehrig: deciphering selective motor neuron death in ALS. *Nat Rev Neurosci* 2001;2:806-19.
2. Swinnen B, Robberecht W. The phenotypic variability of amyotrophic lateral sclerosis. *Nat Rev Neurol* 2014;10:661-70.
3. Rowland LP, Shneider NA. Amyotrophic lateral sclerosis. *N Engl J Med* 2001;344:1688-700.
4. Poppe L, Rue L, Robberecht W, Van Den Bosch L. Translating biological findings into new treatment strategies for amyotrophic lateral sclerosis (ALS). *Exp Neurol* 2014;262 Pt B:138-51.
5. Hugon J. Riluzole and ALS therapy. *Wien Med Wochenschr* 1996;146:185-7.
6. Neary D, Snowden J, Mann D. Frontotemporal dementia. *Lancet Neurol* 2005;4:771-80.
7. Renton AE, Chio A, Traynor BJ. State of play in amyotrophic lateral sclerosis genetics. *Nat Neurosci* 2014;17:17-23.
8. Rosen DR. Mutations in Cu/Zn superoxide dismutase gene are associated with familial amyotrophic lateral sclerosis. *Nature* 1993;364:362.
9. Gurney ME, Pu H, Chiu AY, et al. Motor neuron degeneration in mice that express a human Cu,Zn superoxide dismutase mutation. *Science* 1994;264:1772-5.
10. Shibata N. Transgenic mouse model for familial amyotrophic lateral sclerosis with superoxide dismutase-1 mutation. *Neuropathology* 2001;21:82-92.
11. Jaarsma D, Haasdijk ED, Grashorn JA, et al. Human Cu/Zn superoxide dismutase (SOD1) overexpression in mice causes mitochondrial vacuolization, axonal degeneration, and premature motoneuron death and accelerates motoneuron disease in mice expressing a familial amyotrophic lateral sclerosis mutant SOD1. *Neurobiol Dis* 2000;7:623-43.
12. Reaume AG, Elliott JL, Hoffman EK, et al. Motor neurons in Cu/Zn superoxide dismutase-deficient mice develop normally but exhibit enhanced cell death after axonal injury. *Nat Genet* 1996;13:43-7.
13. Lemmens R, Van Hoecke A, Hersmus N, et al. Overexpression of mutant superoxide dismutase 1 causes a motor axonopathy in the zebrafish. *Hum Mol Genet* 2007;16:2359-65.
14. Deng H, Gao K, Jankovic J. The role of FUS gene variants in neurodegenerative diseases. *Nat Rev Neurol* 2014;10:337-48.
15. Lee Y, Morrison BM, Li Y, et al. Oligodendroglia metabolically support axons and contribute to neurodegeneration. *Nature* 2012;487:443-8.
16. Neumann M, Sampathu DM, Kwong LK, et al. Ubiquitinated TDP-43 in frontotemporal lobar degeneration and amyotrophic lateral sclerosis. *Science* 2006;314:130-3.
17. Deng HX, Zhai H, Bigio EH, et al. FUS-immunoreactive inclusions are a common feature in sporadic and non-SOD1 familial amyotrophic lateral sclerosis. *Ann Neurol* 2010;67:739-48.
18. Da Cruz S, Cleveland DW. Understanding the role of TDP-43 and FUS/TLS in ALS and beyond. *Curr Opin Neurobiol* 2011;21:904-19.
19. Robberecht W, Philips T. The changing scene of amyotrophic lateral sclerosis. *Nat Rev Neurosci* 2013;14:248-64.
20. DeJesus-Hernandez M, Mackenzie IR, Boeve BF, et al. Expanded GGGGCC hexanucleotide repeat in noncoding region of C9ORF72 causes chromosome 9p-linked FTD and ALS. *Neuron* 2011;72:245-56.
21. Renton AE, Majounie E, Waite A, et al. A hexanucleotide repeat expansion in C9ORF72 is the cause of chromosome 9p21-linked ALS-FTD. *Neuron* 2011;72:257-68.
22. Gijssels I, Van Langenhove T, van der Zee J, et al. A C9orf72 promoter repeat expansion in a Flanders-Belgian cohort with disorders of the frontotemporal lobar degeneration-amyotrophic lateral sclerosis spectrum: a gene identification study. *Lancet Neurol* 2012;11:54-65.

23. Belzil VV, Bauer PO, Prudencio M, et al. Reduced C9orf72 gene expression in c9FTD/ALS is caused by histone trimethylation, an epigenetic event detectable in blood. *Acta Neuropathol* 2013;126:895-905.
24. Haeusler AR, Donnelly CJ, Periz G, et al. C9orf72 nucleotide repeat structures initiate molecular cascades of disease. *Nature* 2014;507:195-200.
25. Fratta P, Mizielinska S, Nicoll AJ, et al. C9orf72 hexanucleotide repeat associated with amyotrophic lateral sclerosis and frontotemporal dementia forms RNA G-quadruplexes. *Sci Rep* 2012;2:1016.
26. Mori K, Arzberger T, Grasser FA, et al. Bidirectional transcripts of the expanded C9orf72 hexanucleotide repeat are translated into aggregating dipeptide repeat proteins. *Acta Neuropathol* 2013;126:881-93.
27. Marangi G, Traynor BJ. Genetic causes of amyotrophic lateral sclerosis: New genetic analysis methodologies entailing new opportunities and challenges. *Brain Res* 2014.
28. Regal L, Vanopdenbosch L, Tilkin P, et al. The G93C mutation in superoxide dismutase 1: clinicopathologic phenotype and prognosis. *Arch Neurol* 2006;63:262-7.
29. Dion PA, Daoud H, Rouleau GA. Genetics of motor neuron disorders: new insights into pathogenic mechanisms. *Nat Rev Genet* 2009;10:769-82.
30. Andersen PM, Al-Chalabi A. Clinical genetics of amyotrophic lateral sclerosis: what do we really know? *Nat Rev Neurol* 2011;7:603-15.
31. van Blitterswijk M, Mullen B, Wojtas A, et al. Genetic modifiers in carriers of repeat expansions in the C9ORF72 gene. *Mol Neurodegener* 2014;9:38.
32. Figley MD, Gitler AD. Yeast genetic screen reveals novel therapeutic strategy for ALS. *Rare Dis* 2013;1:e24420.
33. Lee T, Li YR, Ingre C, et al. Ataxin-2 intermediate-length polyglutamine expansions in European ALS patients. *Hum Mol Genet* 2011;20:1697-700.
34. Elden AC, Kim HJ, Hart MP, et al. Ataxin-2 intermediate-length polyglutamine expansions are associated with increased risk for ALS. *Nature* 2010;466:1069-75.
35. Van Hoecke A, Schoonaert L, Lemmens R, et al. EPHA4 is a disease modifier of amyotrophic lateral sclerosis in animal models and in humans. *Nat Med* 2012;18:1418-22.
36. Ling SC, Polymenidou M, Cleveland DW. Converging mechanisms in ALS and FTD: disrupted RNA and protein homeostasis. *Neuron* 2013;79:416-38.
37. Anderson P, Kedersha N. RNA granules: post-transcriptional and epigenetic modulators of gene expression. *Nat Rev Mol Cell Biol* 2009;10:430-6.
38. Li YR, King OD, Shorter J, Gitler AD. Stress granules as crucibles of ALS pathogenesis. *J Cell Biol* 2013;201:361-72.
39. Kato M, Han TW, Xie S, et al. Cell-free formation of RNA granules: low complexity sequence domains form dynamic fibers within hydrogels. *Cell* 2012;149:753-67.
40. Schwartz JC, Wang X, Podell ER, Cech TR. RNA seeds higher-order assembly of FUS protein. *Cell Rep* 2013;5:918-25.
41. King OD, Gitler AD, Shorter J. The tip of the iceberg: RNA-binding proteins with prion-like domains in neurodegenerative disease. *Brain Res* 2012;1462:61-80.
42. Toretzky JA, Wright PE. Assemblages: functional units formed by cellular phase separation. *J Cell Biol* 2014;206:579-88.
43. Rotunno MS, Bosco DA. An emerging role for misfolded wild-type SOD1 in sporadic ALS pathogenesis. *Front Cell Neurosci* 2013;7:253.
44. Blokhuis AM, Groen EJ, Koppers M, van den Berg LH, Pasterkamp RJ. Protein aggregation in amyotrophic lateral sclerosis. *Acta Neuropathol* 2013;125:777-94.
45. Saxena S, Cabuy E, Caroni P. A role for motoneuron subtype-selective ER stress in disease manifestations of FALS mice. *Nat Neurosci* 2009;12:627-36.
46. Seeburg PH. The TIPS/TINS lecture: the molecular biology of mammalian glutamate receptor channels. *Trends Pharmacol Sci* 1993;14:297-303.

47. Heath PR, Shaw PJ. Update on the glutamatergic neurotransmitter system and the role of excitotoxicity in amyotrophic lateral sclerosis. *Muscle Nerve* 2002;26:438-58.
48. Tanaka K, Watase K, Manabe T, et al. Epilepsy and exacerbation of brain injury in mice lacking the glutamate transporter GLT-1. *Science* 1997;276:1699-702.
49. Haugeto O, Ullensvang K, Levy LM, et al. Brain glutamate transporter proteins form homomultimers. *J Biol Chem* 1996;271:27715-22.
50. Baimbridge KG, Celio MR, Rogers JH. Calcium-binding proteins in the nervous system. *Trends Neurosci* 1992;15:303-8.
51. Orrenius S, McConkey DJ, Bellomo G, Nicotera P. Role of Ca<sup>2+</sup> in toxic cell killing. *Trends Pharmacol Sci* 1989;10:281-5.
52. Van Den Bosch L, Van Damme P, Bogaert E, Robberecht W. The role of excitotoxicity in the pathogenesis of amyotrophic lateral sclerosis. *Biochim Biophys Acta* 2006;1762:1068-82.
53. Van Damme P, Van Den Bosch L, Van Houtte E, Callewaert G, Robberecht W. GluR2-dependent properties of AMPA receptors determine the selective vulnerability of motor neurons to excitotoxicity. *J Neurophysiol* 2002;88:1279-87.
54. Maragakis NJ, Dykes-Hoberg M, Rothstein JD. Altered expression of the glutamate transporter EAAT2b in neurological disease. *Ann Neurol* 2004;55:469-77.
55. Fray AE, Ince PG, Banner SJ, et al. The expression of the glial glutamate transporter protein EAAT2 in motor neuron disease: an immunohistochemical study. *Eur J Neurosci* 1998;10:2481-9.
56. Rothstein JD, Van Kammen M, Levey AI, Martin LJ, Kuncl RW. Selective loss of glial glutamate transporter GLT-1 in amyotrophic lateral sclerosis. *Ann Neurol* 1995;38:73-84.
57. Howland DS, Liu J, She Y, et al. Focal loss of the glutamate transporter EAAT2 in a transgenic rat model of SOD1 mutant-mediated amyotrophic lateral sclerosis (ALS). *Proc Natl Acad Sci U S A* 2002;99:1604-9.
58. Bruijn LI, Becher MW, Lee MK, et al. ALS-linked SOD1 mutant G85R mediates damage to astrocytes and promotes rapidly progressive disease with SOD1-containing inclusions. *Neuron* 1997;18:327-38.
59. Kawamata H, Manfredi G. Mitochondrial dysfunction and intracellular calcium dysregulation in ALS. *Mech Ageing Dev* 2010;131:517-26.
60. Van Damme P, Bogaert E, Dewil M, et al. Astrocytes regulate GluR2 expression in motor neurons and their vulnerability to excitotoxicity. *Proc Natl Acad Sci U S A* 2007;104:14825-30.
61. Barber SC, Shaw PJ. Oxidative stress in ALS: key role in motor neuron injury and therapeutic target. *Free Radic Biol Med* 2010;48:629-41.
62. Batulan Z, Shinder GA, Minotti S, et al. High threshold for induction of the stress response in motor neurons is associated with failure to activate HSF1. *J Neurosci* 2003;23:5789-98.
63. Lowenstein DH, Chan PH, Miles MF. The stress protein response in cultured neurons: characterization and evidence for a protective role in excitotoxicity. *Neuron* 1991;7:1053-60.
64. Rordorf G, Koroshetz WJ, Bonventre JV. Heat shock protects cultured neurons from glutamate toxicity. *Neuron* 1991;7:1043-51.
65. Kalmar B, Greensmith L. Induction of heat shock proteins for protection against oxidative stress. *Adv Drug Deliv Rev* 2009;61:310-8.
66. Bruening W, Roy J, Giasson B, Figlewicz DA, Mushynski WE, Durham HD. Up-regulation of protein chaperones preserves viability of cells expressing toxic Cu/Zn-superoxide dismutase mutants associated with amyotrophic lateral sclerosis. *J Neurochem* 1999;72:693-9.
67. Gizzi M, DiRocco A, Sivak M, Cohen B. Ocular motor function in motor neuron disease. *Neurology* 1992;42:1037-46.
68. Kaminski HJ, Richmonds CR, Kusner LL, Mitsumoto H. Differential susceptibility of the ocular motor system to disease. *Ann N Y Acad Sci* 2002;956:42-54.
69. Mannen T. Neuropathological findings of Onuf's nucleus and its significance. *Neuropathology* 2000;20 Suppl:S30-3.
70. Schroder HD, Reske-Nielsen E. Preservation of the nucleus X-pelvic floor motosystem in amyotrophic lateral sclerosis. *Clin Neuropathol* 1984;3:210-6.

71. Brockington A, Ning K, Heath PR, et al. Unravelling the enigma of selective vulnerability in neurodegeneration: motor neurons resistant to degeneration in ALS show distinct gene expression characteristics and decreased susceptibility to excitotoxicity. *Acta Neuropathol* 2013;125:95-109.
72. Lorenzo LE, Barbe A, Portalier P, Fritschy JM, Bras H. Differential expression of GABAA and glycine receptors in ALS-resistant vs. ALS-vulnerable motoneurons: possible implications for selective vulnerability of motoneurons. *Eur J Neurosci* 2006;23:3161-70.
73. Vanselow BK, Keller BU. Calcium dynamics and buffering in oculomotor neurones from mouse that are particularly resistant during amyotrophic lateral sclerosis (ALS)-related motoneurone disease. *J Physiol* 2000;525 Pt 2:433-45.
74. Kaplan A, Spiller KJ, Towne C, et al. Neuronal matrix metalloproteinase-9 is a determinant of selective neurodegeneration. *Neuron* 2014;81:333-48.
75. Frey D, Schneider C, Xu L, Borg J, Spooren W, Caroni P. Early and selective loss of neuromuscular synapse subtypes with low sprouting competence in motoneuron diseases. *J Neurosci* 2000;20:2534-42.
76. Dengler R, Konstanzer A, Kuther G, Hesse S, Wolf W, Struppler A. Amyotrophic lateral sclerosis: macro-EMG and twitch forces of single motor units. *Muscle Nerve* 1990;13:545-50.
77. Pun S, Santos AF, Saxena S, Xu L, Caroni P. Selective vulnerability and pruning of phasic motoneuron axons in motoneuron disease alleviated by CNTF. *Nat Neurosci* 2006;9:408-19.
78. de Carvalho MA, Pinto S, Swash M. Paraspinal and limb motor neuron involvement within homologous spinal segments in ALS. *Clin Neurophysiol* 2008;119:1607-13.
79. Brown MC, Holland RL, Ironton R. Nodal and terminal sprouting from motor nerves in fast and slow muscles of the mouse. *J Physiol* 1980;306:493-510.
80. Scotter EL, Chen HJ, Shaw CE. TDP-43 Proteinopathy and ALS: Insights into Disease Mechanisms and Therapeutic Targets. *Neurotherapeutics* 2015;12:352-63.
81. Souza PV, Pinto WB, Oliveira AS. C9orf72-related disorders: expanding the clinical and genetic spectrum of neurodegenerative diseases. *Arq Neuropsiquiatr* 2015;73:246-56.
82. Lino MM, Schneider C, Caroni P. Accumulation of SOD1 mutants in postnatal motoneurons does not cause motoneuron pathology or motoneuron disease. *J Neurosci* 2002;22:4825-32.
83. Pramatarova A, Laganieri J, Roussel J, Brisebois K, Rouleau GA. Neuron-specific expression of mutant superoxide dismutase 1 in transgenic mice does not lead to motor impairment. *J Neurosci* 2001;21:3369-74.
84. Jaarsma D, Teuling E, Haasdijk ED, De Zeeuw CI, Hoogenraad CC. Neuron-specific expression of mutant superoxide dismutase is sufficient to induce amyotrophic lateral sclerosis in transgenic mice. *J Neurosci* 2008;28:2075-88.
85. Wang L, Sharma K, Deng HX, et al. Restricted expression of mutant SOD1 in spinal motor neurons and interneurons induces motor neuron pathology. *Neurobiol Dis* 2008;29:400-8.
86. Boillee S, Yamanaka K, Lobsiger CS, et al. Onset and progression in inherited ALS determined by motor neurons and microglia. *Science* 2006;312:1389-92.
87. Yamanaka K, Boillee S, Roberts EA, et al. Mutant SOD1 in cell types other than motor neurons and oligodendrocytes accelerates onset of disease in ALS mice. *Proc Natl Acad Sci U S A* 2008;105:7594-9.
88. Ralph GS, Radcliffe PA, Day DM, et al. Silencing mutant SOD1 using RNAi protects against neurodegeneration and extends survival in an ALS model. *Nat Med* 2005;11:429-33.
89. Wang L, Sharma K, Grisotti G, Roos RP. The effect of mutant SOD1 dismutase activity on non-cell autonomous degeneration in familial amyotrophic lateral sclerosis. *Neurobiol Dis* 2009;35:234-40.
90. Beers DR, Henkel JS, Xiao Q, et al. Wild-type microglia extend survival in PU.1 knockout mice with familial amyotrophic lateral sclerosis. *Proc Natl Acad Sci U S A* 2006;103:16021-6.
91. Yamanaka K, Chun SJ, Boillee S, et al. Astrocytes as determinants of disease progression in inherited amyotrophic lateral sclerosis. *Nat Neurosci* 2008;11:251-3.
92. Lepore AC, Rauck B, Dejea C, et al. Focal transplantation-based astrocyte replacement is neuroprotective in a model of motor neuron disease. *Nat Neurosci* 2008;11:1294-301.

93. Kang SH, Li Y, Fukaya M, et al. Degeneration and impaired regeneration of gray matter oligodendrocytes in amyotrophic lateral sclerosis. *Nat Neurosci* 2013;16:571-9.
94. Sofroniew MV, Vinters HV. Astrocytes: biology and pathology. *Acta Neuropathol* 2010;119:7-35.
95. Abbott NJ, Ronnback L, Hansson E. Astrocyte-endothelial interactions at the blood-brain barrier. *Nat Rev Neurosci* 2006;7:41-53.
96. Sofroniew MV. Molecular dissection of reactive astrogliosis and glial scar formation. *Trends Neurosci* 2009;32:638-47.
97. Takano T, He W, Han X, et al. Rapid manifestation of reactive astrogliosis in acute hippocampal brain slices. *Glia* 2014;62:78-95.
98. Molofsky AV, Krencik R, Ullian EM, et al. Astrocytes and disease: a neurodevelopmental perspective. *Genes Dev* 2012;26:891-907.
99. Wilhelmsson U, Bushong EA, Price DL, et al. Redefining the concept of reactive astrocytes as cells that remain within their unique domains upon reaction to injury. *Proc Natl Acad Sci U S A* 2006;103:17513-8.
100. Schiffer D, Cordera S, Cavalla P, Migheli A. Reactive astrogliosis of the spinal cord in amyotrophic lateral sclerosis. *J Neurol Sci* 1996;139 Suppl:27-33.
101. Nagy D, Kato T, Kushner PD. Reactive astrocytes are widespread in the cortical gray matter of amyotrophic lateral sclerosis. *J Neurosci Res* 1994;38:336-47.
102. Kushner PD, Stephenson DT, Wright S. Reactive astrogliosis is widespread in the subcortical white matter of amyotrophic lateral sclerosis brain. *J Neuropathol Exp Neurol* 1991;50:263-77.
103. Vargas MR, Johnson JA. Astrogliosis in amyotrophic lateral sclerosis: role and therapeutic potential of astrocytes. *Neurotherapeutics* 2010;7:471-81.
104. Nagai M, Re DB, Nagata T, et al. Astrocytes expressing ALS-linked mutated SOD1 release factors selectively toxic to motor neurons. *Nat Neurosci* 2007;10:615-22.
105. Di Giorgio FP, Carrasco MA, Siao MC, Maniatis T, Eggan K. Non-cell autonomous effect of glia on motor neurons in an embryonic stem cell-based ALS model. *Nat Neurosci* 2007;10:608-14.
106. Fritz E, Izaurieta P, Weiss A, et al. Mutant SOD1-expressing astrocytes release toxic factors that trigger motoneuron death by inducing hyperexcitability. *J Neurophysiol* 2013;109:2803-14.
107. Haidet-Phillips AM, Hester ME, Miranda CJ, et al. Astrocytes from familial and sporadic ALS patients are toxic to motor neurons. *Nat Biotechnol* 2011;29:824-8.
108. Re DB, Le Verche V, Yu C, et al. Necroptosis drives motor neuron death in models of both sporadic and familial ALS. *Neuron* 2014;81:1001-8.
109. Hanisch UK, Kettenmann H. Microglia: active sensor and versatile effector cells in the normal and pathologic brain. *Nat Neurosci* 2007;10:1387-94.
110. Henkel JS, Beers DR, Zhao W, Appel SH. Microglia in ALS: the good, the bad, and the resting. *J Neuroimmune Pharmacol* 2009;4:389-98.
111. Philips T, Robberecht W. Neuroinflammation in amyotrophic lateral sclerosis: role of glial activation in motor neuron disease. *Lancet Neurol* 2011;10:253-63.
112. Cherry JD, Olschowka JA, O'Banion MK. Neuroinflammation and M2 microglia: the good, the bad, and the inflamed. *J Neuroinflammation* 2014;11:98.
113. Liao B, Zhao W, Beers DR, Henkel JS, Appel SH. Transformation from a neuroprotective to a neurotoxic microglial phenotype in a mouse model of ALS. *Exp Neurol* 2012;237:147-52.
114. Engelhardt JI, Tajti J, Appel SH. Lymphocytic infiltrates in the spinal cord in amyotrophic lateral sclerosis. *Arch Neurol* 1993;50:30-6.
115. Kawamata T, Akiyama H, Yamada T, McGeer PL. Immunologic reactions in amyotrophic lateral sclerosis brain and spinal cord tissue. *Am J Pathol* 1992;140:691-707.
116. Turner MR, Cagnin A, Turkheimer FE, et al. Evidence of widespread cerebral microglial activation in amyotrophic lateral sclerosis: an [<sup>11</sup>C](R)-PK11195 positron emission tomography study. *Neurobiol Dis* 2004;15:601-9.
117. Lewis CA, Manning J, Rossi F, Krieger C. The Neuroinflammatory Response in ALS: The Roles of Microglia and T Cells. *Neurol Res Int* 2012;2012:803701.

118. Hall ED, Oostveen JA, Gurney ME. Relationship of microglial and astrocytic activation to disease onset and progression in a transgenic model of familial ALS. *Glia* 1998;23:249-56.
119. Bradl M, Lassmann H. Oligodendrocytes: biology and pathology. *Acta Neuropathol* 2010;119:37-53.
120. Sowell ER, Thompson PM, Tessner KD, Toga AW. Mapping continued brain growth and gray matter density reduction in dorsal frontal cortex: Inverse relationships during postadolescent brain maturation. *J Neurosci* 2001;21:8819-29.
121. Levine JM, Reynolds R, Fawcett JW. The oligodendrocyte precursor cell in health and disease. *Trends Neurosci* 2001;24:39-47.
122. Niebroj-Dobosz I, Rafalowska J, Fidzianska A, Gadamski R, Grieb P. Myelin composition of spinal cord in a model of amyotrophic lateral sclerosis (ALS) in SOD1G93A transgenic rats. *Folia Neuropathol* 2007;45:236-41.
123. Seilhean D, Cazeneuve C, Thuries V, et al. Accumulation of TDP-43 and alpha-actin in an amyotrophic lateral sclerosis patient with the K17I ANG mutation. *Acta Neuropathol* 2009;118:561-73.
124. Philips T, Bento-Abreu A, Nonneman A, et al. Oligodendrocyte dysfunction in the pathogenesis of amyotrophic lateral sclerosis. *Brain* 2013;136:471-82.
125. Neumann M, Kwong LK, Truax AC, et al. TDP-43-positive white matter pathology in frontotemporal lobar degeneration with ubiquitin-positive inclusions. *J Neuropathol Exp Neurol* 2007;66:177-83.
126. Shi P, Gal J, Kwinter DM, Liu X, Zhu H. Mitochondrial dysfunction in amyotrophic lateral sclerosis. *Biochim Biophys Acta* 2010;1802:45-51.
127. Devasagayam TP, Tilak JC, Bloor KK, Sane KS, Ghaskadbi SS, Lele RD. Free radicals and antioxidants in human health: current status and future prospects. *J Assoc Physicians India* 2004;52:794-804.
128. Uttara B, Singh AV, Zamboni P, Mahajan RT. Oxidative stress and neurodegenerative diseases: a review of upstream and downstream antioxidant therapeutic options. *Curr Neuropharmacol* 2009;7:65-74.
129. Manfredi G, Xu Z. Mitochondrial dysfunction and its role in motor neuron degeneration in ALS. *Mitochondrion* 2005;5:77-87.
130. Wang C, Youle RJ. The role of mitochondria in apoptosis\*. *Annu Rev Genet* 2009;43:95-118.
131. Tan W, Pasinelli P, Trotti D. Role of mitochondria in mutant SOD1 linked amyotrophic lateral sclerosis. *Biochim Biophys Acta* 2014;1842:1295-301.
132. Kirkinezos IG, Bacman SR, Hernandez D, et al. Cytochrome c association with the inner mitochondrial membrane is impaired in the CNS of G93A-SOD1 mice. *J Neurosci* 2005;25:164-72.
133. Bilsland LG, Sahai E, Kelly G, Golding M, Greensmith L, Schiavo G. Deficits in axonal transport precede ALS symptoms in vivo. *Proc Natl Acad Sci U S A* 2010;107:20523-8.
134. Perlson E, Jeong GB, Ross JL, et al. A switch in retrograde signaling from survival to stress in rapid-onset neurodegeneration. *J Neurosci* 2009;29:9903-17.
135. Warita H, Itoyama Y, Abe K. Selective impairment of fast anterograde axonal transport in the peripheral nerves of asymptomatic transgenic mice with a G93A mutant SOD1 gene. *Brain Res* 1999;819:120-31.
136. Williamson TL, Cleveland DW. Slowing of axonal transport is a very early event in the toxicity of ALS-linked SOD1 mutants to motor neurons. *Nat Neurosci* 1999;2:50-6.
137. Carpenter S. Proximal axonal enlargement in motor neuron disease. *Neurology* 1968;18:841-51.
138. Hirano A. Cytopathology of amyotrophic lateral sclerosis. *Adv Neurol* 1991;56:91-101.
139. Hirano A, Donnerfeld H, Sasaki S, Nakano I. Fine structural observations of neurofilamentous changes in amyotrophic lateral sclerosis. *J Neuropathol Exp Neurol* 1984;43:461-70.
140. Julien JP. A role for neurofilaments in the pathogenesis of amyotrophic lateral sclerosis. *Biochem Cell Biol* 1995;73:593-7.
141. Julien JP. Neurofilaments and motor neuron disease. *Trends Cell Biol* 1997;7:243-9.

142. Hirai H, Maru Y, Hagiwara K, Nishida J, Takaku F. A novel putative tyrosine kinase receptor encoded by the eph gene. *Science* 1987;238:1717-20.
143. Unified nomenclature for Eph family receptors and their ligands, the ephrins. Eph Nomenclature Committee. *Cell* 1997;90:403-4.
144. Bowden TA, Aricescu AR, Nettleship JE, et al. Structural plasticity of eph receptor A4 facilitates cross-class ephrin signaling. *Structure* 2009;17:1386-97.
145. Himanen JP, Chumley MJ, Lackmann M, et al. Repelling class discrimination: ephrin-A5 binds to and activates EphB2 receptor signaling. *Nat Neurosci* 2004;7:501-9.
146. Qin H, Noberini R, Huan X, Shi J, Pasquale EB, Song J. Structural characterization of the EphA4-Ephrin-B2 complex reveals new features enabling Eph-ephrin binding promiscuity. *J Biol Chem* 2010;285:644-54.
147. Gale NW, Holland SJ, Valenzuela DM, et al. Eph receptors and ligands comprise two major specificity subclasses and are reciprocally compartmentalized during embryogenesis. *Neuron* 1996;17:9-19.
148. Klein R. Eph/ephrin signalling during development. *Development* 2012;139:4105-9.
149. Pitulescu ME, Adams RH. Eph/ephrin molecules--a hub for signaling and endocytosis. *Genes Dev* 2010;24:2480-92.
150. Cheng N, Brantley DM, Chen J. The ephrins and Eph receptors in angiogenesis. *Cytokine Growth Factor Rev* 2002;13:75-85.
151. Egea J, Klein R. Bidirectional Eph-ephrin signaling during axon guidance. *Trends Cell Biol* 2007;17:230-8.
152. Holder N, Klein R. Eph receptors and ephrins: effectors of morphogenesis. *Development* 1999;126:2033-44.
153. Durbin L, Brennan C, Shiomi K, et al. Eph signaling is required for segmentation and differentiation of the somites. *Genes Dev* 1998;12:3096-109.
154. Klein R. Bidirectional modulation of synaptic functions by Eph/ephrin signaling. *Nat Neurosci* 2009;12:15-20.
155. Wu J, Luo H. Recent advances on T-cell regulation by receptor tyrosine kinases. *Curr Opin Hematol* 2005;12:292-7.
156. Matsuo K, Otaki N. Bone cell interactions through Eph/ephrin: bone modeling, remodeling and associated diseases. *Cell Adh Migr* 2012;6:148-56.
157. Genander M, Frisen J. Ephrins and Eph receptors in stem cells and cancer. *Curr Opin Cell Biol* 2010;22:611-6.
158. McCarron JK, Stringer BW, Day BW, Boyd AW. Ephrin expression and function in cancer. *Future Oncol* 2010;6:165-76.
159. Pasquale EB. Eph-ephrin bidirectional signaling in physiology and disease. *Cell* 2008;133:38-52.
160. Pasquale EB. Eph receptors and ephrins in cancer: bidirectional signalling and beyond. *Nat Rev Cancer* 2010;10:165-80.
161. Himanen JP, Nikolov DB. Eph signaling: a structural view. *Trends Neurosci* 2003;26:46-51.
162. Janes PW, Nievergall E, Lackmann M. Concepts and consequences of Eph receptor clustering. *Semin Cell Dev Biol* 2012;23:43-50.
163. Seiradake E, Harlos K, Sutton G, Aricescu AR, Jones EY. An extracellular steric seeding mechanism for Eph-ephrin signaling platform assembly. *Nat Struct Mol Biol* 2010;17:398-402.
164. Hubbard SR. Juxtamembrane autoinhibition in receptor tyrosine kinases. *Nat Rev Mol Cell Biol* 2004;5:464-71.
165. Johnson LN, Noble ME, Owen DJ. Active and inactive protein kinases: structural basis for regulation. *Cell* 1996;85:149-58.
166. Hubbard SR. Autoinhibitory mechanisms in receptor tyrosine kinases. *Front Biosci* 2002;7:d330-40.



167. Wybenga-Groot LE, Baskin B, Ong SH, Tong J, Pawson T, Sicheri F. Structural basis for autoinhibition of the Ephb2 receptor tyrosine kinase by the unphosphorylated juxtamembrane region. *Cell* 2001;106:745-57.
168. Himanen JP, Yermekbayeva L, Janes PW, et al. Architecture of Eph receptor clusters. *Proc Natl Acad Sci U S A* 2010;107:10860-5.
169. Murai KK, Pasquale EB. 'Eph'ective signaling: forward, reverse and crosstalk. *J Cell Sci* 2003;116:2823-32.
170. Himanen JP, Saha N, Nikolov DB. Cell-cell signaling via Eph receptors and ephrins. *Curr Opin Cell Biol* 2007;19:534-42.
171. Falivelli G, Lisabeth EM, Rubio de la Torre E, et al. Attenuation of eph receptor kinase activation in cancer cells by coexpressed ephrin ligands. *PLoS One* 2013;8:e81445.
172. Carvalho RF, Beutler M, Marler KJ, et al. Silencing of EphA3 through a cis interaction with ephrinA5. *Nat Neurosci* 2006;9:322-30.
173. Singh DR, Cao Q, King C, et al. Unliganded EphA3 dimerization promoted by the SAM domain. *Biochem J* 2015;471:101-9.
174. Stapleton D, Balan I, Pawson T, Sicheri F. The crystal structure of an Eph receptor SAM domain reveals a mechanism for modular dimerization. *Nat Struct Biol* 1999;6:44-9.
175. Boyd AW, Bartlett PF, Lackmann M. Therapeutic targeting of EPH receptors and their ligands. *Nat Rev Drug Discov* 2014;13:39-62.
176. Serra-Pages C, Kedersha NL, Fazikas L, Medley Q, Debant A, Streuli M. The LAR transmembrane protein tyrosine phosphatase and a coiled-coil LAR-interacting protein co-localize at focal adhesions. *EMBO J* 1995;14:2827-38.
177. Stein E, Lane AA, Cerretti DP, et al. Eph receptors discriminate specific ligand oligomers to determine alternative signaling complexes, attachment, and assembly responses. *Genes Dev* 1998;12:667-78.
178. Lim YS, McLaughlin T, Sung TC, Santiago A, Lee KF, O'Leary DD. p75(NTR) mediates ephrin-A reverse signaling required for axon repulsion and mapping. *Neuron* 2008;59:746-58.
179. Bonanomi D, Chivatakarn O, Bai G, et al. Ret is a multifunctional coreceptor that integrates diffusible- and contact-axon guidance signals. *Cell* 2012;148:568-82.
180. Marler KJ, Becker-Barroso E, Martinez A, et al. A TrkB/EphrinA interaction controls retinal axon branching and synaptogenesis. *J Neurosci* 2008;28:12700-12.
181. Daar IO. Non-SH2/PDZ reverse signaling by ephrins. *Semin Cell Dev Biol* 2012;23:65-74.
182. Palmer A, Zimmer M, Erdmann KS, et al. EphrinB phosphorylation and reverse signaling: regulation by Src kinases and PTP-BL phosphatase. *Mol Cell* 2002;9:725-37.
183. Kullander K, Klein R. Mechanisms and functions of Eph and ephrin signalling. *Nat Rev Mol Cell Biol* 2002;3:475-86.
184. Himanen JP, Rajashankar KR, Lackmann M, Cowan CA, Henkemeyer M, Nikolov DB. Crystal structure of an Eph receptor-ephrin complex. *Nature* 2001;414:933-8.
185. Himanen JP. Ectodomain structures of Eph receptors. *Semin Cell Dev Biol* 2012;23:35-42.
186. Wimmer-Kleikamp SH, Janes PW, Squire A, Bastiaens PI, Lackmann M. Recruitment of Eph receptors into signaling clusters does not require ephrin contact. *J Cell Biol* 2004;164:661-6.
187. Smith FM, Vearing C, Lackmann M, et al. Dissecting the EphA3/Ephrin-A5 interactions using a novel functional mutagenesis screen. *J Biol Chem* 2004;279:9522-31.
188. Davis S, Gale NW, Aldrich TH, et al. Ligands for EPH-related receptor tyrosine kinases that require membrane attachment or clustering for activity. *Science* 1994;266:816-9.
189. Carter N, Nakamoto T, Hirai H, Hunter T. EphrinA1-induced cytoskeletal re-organization requires FAK and p130(cas). *Nat Cell Biol* 2002;4:565-73.
190. Dobrzanski P, Hunter K, Jones-Bolin S, et al. Antiangiogenic and antitumor efficacy of EphA2 receptor antagonist. *Cancer Res* 2004;64:910-9.
191. Lawrenson ID, Wimmer-Kleikamp SH, Lock P, et al. Ephrin-A5 induces rounding, blebbing and de-adhesion of EphA3-expressing 293T and melanoma cells by CrkII and Rho-mediated signalling. *J Cell Sci* 2002;115:1059-72.

192. Gauthier LR, Robbins SM. Ephrin signaling: One raft to rule them all? One raft to sort them? One raft to spread their call and in signaling bind them? *Life Sci* 2003;74:207-16.
193. Marquardt T, Shirasaki R, Ghosh S, et al. Coexpressed EphA receptors and ephrin-A ligands mediate opposing actions on growth cone navigation from distinct membrane domains. *Cell* 2005;121:127-39.
194. Miao H, Burnett E, Kinch M, Simon E, Wang B. Activation of EphA2 kinase suppresses integrin function and causes focal-adhesion-kinase dephosphorylation. *Nat Cell Biol* 2000;2:62-9.
195. Arvanitis DN, Davy A. Regulation and misregulation of Eph/ephrin expression. *Cell Adh Migr* 2012;6:131-7.
196. Shintani T, Ihara M, Sakuta H, Takahashi H, Watakabe I, Noda M. Eph receptors are negatively controlled by protein tyrosine phosphatase receptor type O. *Nat Neurosci* 2006;9:761-9.
197. Nievergall E, Janes PW, Stegmayer C, et al. PTP1B regulates Eph receptor function and trafficking. *J Cell Biol* 2010;191:1189-203.
198. Georgakopoulos A, Litterst C, Ghersi E, et al. Metalloproteinase/Presenilin1 processing of ephrinB regulates EphB-induced Src phosphorylation and signaling. *EMBO J* 2006;25:1242-52.
199. Arvanitis D, Davy A. Eph/ephrin signaling: networks. *Genes Dev* 2008;22:416-29.
200. Litterst C, Georgakopoulos A, Shioi J, et al. Ligand binding and calcium influx induce distinct ectodomain/gamma-secretase-processing pathways of EphB2 receptor. *J Biol Chem* 2007;282:16155-63.
201. Inoue E, Deguchi-Tawarada M, Togawa A, et al. Synaptic activity prompts gamma-secretase-mediated cleavage of EphA4 and dendritic spine formation. *J Cell Biol* 2009;185:551-64.
202. Halford MM, Chumley MJ, Henkemeyer M. Ephective endocytosis. *Dev Cell* 2003;5:536-7.
203. Martone ME, Holash JA, Bayardo A, Pasquale EB, Ellisman MH. Immunolocalization of the receptor tyrosine kinase EphA4 in the adult rat central nervous system. *Brain Res* 1997;771:238-50.
204. Tremblay ME, Riad M, Bouvier D, et al. Localization of EphA4 in axon terminals and dendritic spines of adult rat hippocampus. *J Comp Neurol* 2007;501:691-702.
205. Filosa A, Paixao S, Honsek SD, et al. Neuron-glia communication via EphA4/ephrin-A3 modulates LTP through glial glutamate transport. *Nat Neurosci* 2009;12:1285-92.
206. Grunwald IC, Korte M, Adelmann G, et al. Hippocampal plasticity requires postsynaptic ephrinBs. *Nat Neurosci* 2004;7:33-40.
207. Fu AK, Hung KW, Fu WY, et al. APC(Cdh1) mediates EphA4-dependent downregulation of AMPA receptors in homeostatic plasticity. *Nat Neurosci* 2011;14:181-9.
208. Frugier T, Conquest A, McLean C, Currie P, Moses D, Goldshmit Y. Expression and activation of EphA4 in the human brain after traumatic injury. *J Neuropathol Exp Neurol* 2012;71:242-50.
209. Hanell A, Clausen F, Djupsjo A, et al. Functional and histological outcome after focal traumatic brain injury is not improved in conditional EphA4 knockout mice. *J Neurotrauma* 2012;29:2660-71.
210. Goldshmit Y, Galea MP, Wise G, Bartlett PF, Turnley AM. Axonal regeneration and lack of astrocytic gliosis in EphA4-deficient mice. *J Neurosci* 2004;24:10064-73.
211. Willson CA, Irizarry-Ramirez M, Gaskins HE, et al. Upregulation of EphA receptor expression in the injured adult rat spinal cord. *Cell Transplant* 2002;11:229-39.
212. Fabes J, Anderson P, Yanez-Munoz RJ, Thrasher A, Brennan C, Bolsover S. Accumulation of the inhibitory receptor EphA4 may prevent regeneration of corticospinal tract axons following lesion. *Eur J Neurosci* 2006;23:1721-30.
213. Fabes J, Anderson P, Brennan C, Bolsover S. Regeneration-enhancing effects of EphA4 blocking peptide following corticospinal tract injury in adult rat spinal cord. *Eur J Neurosci* 2007;26:2496-505.
214. Parmentier-Batteur S, Finger EN, Krishnan R, et al. Attenuation of scratch-induced reactive astrogliosis by novel EphA4 kinase inhibitors. *J Neurochem* 2011;118:1016-31.
215. Cruz-Orengo L, Figueroa JD, Velazquez I, et al. Blocking EphA4 upregulation after spinal cord injury results in enhanced chronic pain. *Exp Neurol* 2006;202:421-33.

216. Li J, Liu N, Wang Y, Wang R, Guo D, Zhang C. Inhibition of EphA4 signaling after ischemia-reperfusion reduces apoptosis of CA1 pyramidal neurons. *Neurosci Lett* 2012;518:92-5.
217. Li S, Overman JJ, Katsman D, et al. An age-related sprouting transcriptome provides molecular control of axonal sprouting after stroke. *Nat Neurosci* 2010;13:1496-504.
218. Overman JJ, Clarkson AN, Wanner IB, et al. A role for ephrin-A5 in axonal sprouting, recovery, and activity-dependent plasticity after stroke. *Proc Natl Acad Sci U S A* 2012;109:E2230-9.
219. Lemmens R, Jaspers T, Robberecht W, Thijs VN. Modifying expression of EphA4 and its downstream targets improves functional recovery after stroke. *Hum Mol Genet* 2013;22:2214-20.
220. Sobel RA. Ephrin A receptors and ligands in lesions and normal-appearing white matter in multiple sclerosis. *Brain Pathol* 2005;15:35-45.
221. Munro KM, Dixon KJ, Gresle MM, et al. EphA4 receptor tyrosine kinase is a modulator of onset and disease severity of experimental autoimmune encephalomyelitis (EAE). *PLoS One* 2013;8:e55948.
222. Murai KK, Nguyen LN, Koolpe M, McLennan R, Krull CE, Pasquale EB. Targeting the EphA4 receptor in the nervous system with biologically active peptides. *Mol Cell Neurosci* 2003;24:1000-11.
223. Simon AM, de Maturana RL, Ricobaraza A, et al. Early changes in hippocampal Eph receptors precede the onset of memory decline in mouse models of Alzheimer's disease. *J Alzheimers Dis* 2009;17:773-86.
224. Matsui C, Inoue E, Kakita A, et al. Involvement of the gamma-secretase-mediated EphA4 signaling pathway in synaptic pathogenesis of Alzheimer's disease. *Brain Pathol* 2012;22:776-87.
225. Rosenberger AF, Rozemuller AJ, van der Flier WM, Scheltens P, van der Vies SM, Hoozemans JJ. Altered distribution of the EphA4 kinase in hippocampal brain tissue of patients with Alzheimer's disease correlates with pathology. *Acta Neuropathol Commun* 2014;2:79.
226. Lai WB, Wang BJ, Hu MK, Hsu WM, Her GM, Liao YF. Ligand-dependent activation of EphA4 signaling regulates the proteolysis of amyloid precursor protein through a Lyn-mediated pathway. *Mol Neurobiol* 2014;49:1055-68.
227. Fu AK, Hung KW, Huang H, et al. Blockade of EphA4 signaling ameliorates hippocampal synaptic dysfunctions in mouse models of Alzheimer's disease. *Proc Natl Acad Sci U S A* 2014;111:9959-64.
228. Vargas LM, Leal N, Estrada LD, et al. EphA4 activation of c-Abl mediates synaptic loss and LTP blockade caused by amyloid-beta oligomers. *PLoS One* 2014;9:e92309.
229. Shi M, Movius J, Dator R, et al. Cerebrospinal fluid peptides as potential Parkinson disease biomarkers: a staged pipeline for discovery and validation. *Mol Cell Proteomics* 2015;14:544-55.
230. Fang Q, Strand A, Law W, et al. Brain-specific proteins decline in the cerebrospinal fluid of humans with Huntington disease. *Mol Cell Proteomics* 2009;8:451-66.
231. Saxena S, Caroni P. Selective neuronal vulnerability in neurodegenerative diseases: from stressor thresholds to degeneration. *Neuron* 2011;71:35-48.
232. Fischer LR, Culver DG, Tennant P, et al. Amyotrophic lateral sclerosis is a distal axonopathy: evidence in mice and man. *Exp Neurol* 2004;185:232-40.
233. Gordon T, Tyreman N, Li S, Putman CT, Hegedus J. Functional over-load saves motor units in the SOD1-G93A transgenic mouse model of amyotrophic lateral sclerosis. *Neurobiol Dis* 2010;37:412-22.
234. Egea J, Nissen UV, Dufour A, et al. Regulation of EphA 4 kinase activity is required for a subset of axon guidance decisions suggesting a key role for receptor clustering in Eph function. *Neuron* 2005;47:515-28.
235. Dufour A, Seibt J, Passante L, et al. Area specificity and topography of thalamocortical projections are controlled by ephrin/Eph genes. *Neuron* 2003;39:453-65.
236. Dottori M, Hartley L, Galea M, et al. EphA4 (Sek1) receptor tyrosine kinase is required for the development of the corticospinal tract. *Proc Natl Acad Sci U S A* 1998;95:13248-53.
237. Janes PW, Saha N, Barton WA, et al. Adam meets Eph: an ADAM substrate recognition module acts as a molecular switch for ephrin cleavage in trans. *Cell* 2005;123:291-304.

238. Gatto G, Morales D, Kania A, Klein R. EphA4 receptor shedding regulates spinal motor axon guidance. *Curr Biol* 2014;24:2355-65.
239. Sorkin A, von Zastrow M. Endocytosis and signalling: intertwining molecular networks. *Nat Rev Mol Cell Biol* 2009;10:609-22.
240. Deininger K, Eder M, Kramer ER, et al. The Rab5 guanylate exchange factor Rin1 regulates endocytosis of the EphA4 receptor in mature excitatory neurons. *Proc Natl Acad Sci U S A* 2008;105:12539-44.
241. Cowan CW, Shao YR, Sahin M, et al. Vav family GEFs link activated Ephs to endocytosis and axon guidance. *Neuron* 2005;46:205-17.
242. Kullander K, Mather NK, Diella F, Dottori M, Boyd AW, Klein R. Kinase-dependent and kinase-independent functions of EphA4 receptors in major axon tract formation in vivo. *Neuron* 2001;29:73-84.
243. Dufour A, Egea J, Kullander K, Klein R, Vanderhaeghen P. Genetic analysis of EphA-dependent signaling mechanisms controlling topographic mapping in vivo. *Development* 2006;133:4415-20.
244. Cowan CA, Yokoyama N, Saxena A, et al. Ephrin-B2 reverse signaling is required for axon pathfinding and cardiac valve formation but not early vascular development. *Dev Biol* 2004;271:263-71.
245. Ilieva H, Polymenidou M, Cleveland DW. Non-cell autonomous toxicity in neurodegenerative disorders: ALS and beyond. *J Cell Biol* 2009;187:761-72.
246. Swartz ME, Eberhart J, Pasquale EB, Krull CE. EphA4/ephrin-A5 interactions in muscle precursor cell migration in the avian forelimb. *Development* 2001;128:4669-80.
247. Donoghue MJ, Merlie JP, Sanes JR. The Eph Kinase Ligand AL-1 Is Expressed by Rostral Muscles and Inhibits Outgrowth from Caudal Neurons. *Mol Cell Neurosci* 1996;8:185-98.
248. Linneberg C, Harboe M, Laursen LS. Axo-Glia Interaction Preceding CNS Myelination Is Regulated by Bidirectional Eph-Ephrin Signaling. *ASN Neuro* 2015;7.
249. Prestoz L, Chatzopoulou E, Lemkine G, et al. Control of axonophilic migration of oligodendrocyte precursor cells by Eph-ephrin interaction. *Neuron Glia Biol* 2004;1:73-83.
250. Benson MD, Romero MI, Lush ME, Lu QR, Henkemeyer M, Parada LF. Ephrin-B3 is a myelin-based inhibitor of neurite outgrowth. *Proc Natl Acad Sci U S A* 2005;102:10694-9.
251. Jiao JW, Feldheim DA, Chen DF. Ephrins as negative regulators of adult neurogenesis in diverse regions of the central nervous system. *Proc Natl Acad Sci U S A* 2008;105:8778-83.
252. Ashton RS, Conway A, Pangarkar C, et al. Astrocytes regulate adult hippocampal neurogenesis through ephrin-B signaling. *Nat Neurosci* 2012;15:1399-406.
253. Murai KK, Nguyen LN, Irie F, Yamaguchi Y, Pasquale EB. Control of hippocampal dendritic spine morphology through ephrin-A3/EphA4 signaling. *Nat Neurosci* 2003;6:153-60.
254. Carmona MA, Murai KK, Wang L, Roberts AJ, Pasquale EB. Glial ephrin-A3 regulates hippocampal dendritic spine morphology and glutamate transport. *Proc Natl Acad Sci U S A* 2009;106:12524-9.
255. Yang J, Luo X, Huang X, Ning Q, Xie M, Wang W. Ephrin-A3 reverse signaling regulates hippocampal neuronal damage and astrocytic glutamate transport after transient global ischemia. *J Neurochem* 2014;131:383-94.
256. Bundesen LQ, Scheel TA, Bregman BS, Kromer LF. Ephrin-B2 and EphB2 regulation of astrocyte-meningeal fibroblast interactions in response to spinal cord lesions in adult rats. *J Neurosci* 2003;23:7789-800.
257. Ren Z, Chen X, Yang J, et al. Improved axonal regeneration after spinal cord injury in mice with conditional deletion of ephrin B2 under the GFAP promoter. *Neuroscience* 2013;241:89-99.
258. Adams RH, Wilkinson GA, Weiss C, et al. Roles of ephrinB ligands and EphB receptors in cardiovascular development: demarcation of arterial/venous domains, vascular morphogenesis, and sprouting angiogenesis. *Genes Dev* 1999;13:295-306.
259. Bajenaru ML, Zhu Y, Hedrick NM, Donahoe J, Parada LF, Gutmann DH. Astrocyte-specific inactivation of the neurofibromatosis 1 gene (NF1) is insufficient for astrocytoma formation. *Mol Cell Biol* 2002;22:5100-13.

260. Srinivas S, Watanabe T, Lin CS, et al. Cre reporter strains produced by targeted insertion of EYFP and ECFP into the ROSA26 locus. *BMC Dev Biol* 2001;1:4.
261. Slezak M, Goritz C, Niemiec A, et al. Transgenic mice for conditional gene manipulation in astroglial cells. *Glia* 2007;55:1565-76.
262. Sawamiphak S, Seidel S, Essmann CL, et al. Ephrin-B2 regulates VEGFR2 function in developmental and tumour angiogenesis. *Nature* 2010;465:487-91.
263. Wang Y, Nakayama M, Pitulescu ME, et al. Ephrin-B2 controls VEGF-induced angiogenesis and lymphangiogenesis. *Nature* 2010;465:483-6.
264. Zhang Y, Chen K, Sloan SA, et al. An RNA-sequencing transcriptome and splicing database of glia, neurons, and vascular cells of the cerebral cortex. *J Neurosci* 2014;34:11929-47.
265. Roessmann U, Velasco ME, Sindely SD, Gambetti P. Glial fibrillary acidic protein (GFAP) in ependymal cells during development. An immunocytochemical study. *Brain Res* 1980;200:13-21.
266. Buniatian G, Traub P, Albinus M, et al. The immunoreactivity of glial fibrillary acidic protein in mesangial cells and podocytes of the glomeruli of rat kidney in vivo and in culture. *Biol Cell* 1998;90:53-61.
267. von Koskull H. Rapid identification of glial cells in human amniotic fluid with indirect immunofluorescence. *Acta Cytol* 1984;28:393-400.
268. Apte MV, Haber PS, Applegate TL, et al. Periacinar stellate shaped cells in rat pancreas: identification, isolation, and culture. *Gut* 1998;43:128-33.
269. Kasantikul V, Shuangshoti S. Positivity to glial fibrillary acidic protein in bone, cartilage, and chordoma. *J Surg Oncol* 1989;41:22-6.
270. Boulay AC, del Castillo FJ, Giraudet F, et al. Hearing is normal without connexin30. *J Neurosci* 2013;33:430-4.
271. Xu J, Nicholson BJ. The role of connexins in ear and skin physiology - functional insights from disease-associated mutations. *Biochim Biophys Acta* 2013;1828:167-78.
272. Alvarez JI, Katayama T, Prat A. Glial influence on the blood brain barrier. *Glia* 2013;61:1939-58.
273. Miyazaki K, Ohta Y, Nagai M, et al. Disruption of neurovascular unit prior to motor neuron degeneration in amyotrophic lateral sclerosis. *J Neurosci Res* 2011;89:718-28.
274. Garbuzova-Davis S, Saporta S, Haller E, et al. Evidence of compromised blood-spinal cord barrier in early and late symptomatic SOD1 mice modeling ALS. *PLoS One* 2007;2:e1205.
275. Garbuzova-Davis S, Haller E, Saporta S, Kolomey I, Nicosia SV, Sanberg PR. Ultrastructure of blood-brain barrier and blood-spinal cord barrier in SOD1 mice modeling ALS. *Brain Res* 2007;1157:126-37.
276. Garbuzova-Davis S, Sanberg PR. Blood-CNS Barrier Impairment in ALS patients versus an animal model. *Front Cell Neurosci* 2014;8:21.
277. Zhong Z, Deane R, Ali Z, et al. ALS-causing SOD1 mutants generate vascular changes prior to motor neuron degeneration. *Nat Neurosci* 2008;11:420-2.
278. Emmert-Buck MR, Bonner RF, Smith PD, et al. Laser capture microdissection. *Science* 1996;274:998-1001.
279. Boyd AW, Bartlett PF, Lackmann M. Therapeutic targeting of EPH receptors and their ligands. *Nat Rev Drug Discov* 2014;13:39-62.
280. Fu AKY, Hung KW, Huang HQ, et al. Blockade of EphA4 signaling ameliorates hippocampal synaptic dysfunctions in mouse models of Alzheimer's disease. *P Natl Acad Sci USA* 2014;111:9959-64.
281. Van Hoecke A, Schoonaert L, Lemmens R, et al. EPHA4 is a disease modifier of amyotrophic lateral sclerosis in animal models and in humans. *Nat Med* 2012;18:1418-+.
282. Noberini R, Lamberto I, Pasquale EB. Targeting Eph receptors with peptides and small molecules: progress and challenges. *Semin Cell Dev Biol* 2012;23:51-7.
283. Tognolini M, Hassan-Mohamed I, Giorgio C, Zanotti I, Lodola A. Therapeutic perspectives of Eph-ephrin system modulation. *Drug Discov Today* 2014;19:661-9.

284. Lamberto I, Lechtenberg BC, Olson EJ, et al. Development and structural analysis of a nanomolar cyclic peptide antagonist for the EphA4 receptor. *ACS Chem Biol* 2014;9:2787-95.
285. Guo FY, Lesk AM. Sizes of interface residues account for cross-class binding affinity patterns in Eph receptor-ephrin families. *Proteins* 2014;82:349-53.
286. Singla N, Goldgur Y, Xu K, Paavilainen S, Nikolov DB, Himanen JP. Crystal structure of the ligand-binding domain of the promiscuous EphA4 receptor reveals two distinct conformations. *Biochem Biophys Res Commun* 2010;399:555-9.
287. Lamberto I, Qin H, Noberini R, et al. Distinctive binding of three antagonistic peptides to the ephrin-binding pocket of the EphA4 receptor. *Biochem J* 2012;445:47-56.
288. Wu B, Zhang Z, Noberini R, et al. HTS by NMR of combinatorial libraries: a fragment-based approach to ligand discovery. *Chem Biol* 2013;20:19-33.
289. Han X, Xu Y, Yang Y, et al. Discovery and characterization of a novel cyclic peptide that effectively inhibits ephrin binding to the EphA4 receptor and displays anti-angiogenesis activity. *PLoS One* 2013;8:e80183.
290. Noberini R, Koolpe M, Peddibhotla S, et al. Small molecules can selectively inhibit ephrin binding to the EphA4 and EphA2 receptors. *J Biol Chem* 2008;283:29461-72.
291. Muyldermans S. Nanobodies: natural single-domain antibodies. *Annu Rev Biochem* 2013;82:775-97.
292. De Meyer T, Muyldermans S, Depicker A. Nanobody-based products as research and diagnostic tools. *Trends Biotechnol* 2014;32:263-70.
293. Steyaert J, Kobilka BK. Nanobody stabilization of G protein-coupled receptor conformational states. *Curr Opin Struct Biol* 2011;21:567-72.
294. Qin H, Shi J, Noberini R, Pasquale EB, Song J. Crystal structure and NMR binding reveal that two small molecule antagonists target the high affinity ephrin-binding channel of the EphA4 receptor. *J Biol Chem* 2008;283:29473-84.
295. Noberini R, De SK, Zhang Z, et al. A disalicylic acid-furanyl derivative inhibits ephrin binding to a subset of Eph receptors. *Chem Biol Drug Des* 2011;78:667-78.
296. Tognolini M, Incerti M, Lodola A. Are we using the right pharmacological tools to target EphA4? *ACS Chem Neurosci* 2014;5:1146-7.
297. Baell JB, Holloway GA. New substructure filters for removal of pan assay interference compounds (PAINS) from screening libraries and for their exclusion in bioassays. *J Med Chem* 2010;53:2719-40.
298. Hamers-Casterman C, Atarhouch T, Muyldermans S, et al. Naturally occurring antibodies devoid of light chains. *Nature* 1993;363:446-8.
299. Conrath K, Vincke C, Stijlemans B, et al. Antigen binding and solubility effects upon the veneering of a camel VHH in framework-2 to mimic a VH. *J Mol Biol* 2005;350:112-25.
300. Vincke C, Loris R, Saerens D, Martinez-Rodriguez S, Muyldermans S, Conrath K. General strategy to humanize a camelid single-domain antibody and identification of a universal humanized nanobody scaffold. *J Biol Chem* 2009;284:3273-84.
301. Nguyen VK, Hamers R, Wyns L, Muyldermans S. Camel heavy-chain antibodies: diverse germline V(H)H and specific mechanisms enlarge the antigen-binding repertoire. *EMBO J* 2000;19:921-30.
302. Rissiek B, Koch-Nolte F, Magnus T. Nanobodies as modulators of inflammation: potential applications for acute brain injury. *Front Cell Neurosci* 2014;8:344.
303. Vincke C, Gutierrez C, Wernery U, Devoogdt N, Hassanzadeh-Ghassabeh G, Muyldermans S. Generation of single domain antibody fragments derived from camelids and generation of manifold constructs. *Methods Mol Biol* 2012;907:145-76.
304. Truitt L, Freywald A. Dancing with the dead: Eph receptors and their kinase-null partners. *Biochem Cell Biol* 2011;89:115-29.
305. Figueroa JD, Benton RL, Velazquez I, et al. Inhibition of EphA7 up-regulation after spinal cord injury reduces apoptosis and promotes locomotor recovery. *J Neurosci Res* 2006;84:1438-51.

306. Figueroa JD, Benton RL, Velazquez I, et al. Inhibition of EphA7 up-regulation after spinal cord injury reduces apoptosis and promotes locomotor recovery. *J Neurosci Res* 2006;84:1438-51.
307. Coppieters K, Dreier T, Silence K, et al. Formatted anti-tumor necrosis factor alpha VHH proteins derived from camelids show superior potency and targeting to inflamed joints in a murine model of collagen-induced arthritis. *Arthritis Rheum* 2006;54:1856-66.
308. Dennis MS, Zhang M, Meng YG, et al. Albumin binding as a general strategy for improving the pharmacokinetics of proteins. *Journal of Biological Chemistry* 2002;277:35035-43.
309. Dixon FJ, Maurer PH, Deichmiller MP. Half-lives of homologous serum albumins in several species. *Proc Soc Exp Biol Med* 1953;83:287-8.
310. Veronese FM, Mero A. The impact of PEGylation on biological therapies. *Biodrugs* 2008;22:315-29.
311. Chapman AP. PEGylated antibodies and antibody fragments for improved therapy: a review. *Adv Drug Deliv Rev* 2002;54:531-45.
312. Saerens D, Ghassabeh GH, Muyldermans S. Single-domain antibodies as building blocks for novel therapeutics. *Curr Opin Pharmacol* 2008;8:600-8.
313. Sheedy C, MacKenzie CR, Hall JC. Isolation and affinity maturation of hapten-specific antibodies. *Biotechnol Adv* 2007;25:333-52.
314. Bashaw GJ, Klein R. Signaling from axon guidance receptors. *Cold Spring Harb Perspect Biol* 2010;2:a001941.
315. Noren NK, Pasquale EB. Eph receptor-ephrin bidirectional signals that target Ras and Rho proteins. *Cell Signal* 2004;16:655-66.
316. Shi L, Fu WY, Hung KW, et al. Alpha2-chimaerin interacts with EphA4 and regulates EphA4-dependent growth cone collapse. *Proc Natl Acad Sci U S A* 2007;104:16347-52.
317. Murai KK, Pasquale EB. New exchanges in eph-dependent growth cone dynamics. *Neuron* 2005;46:161-3.
318. Bartanusz V, Jezova D, Alajajian B, Digicaylioglu M. The blood-spinal cord barrier: morphology and clinical implications. *Ann Neurol* 2011;70:194-206.
319. Garbuzova-Davis S, Hernandez-Ontiveros DG, Rodrigues MC, et al. Impaired blood-brain/spinal cord barrier in ALS patients. *Brain Res* 2012;1469:114-28.
320. Nicaise C, Mitrecic D, Demetter P, et al. Impaired blood-brain and blood-spinal cord barriers in mutant SOD1-linked ALS rat. *Brain Res* 2009;1301:152-62.
321. Henkel JS, Beers DR, Wen S, Bowser R, Appel SH. Decreased mRNA expression of tight junction proteins in lumbar spinal cords of patients with ALS. *Neurology* 2009;72:1614-6.
322. Salvucci O, de la Luz Sierra M, Martina JA, McCormick PJ, Tosato G. EphB2 and EphB4 receptors forward signaling promotes SDF-1-induced endothelial cell chemotaxis and branching remodeling. *Blood* 2006;108:2914-22.
323. Fuller T, Korff T, Kilian A, Dandekar G, Augustin HG. Forward EphB4 signaling in endothelial cells controls cellular repulsion and segregation from ephrinB2 positive cells. *J Cell Sci* 2003;116:2461-70.
324. Salvucci O, Tosato G. Essential roles of EphB receptors and EphrinB ligands in endothelial cell function and angiogenesis. *Adv Cancer Res* 2012;114:21-57.
325. Bernal GM, Peterson DA. Phenotypic and gene expression modification with normal brain aging in GFAP-positive astrocytes and neural stem cells. *Aging Cell* 2011;10:466-82.
326. Krum JM, Mani N, Rosenstein JM. Roles of the endogenous VEGF receptors flt-1 and flk-1 in astroglial and vascular remodeling after brain injury. *Exp Neurol* 2008;212:108-17.
327. Germain S, Eichmann A. VEGF and ephrin-B2: a bloody duo. *Nat Med* 2010;16:752-4.
328. Masumura T, Yamamoto K, Shimizu N, Obi S, Ando J. Shear stress increases expression of the arterial endothelial marker ephrinB2 in murine ES cells via the VEGF-Notch signaling pathways. *Arterioscler Thromb Vasc Biol* 2009;29:2125-31.
329. Bochenek ML, Dickinson S, Astin JW, Adams RH, Nobes CD. Ephrin-B2 regulates endothelial cell morphology and motility independently of Eph-receptor binding. *J Cell Sci* 2010;123:1235-46.

330. Lambrechts D, Storkebaum E, Morimoto M, et al. VEGF is a modifier of amyotrophic lateral sclerosis in mice and humans and protects motoneurons against ischemic death. *Nat Genet* 2003;34:383-94.
331. Storkebaum E, Lambrechts D, Dewerchin M, et al. Treatment of motoneuron degeneration by intracerebroventricular delivery of VEGF in a rat model of ALS. *Nat Neurosci* 2005;8:85-92.
332. Llado J, Tolosa L, Olmos G. Cellular and molecular mechanisms involved in the neuroprotective effects of VEGF on motoneurons. *Front Cell Neurosci* 2013;7:181.
333. Bogaert E, Van Damme P, Van Den Bosch L, Robberecht W. Vascular endothelial growth factor in amyotrophic lateral sclerosis and other neurodegenerative diseases. *Muscle Nerve* 2006;34:391-405.
334. Rasmussen SG, Choi HJ, Fung JJ, et al. Structure of a nanobody-stabilized active state of the beta(2) adrenoceptor. *Nature* 2011;469:175-80.
335. Meier C, Anastasiadou S, Knoll B. Ephrin-A5 suppresses neurotrophin evoked neuronal motility, ERK activation and gene expression. *PLoS One* 2011;6:e26089.
336. Fridy PC, Li Y, Keegan S, et al. A robust pipeline for rapid production of versatile nanobody repertoires. *Nat Methods* 2014;11:1253-60.
337. Vearing C, Lee FT, Wimmer-Kleikamp S, et al. Concurrent binding of anti-EphA3 antibody and ephrin-A5 amplifies EphA3 signaling and downstream responses: potential as EphA3-specific tumor-targeting reagents. *Cancer Res* 2005;65:6745-54.





## List of publications

**Schoonaert L**, Roucourt B, Timmers M, Rue L, Haustraete J, Scheveneels W, Chavez Gutierrez L, Dewilde M, Destrooper B, Van Den Bosch L, Van Damme P, Lemmens R, Robberecht W. Identification and characterization of Nanobodies specific for the ephrin A4 receptor. Manuscript in preparation

Defourny J, Mateo Sanchez S, **Schoonaert L**, Robberecht W, Davy A, Nguyen L, Malgrange B. Cochlear supporting cell transdifferentiation *and integration into hair cell layers by inhibition of ephrin-B2 signalling* (2015). *Nature Communications*

Van Hoecke A, **Schoonaert L**, Lemmens R, Timmers M, Staats KA, Laird AS, Peeters E, Philips T, Goris A, Dubois B, Andersen PM, Al-Chalabi A, Thijs V, Turnley AM, van Vught PM, Veldink JH, Hardiman O, Van Den Bosch L, Gonzalez-Perez P, Van Damme P, Brown RH Jr, van den Berg LH, Robberecht W. EphA4 is a disease modifier of amyotrophic lateral sclerosis in animal models and in humans (2012). *Nature Medicine*



## **Presentations at international symposia**

Society for Neuroscience (Sfn), San Diego, USA, 2013; poster presentation entitled 'Deleting ephrin-b2 from reactive astrocytes is beneficial in ALS'

European Network for the Cure of ALS (ENCALS), Sheffield, UK, 2013; oral presentation entitled 'Deleting ephrin-b2 from reactive astrocytes is beneficial in ALS'

Society for Neuroscience (Sfn), New Orleans, USA, 2012; poster presentation entitled 'Genetic screening in zebrafish identifies EphA4 of the ephrin axonal repellent system as a disease modifier of amyotrophic lateral sclerosis in rodent models and patients'

European Network for the Cure of ALS (ENCALS), Dublin, Ireland, 2012; oral presentation entitled 'EphA4 inhibition rescues the motor axon phenotype in a zebrafish model for ALS and SMA'

Society for Neuroscience (Sfn), Washington D.C., USA, 2011; poster presentation entitled 'Inhibition of the EphA4 receptor rescues the axonopathy in a zebrafish model for ALS'







